Artificial amyloid-like aggregating proteins cause cytotoxicity in vitro and in vivo

Irene Riera Tur

München 2019

Artificial amyloid-like aggregating proteins cause cytotoxicity in vitro and in vivo

Irene Riera Tur

Dissertation
an der Fakultät für Biologie
der Ludwig–Maximilians–Universität
München

vorgelegt von
Irene Riera Tur
aus Ibiza, Spanien

München, den 04 Juli 2019

Die wissenschaftliche Arbeit, die dieser Dissertation zugrunde liegt, wurde im Labor von Prof. Dr. Rüdiger Klein, Abteilung Moleküle-Signale-Entwicklung, am Max-Planck-Institut für Neurobiologie, Martinsried, Deutschland durchgeführt.

Erstgutachter: Prof. Dr. Rüdiger Klein

Zweitgutachter: Prof. Dr. Laura Busse

Tag der mündlichen Prüfung: 26 November 2019

Erklärung

Ich versichere hiermit an Eides Statt, dass die vorgelegte Dissertation von mir selbständig und ohne unerlaubte Hilfe angefertigt ist.

München, den 04 Juli 2019

Irene Riera Tur

Eidesstattliche Erklärung

Hiermit erkläre ich, dass die Dissertation nicht ganz oder in wesentlichen Teilen einer anderen Prüfungskommission vorgelegt worden ist und ich mich anderweitig einer Doktorprüfung ohne Erfolg nicht unterzogen habe.

München, den 04 Juli 2019

Irene Riera Tur

Contents

1 Abstract

Neurodegenerative diseases (NDs), such as Alzheimer's disease and Parkinson's disease, are devastating disorders that progress to severe disability and death. Currently, there is no cure for these diseases.

The common hallmark of NDs is the progressive deposition of misfolded protein aggregates, rich in amyloid-like β-sheet structures. Moreover, the etiology of these diseases at the molecular level is extremely complex and malfunction of diverse cellular pathways, including protein degradation mechanisms, mitochondrial homeostasis, neurotrophic signaling, and nucleocytoplasmic transport have been shown to be involved. Despite great advances in last decades in the comprehension of how these diseases develop, the precise mechanisms leading to neurodegeneration are still not fully understood. One difficulty in deciphering these mechanisms is the co-existence of loss of function effects, due to the impaired structure of the aggregating protein, and gain of function effects, due to the cytotoxic properties of the misfolded conformation.

In this thesis, I have used rationally designed proteins which form amyloid-like β-sheet structures as a tool to investigate the toxicity mechanisms of protein aggregation in the absence of potential loss of function effects. First, we confirmed that β-sheet proteins form aggregates in primary cultured neurons. Moreover, expression of these proteins resulted in impaired neuronal morphology and progressive neuronal death. Reduced Akt phosphorylation suggested that impaired neurotrophic signaling might be involved in the cause of neuronal death.

To further investigate the molecular signature of β-sheet-induced toxicity, we performed interactome mass spectrometry analysis in primary neurons. This approach revealed that a variety of proteins, some of them essential for neuronal survival, form aberrant interactions with the β-sheet proteins. Therefore, the list of interacting proteins constitutes a resource of candidates which might be potentially involved in common mechanisms of aggregation toxicity.

In addition, we generated a novel inducible transgenic mouse line to study amyloid-like aggregation effects *in vivo*. β-sheet protein expression in the forebrain resulted in aggregate formation, brain atrophy and interfered with nucleocytoplasmic transport components, while no effects on mouse behavior were detected. Moreover, β-sheet protein expression in the whole central nervous system during embryogenesis was lethal, suggesting a strong cellular toxicity phenotype. Hence, the observed lethality requires further investigation.

Overall, we adopted an integrative and multidisciplinary approach that confirmed the use of artificial aggregating proteins as an asset to decipher gain of function effects of protein aggregation. Further studies using the β-sheet proteins to unravel common underlying mechanisms of aggregation toxicity in NDs may enable the therapeutic targeting of a whole range of disorders.

2 Introduction

2.1 Protein aggregation in neurodegenerative diseases

Life expectancy has risen worldwide at fast pace during the last century. Since aging is a common risk factor for Neurodegenerative diseases (NDs), their prevalence is also rising. As an example, in 2015 around 47 million people were living with dementia worldwide, and this number is expected to increase to approximately 131 million people by 2050. This does not only affect people who suffer from these illnesses, but also relatives, friends, and eventually, the whole society [1, 2]. In spite of great efforts in research, industry, and clinics, there is currently no cure for neurodegenerative diseases. However, our knowledge about these diseases has vastly improved in last decades.

The group of neurodegenerative diseases includes some of the most debilitating disorders, such as Alzheimer's disease (AD), Parkinson's disease (PD), Huntington's disease (HD), Amyotrophic lateral sclerosis (ALS), Spinocerebellar ataxia (SCA), Frontotemporal dementia (FTD), dementia with Lewy bodies, and Prion diseases (PrD), among others. These diseases present diverse clinical symptoms, affecting cognition and movements. In AD, which is the most prevalent ND, patients suffer from progressive memory loss and dementia. In contrast, PD characteristic symptoms are resting tremor, rigidity, bradikynesia, and occasionally dementia [3, 4]. HD has a broad impact on a person's functional abilities, resulting in movement problems (including involuntary movements and impairments in voluntary movements), cognitive problems, and psychiatric problems as depression [5]. People affected by ALS, which is a type of motor neuron disease, experience lack of control in muscles needed to move, eat, and breathe. Interestingly, ALS and FTD show clinical overlap, as dementia symptoms can be seen in ALS patients and neuromuscular signs can be seen in FTD patients [6].

Despite the variety in clinical manifestations, NDs share some common features: most of them have both sporadic and inherited origin (except for HD and SCA, which are inherited in an autosomal dominant manner), they appear late in life, and patients

present brain mass loss with characteristic neuronal loss and synaptic abnormalities, which are in turn reflected in specific clinical symptoms. Moreover, the common hallmark of NDs is the progressive deposition of intra- and/or extracellular protein aggregates. This commonality of protein misfolding and aggregate accumulation accros diseases has prompted researchers to refer to NDs as protein misfolding diseases [7].

The aggregating proteins in each disease have different sequence, structure, expression levels, and function. Nevertherless, they all misfold and self-assemble forming well-ordered β-sheet-rich structures (except for SOD1, TDP-43, and FUS in ALS; their structure is under discussion), ranging from small oligomers to large fibrillar aggregates, the latter usually referred to as amyloid. Structural analysis has shown that amyloid consists of ordered arrays of β-sheets running parallel to the long axis of the fibrils, a structure known as cross-β [8]. Moreover, amyloid fibrils are thread-like structures typically 7–13 nm in diameter, as observed by electron microscopy (EM), and often microns in length. Finally, amyloid structures are characteristically identified by the binding of dyes, such as thioflavin-T, Congo red, or their derivatives [9].

The amyloid polymerization mechanism can be best described by the seeding-nucleation model [10, 11], shown in schematics in Figure 2.1. This model proposes that the formation of a stable protein nucleus that acts as a seed to further propagate protein misfolding is the critical event. The process of seed formation is slow, thermodynamically unfavorable, and followed by a rapid elongation with incorporation of soluble monomeric protein into the aggregate. Likely, conformational changes to form the β-strands facilitate aggregation. In particular, hydrophobic groups usually buried inside the protein structure become exposed to the solvent and this makes proteins prone to intermolecular interactions [9]. Interestingly, evolutionary selection might have reduced segments of alternating hydrophilic and hydrophobic residues that favor β-sheet formation. Analysis of a large database of protein sequences derived from many different organisms revealed that alternating patterns occur less frequently than other patterns with the same polar/non-polar composition [12].

Remarkably, secondary processes, such as fragmentation events and secondary nucleation reactions, can as well be important in aggregation kinetics. Fragmentation events refer to a growing fibrillar aggregate breaking into smaller pieces, which can free oligomeric species. In secondary nucleation reactions the surfaces of growing fibrils

catalyze the formation of new clusters of monomers that act as nuclei, increasing the number of growth-competent aggregate species and hence accelerating the overall aggregation rate. Finally, it is also important to note, that variations on the common cross-β-sheet conformation might be present at detailed structural level due to differences in aminoacid sequence, chain lengths, as well as solution conditions [9].

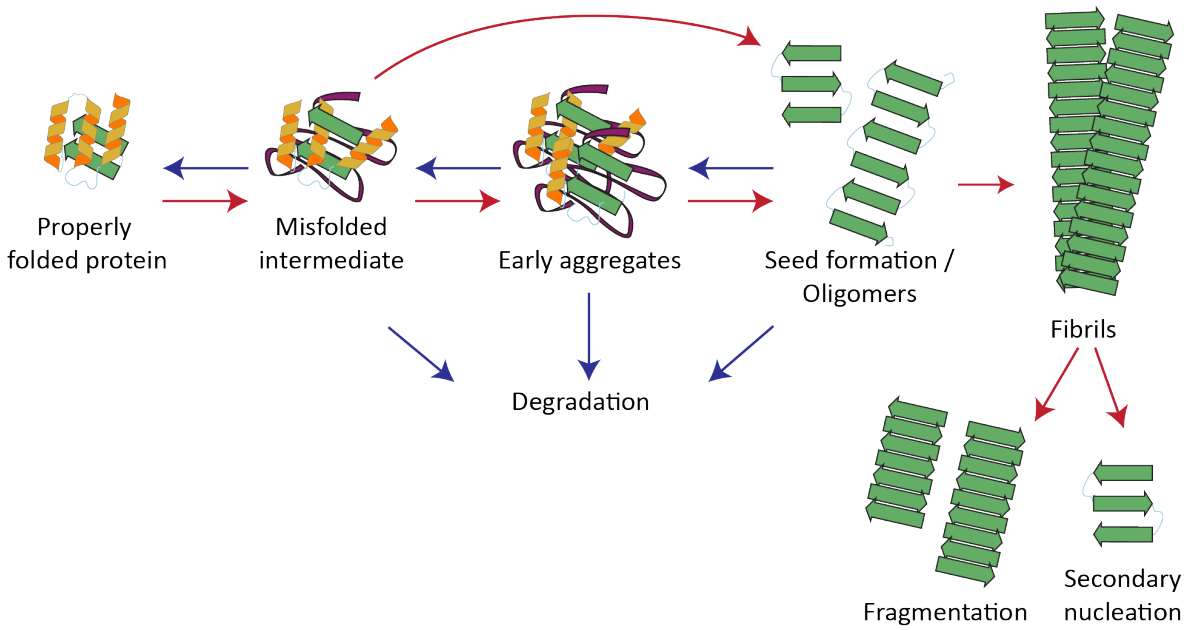

Figure 2.1: **Mechanism of amyloid fibril formation.** Monomeric proteins can misfold and aggregate in a thermodynamically unfavorable process to form a protein seed or nuclei (red arrows). Such seeds can be considered as the smallest structures that are able to initiate fibril elongation. During the misfolding process, the folding or degradation machineries of the cell can intervene to properly fold or degrade the misfolded protein species (blue arrows). Otherwise, fibrils grow rapidly through the addition of monomers to these seeds. Finally, secondary processes, such as fragmentation or secondary nucleation can occur, leading to further misfolding. Adapted from [7, 9, 13].

2.1.1 Key aggregating proteins and genetics in neurodegeneration

Within the different diseases, specific proteins form aggregates in particular locations. Extracellular deposits of amyloid-β protein (Aβ), so called amyloid plaques, and cytoplasmic neurofibrillary tangles (NFTs) of hyperphosphorylated tau protein are characteristic in AD. Cases of familial AD account for 1–5% of patients and

lead to inherited, early onset AD [3]. These cases are the result of autosomal, dominant mutations in three genes: the amyloid-β precursor protein gene (*APP*) [14], presenilin-1 (*PSEN1*), or presenilin-2 (*PSEN2*) [15, 16]. *PSEN1* and *PSEN2* encode for active subunits of the gamma secretase complex, an amyloid-β processing-pathway component [17, 18, 19]. Moreover, duplications of the *APP* locus also cause familial AD [20]. These first discoveries and the consequent advances in understanding the disease genetics, favored the postulation of the amyloid cascade hypothesis, which places the changes in Aβ metabolism as triggers of AD pathophysiology, leading to neurofibrillary tangles and neurodegeneration that cause memory loss [21]. Moreover, other heritable genetic risk factors contribute to an individual's susceptibility to late-onset AD, be it because they increase Aβ accumulation, as for apolipoprotein E (APOE) mutations [22, 23], or because they result in impaired Aβ clearance, as for mutations in TREM2 (a transmembrane receptor highly expressed in microglia and myeloid cells) [24]. Mutations in the *MAPT* gene, encoding for protein tau, usually result in FTD, a tauopathy causing dementia [25].

Intraneural aggregates of α-synuclein, termed Lewy bodies and Lewy neurites [26], are typical in neurons of the substantia nigra in PD patients. PD is the most common neurodegenerative movement disorder and its motor symptoms result from selective loss of dopaminergic neurons in the pars compacta of the substancia nigra in the midbrain, together with the loss of their axon terminals, which project to the dorsal striatum [4]. Approximately 5-10% of PD cases are caused by familial genetic mutations and the first gene to be linked to familial PD was *SNCA*, coding for α-synuclein protein (α-syn) [27]. Missense, as well as multiplication mutations (duplication or triplication of the loci) in *SNCA* result in genetic dominant forms of PD [28, 29]. Alternatively, the most prevalent genetic cause of familial PD are mutations in *LRRK2*, which lead to diverse pathologies including Lewy bodies and nigral degeneration [30, 31]. Moreover, autosomal recessive mutations in the lysosomal hydrolase glucocerebrosidase (GBA) lead to Gaucher's disease, which is characterized by neurological features that include parkinsonism. A feedback loop between α-synuclein and GBA has been suggested, since GBA loss in iPS neurons causes accumulation of α-synuclein [32]. Mutations in other genes including *Parkin* [33, 34], PTEN-induced putative kinase 1 *PINK1* [35], and *DJ-1* [36] are as well causes of autosomal recessive PD.

HD is a monogenic, fully penetrant disease, caused by a CAG trinucleotide repeat

expansion within exon 1 of the *HTT* gene on chromosome 4. People with more than 39 CAG repeats are certain to develop the disease, whereas 36 to 39 repeats are associated with reduced penetrance. A range between 27-35 repeats is considered intermediate because it may increase the likelihood of repeat instability, while below 27 is normal. CAG expansions result in an elongated polyglutamine (polyQ) tract at the N-terminal of the huntingtin protein (HTT) which leads to protein aggregation. Longer CAG repeats predict earlier onset, accounting for approximately 56% of the variability in age onset [37]. At the cellular level, patients suffer from massive striatal neuronal death, with up to 95% loss of GABAergic medium spiny neurons (MSNs), whereas large interneurons are selectively spared [38]. Furthermore, atrophy is also detected in the cortex, thalamus, sub-thalamic nucleus, white matter, and cerebellum, although less severe than in the striatum [39, 5]. In spite of the early discovery of the *HTT* gene [40], understanding of HD mechanisms is still evolving, due to its tremendously complex pathogenesis.

In ALS, motor neurons accumulate inclusions of aggregated proteins that vary depending on the ALS subtype. This disease is invariably fatal, with death typically occurring 3 to 5 years after diagnosis, and about 10% of cases are transmitted within families. Autopsies of people with ALS reveal the degeneration of motor neurons in the motor cortex of the brain, in the brainstem motor nuclei and in the anterior horns of the spinal cord [6]. In familial cases, protein aggregates are often composed of mutated superoxide dismutase 1 (SOD1), and mutations in the *SOD1* gene cause ALS [41]. Misfolded SOD1 forms ubiquitinated cytoplasmic inclusions that progressively accumulate as disease progresses [42]. Moreover, inclusions of mutated TDP-43 [43], FUS [44], or Optineurin [45] can be detected in approximately 5% of familial cases. Notably, TDP-43 and FUS are usually harbored in the nucleus, whilst in ALS they are accumulated in the cytoplasm [46, 44].

In 2011, the most common genetic cause of ALS and FTD was identified, a pathogenic hexanucleotide repeat in the non-coding region of the C9orf72 (C9) gene. The sequence GGGGCC (G_4C_2) was detected to be expanded to hundreds or thousands of repeats in affected individuals, while 2 to 23 repeats are present in healthy ones [47, 48]. Apart from a reduction in the expression levels of the C9orf72 gene and the accumulation of RNA foci containing the G_4C_2 repeats in the brains and spinal cord of people with C9 ALS-FTD, also dipeptide-repeat proteins (DPRs) accumulate

in neuronal cytoplasmic and intranuclear inclusions. DPR inclusions contain p62 and are distinct from TDP-43 inclusions, which are also present in these individuals [49]. DPR toxicity mechanisms have gained a lot of attention in recent years, particularly because DPRs are produced by repeat-associated non-AUG (RAN) translation [50, 51]. RAN is an unconventional type of translation firstly described in SCA8 [52], which occurs in absence of an AUG initiation codon. RAN translation in C9 ALS-FTD occurs in all reading frames and from both sense and antisense transcripts, resulting in five DRP proteins (GA, GR, PR, PA, and GP). Strikingly, sense and antisense RAN proteins derived from the CAG expansion in HTT have been reported to accumulate in Huntington brains [53].

2.1.2 Cytotoxicity in neurodegeneration: loss or gain of function?

The link between pathogenic mutations and aggregation provides strong genetic evidence that protein aggregation is a primary event in disease pathogenesis, rather than a secondary event. Nevertheless, the relationship between protein aggregation and cell death is currently not fully understood. Classically, three non-exclussive hypotheses have been proposed to give an explanation for how misfolding and aggregation associate with neuronal apoptosis [54]. Intuitively, one of them is the loss of normal activity of the aggregating protein, referred to as loss of function hypothesis. This hypothesis is backed-up by the fact that HTT knock-out (KO) mice are not viable and die early in development [55, 56]. However, heterozygous mice reach adulthood with a normal phenotype. As for proteins related to other diseases, SOD1 deficient mice develop normally and show no motor symptoms [57]. APP and α-synuclein KO mice are viable and show no signs of neurodegeneration, although α-synuclein loss results in functional deficits in the nigrostriatal dopamine system [58, 59]. Finally, a recent study has reported that conditional C9orf72 loss does not cause motor neuron degeneration or motor deficits [60]. Nonetheless, another study showed that loss of C9orf72 in mice leads to lysosomal accumulation and altered immune responses [61]. Overall, although loss of function of the aggregating protein might contribute to disease, evidence suggests that it is not the sole cause of neurodegeneration.

Alternatively, the brain inflammation hypothesis poses chronic inflammatory reactions triggered by protein aggregation as the leading cause of neuronal death and synaptic changes. Evidence for chronic inflammation reactions in patients include:

extensive astrogliosis and microgliosis, especially around protein aggregates, and accumulation of inflammatory proteins such as cytokines and chemokines [62]. Glia not only become reactive in response to degenerative cues, but can also participate in trying to combat them. For example, both microglia and astrocytes are thought to contribute to clearing Aβ [63, 64].

Maladaptive immune responses were initially thought to be caused by neurodegeneration. However, recent investigations suggest that inflammation might be involved as a driving force in neurodegenerative disease pathogenesis [65]. For example, astrogliosis has been detected in prodromal AD [66]. Moreover, in a coculture model composed of human adult primary sporadic ALS astrocytes and human embryonic stem-cell-derived motor neurons, ALS astrocytes, but not control astrocytes, triggered selective motor neuron death by necroptosis [67]. Whole-genome sequencing studies revealed that rare mutations in the microglia-enriched gene triggering receptor expressed on myeloid cells 2 (TREM2) significantly increased the risk of late onset AD [68, 69]. In a bioinformatics study, module group innate immunity/microglia related genes correlated best with clinical disease in sporadic AD [70]. In addition, progranulin, which is highly expressed in microglia, is a major cause of familial FTD in haploinsufficient patients [71]. As a final example, it was recently described that maladaptive microglia might damage neuronal circuits through synaptic pruning or cytokine signaling [72]. In summary, the involvement of glia in NDs is a matter of current intensive research and discussion, and defining the molecular basis of protective and detrimental aspects of glial reactivity may help to identify novel therapeutic strategies.

The third and most accepted hypothesis is the gain of function, by which misfolded proteins acquire neurotoxic functions. As mentioned above, plenty of genetic evidence suggest that protein misfolding, oligomerization, and aggregation are causative to disease pathogenesis, and this may be entirely unrelated to the normal function of the affected protein. Eearly *in vitro* studies recapitulated neuronal apoptosis induction by protein aggregates: murine cortical cultures went into apoptosis when treated with Aβ-42 [73], overexpression of mutant HTT in a neuroblastoma cell line resulted in enhanced apoptosis [74], and SH-SY5Y cells entered apoptotic cell death upon α-synuclein aggregate formation [75].

Additional support for this hypothesis has been provided by experiments in

transgenic animals in which incorporation of the human mutated gene encoding the misfolded protein can trigger neurodegeneration. For instance, the widely studied R6/2 mouse model expresses the mutated exon 1 of the human *HTT* gene, with over 100 CAG repeats, which leads to a fast progressing HD-like phenotype [76]. Mutated human tau expression in mice results in age-related NFTs, neuronal loss, and behavioral impairments [77]. Several AD mouse models, such as the APP/PS1 [78] and the 5xFAD [79], have been generated to express mutated forms of human APP, PS1 and PS2, leading to amyloid plaque formation, as well as to behavioral traits presented by AD patients. Importantly, not only mice, but also other animals such as the fruit fly *Drosophila melanogaster*, rats, and non-human primates have been used to show that protein misfolding and aggregation result in neuronal death [80]. Finally, aggregation of non-disease related proteins can also result in cytotoxicity in cell lines [81, 82], highlighting the possibility of common disease mechanisms among different diseases.

2.1.3 Toxic protein species

Not only the *how* in protein aggregation is a matter of research, but also the *what*. Nowadays, it has not yet been established, if either large insoluble aggregates, or smaller oligomeric species represent the main neurotoxic agents. Although it was initially thought that large protein deposits were the neurotoxic species in the brain, studies indicate that prefibrillar aggregates or soluble oligomers might be the most toxic species [83].

Aβ oligomers extracted from the cerebral cortex of AD patients caused memory deficits and disrupted synaptic plasticity in rats. In contrast, insoluble amyloid plaque cores from AD cortex did not impair long-term potentiation (LTP) unless they were first solubilized to release Aβ dimers [84]. In an AD transgenic mouse model which presented no extracellular plaques, Aβ oligomers accumulated in the neurons, leading to memory and synaptic dysfunction, and tau hyperphosphorilation [85]. Furthermore, by lentivirus injections into the rat brain, it was observed that most severe dopaminergic loss in the substantia nigra occured in animals with the α-syn variants that formed oligomers, whereas the rapidly forming fibrils variants of α-syn were less toxic [86]. Finally, biochemically-measured levels of soluble Aβ, including soluble oligomers, correlate better with the presence and degree of cognitive deficits in AD

than do plaque counts [87]. This evidence suggests that soluble forms might be better candidates for inducing neuronal and synaptic dysfunction than fibrillar aggregates. Indeed, it is this association with pathogenesis that favored research aiming at isolating and determining the structure of oligomeres, as well as their structural determinants of toxicity. However, the structural heterogeneity and transient nature of any given oligomer population, combined with the frequently multiple parallel pathways to oligomeric species formation, greatly complicate the task [9].

Two major structural determinants have been shown to explain the differential toxicity of amyloid oligomers and fibrils. The first is the exposure of hydrophobic groups on the oligomeric surface. In fact, oligomeric species of similar sizes and morphologies, but having very different toxicities, have been isolated and shown to differ in their solvent-exposed hydrophobicity [88, 89]. The second determinant is the size, oligomers are smaller than fibrils and can therefore diffuse better in membranes and tissues [90, 91]. Moreover, oligomers can also aberrantly interact with different molecular targets, leading to a variety of toxicity mechanisms. Therefore, it has been proposed that formation of big fibrillar aggregates could be a protective mechanism designed to reduce the pool of sites for aberrant interactions, as shown for HTT in a cell culture study of HD [92].

However, it is important to note that amyloid fibrils are far from innocuous material. They can as well form aberrant interactions with cellular components and deplete key members of the protein homeostasis network [13]. Perhaps most importantly, fibrils can act as a reservoir of protein oligomers that can be released, and act as potent catalysts for the generation of toxic oligomers through secondary nucleation [93]. Hence it is unlikely that there is a sole neurotoxic agent causing neurodegenerative diseases, but rather a variety of toxic misfolded protein species.

The importance of characterizing the different structural conformations of misfolded proteins lies not only in the cytotoxicity they can directly exert, but also in their propagation capacity. In recent years, it has been gradually accepted that misfolded protein aggregates can spread pathologically by a prion-like mechanism in various cellular and animal models of diverse diseases. Studies with Aβ [94], tau [95, 96], α-syn [97], SOD1 [98], and HTT [99, 100] have shown that inoculation with tissue homogenates rich in misfolded proteins from patients or transgenic mouse

models of NDs results in disease pathology induction in the recipient cells or animals. Furthermore, transmission of α-syn and tau disease pathology has been observed in inoculated nontransgenic mice [101, 102].

Remarkably, several studies have reported the existence of conformational variants, referred as conformational strains, for misfolded protein aggregates composed of Aβ [103], tau [104, 105], and α-syn [106, 107]. These findings may provide an explanation for the heterogeneity observed in AD and PD patients. Altogether, these studies indicate that promoting protein misfolding not only leads to increased protein aggregation, but might accelerate disease progression. In that regard, it however remains an open issue whether spreading of protein misfolding is equivalent to disease spreading [7]. Pathology-mapping studies in postmortem brain tissue suggest that disease proteins accumulate in regions of primary vulnerability and spread to regions of secondary vulnerability along anatomical connections [108, 109]. However, why specific proteins initially accumulate in one and not another set of cells, presenting selective neuronal vulnerability, remains an open question [110].

2.2 Molecular mechanisms of toxicity in neurodegeneration

The molecular underpinnings of neurodegenerative diseases are subject of extensive research and a number of studies have revealed the multifactorial etiology of neurodegeneration [111]. Interestingly, alterations of common neuronal pathways such as protein quality control and degradation mechanisms, mitochondrial homeostasis, and synaptic toxicity have been described. Mechanisms that will be highlighted here because they have been especially investigated during the development of this thesis include: aberrant protein interactions with misfolded aggregating proteins, nucleocytoplasmic transport (NCT) impairments, and defects in trophic signaling. Other research areas in neurodegeneration, such as non-cell-autonomous mechanisms and dysfunctional neuronal connectivity, will not be referred to as in detail.

2.2.1 Aberrant protein interactions: interactome studies

As mentioned above, protein misfolding and aggregation result in exposure of hydrophobic residues, rendering the misfolded protein prone to aberrant interactions.

To try to pin down which molecules and pathways are affected by these aberrant interactions, probably contributing to pathogenesis, interactome studies have been performed. Broadly, these studies can be divided according to their approach: focusing either on a single aggregating protein and identifying its interaction partners, or analyzing several aggregating proteins and their common and specific interactors.

Within the first group, HTT has been mostly studied. In a combination of yeast two-hybrid screening with affinity pull down followed by Mass Spectrometry (MS), several genetic modifiers of neurodegeneration were identified and validated in a Drosophila HD model. Interacting proteins confirmed as modifiers of the neurodegeneration phenotype represented a diverse array of biological functions, including synaptic transmission, cytoskeletal organization, and signal transduction [112]. An *in vivo* study using lysates from different brain regions of BACHD mice (a bacterial artificial chromosome (BAC)-mediated transgenic mouse model expressing full-length human mutant huntingtin with 97Q repeats [113]), reported a spatiotemporal analysis of HTT interacting proteins via affinity-purification mass spectrometry (AP-MS). The authors of this study identified that proteins involved in protein kinase A signalling and mitochondrial dysfunction are enriched in the HTT interactome [114]. Moreover, a recent study dissected the interactomes of oligomers and insoluble inclusions of mutant HTT in neuroblastoma cells. Interestingly, oligomers interacted with nuclear proteins and proteins associated with RNA and DNA binding/translation, intracellular transport and ribosome biogenesis, whereas the interactome of insoluble HTT was significantly enriched in chaperones and proteolysis-related proteins [115].

With regard to other aggregating proteins, the interactome of mutant tau P301L was analyzed by tandem mass spectrometry in neuroblastoma N2A cells, reporting an association of tau with the ribonucleoproteome [116]. Recently, another group identified the tau interactor Otub1, which functions as a tau deubiquitinating enzyme *in vitro* and *in vivo*, and impairs tau degradation [117]. In terms of ALS-related proteins, quantitative mass spectrometry analysis to identify DPR poly-GA co-aggregating proteins revealed a significant enrichment of proteins of the Ubiquitin-proteasome system (UPS) and identified the transport factor Unc119 as a modifier of toxicity in neurons [118]. Finally, another study characterizing the neuronal interactomes of DPRs poly-GR and poly-PR, detected components of stress granules, nucleoli, and ribosomes. Furthermore, it highlighted the partial sequestration of ribosomes as a

pathogenic mechanism, by potential chronic impairment of protein synthesis [119].

Two other reports aimed at unraveling and comparing the interactomes of multiple proteins related to neurodegenerative diseases. In the first study, the authors performed analysis to identify binding partners of wild-type (wt) and ALS-associated mutant versions of Ataxin-2 (ATXN2), C9orf72, Fus, Optineurin (OPTN), TDP-43 and Ubiquilin-2 (UBQLN2) in N2A cells [120]. Surprisingly, interactomes of WT and mutant ALS proteins were very similar, except for OPTN and UBQLN2. Shared binding partners of ATXN2, FUS and TDP-43 had roles in RNA metabolism; OPTN- and UBQLN2-interacting proteins were related to protein degradation and protein transport, and C9orf72 interactors had mitochondria-associated functions [120]. In the second study, the interactomes of APP, PSEN1, PD related Parkin (PARK2), HTT, and ATXN1 were described [121]. In this case, these proteins were overexpressed in HEK293T cells and lysates measured by quantitative AP-MS. Strikingly, some shared interaction partners were detected, although most protein-protein interactions were unique for a single disease [121]. In conclusion, interactomic analysis represent a powerful tool to unravel dysfunctional cellular mechanisms in neurodegeneration.

Furthermore, total proteome studies have been very useful in neurodegeneration research. For example, analysis of the insoluble fraction of human brain proteomes of non-demented individuals, Mild cognitive impairment (MCI) cases, and symptomatic AD cases, showed an upregulation of U1 small nuclear ribonucleoproteins [122]. This result was confirmed by an independent study [123]. Moreover, an elegant research combined transcriptomic and proteomic analysis in several mouse models of HD at different ages. This study linked mutant HTT CAG repeat length and age to the degree of impairment in the expression of identity genes for striatal medium spiny neurons, the dysregulation of cyclic AMP signaling, and to cell death [124]. A complementary and labor-intensive report, characterized the soluble and insoluble proteome of the R6/2 mouse model of HD at several ages and brain regions, identifying particular loss of function protein candidates with potential therapeutic interest [125]. Finally, another group reported the association between changes in solubility of hundreds of proteins in the central nervous system (CNS), with pathological accumulations of misfolded tau, α-synuclein and mutant SOD1 in CNS of transgenic mice. Remarkably, a subset of the proteins that display a shift towards insolubility were common between these different models, suggesting that a specific subset of the proteome is vulnerable to

proteostatic disruption [126]. In summary, besides interactomic studies, analysis of the total proteome has proven crucial to gain insight into protein misfolding pathogenesis.

2.2.2 Nucleocytoplasmic transport impairment

A notable commonality among several aggregated proteins is that they alter nucleocytoplasmic transport, which can have toxic consequences. NCT refers to the import of molecules from the cytoplasm to the nucleus and export from the nucleus to the cytoplasm. NCT is regulated by nuclear pore complexes (NPC), large protein complexes embedded in the nuclear membrane which allow communication between the nucleoplasm and the cytoplasm. Each NPC is composed of multiple copies of 30 different and evolutionary conserved proteins termed nucleoporins (Nups). Interestingly, the central channel of nuclear pores is formed by Nups containing low complexity phenylalanine–glycine (FG) domains that are thought to form hydrogel-like structures to create a selective permeable sieve. Indeed, small molecules can passively diffuse through the NPC, while molecules exceeding around 40 nm are actively transported, requiring energy. Active protein transport through the NPC is regulated via nuclear transport receptors, known as importins and exportins [127].

Moreover, active transport is dependent on Ran, a nuclear GTP-binding protein, which regulates the ability of importins and exportins to transport their cargo across the nuclear membrane depending on the bound nucleotide state. That is, during export, exportins in the nucleus bind to both cargo and Ran-GTP and then pass through the NPC. In the cytoplasm, cargo is released when Ran GTPase activating protein 1 (RanGAP1), which is located on the cytoplasmic side of the NPC, catalizes the hydrolysis of Ran-GTP to Ran-GDP. Ran-GDP recycles back into the nucleus, where its guanine nucleotide exchange factor (GEF) RCC1 exchanges the GDP for GTP to continue the cycle. The gradient of Ran-GTP in the nucleus and Ran-GDP in the cytoplasm provides directionality to nucleocytoplasmic transport. Therefore, alterations in the ratio of nuclear Ran or RanGAP1 can modify the rate and direction of active transport [128].

The first evidence of a mechanistic link between nucleocytoplasmic transport and neurodegeneration came from studies from two independent laboratories focusing on C9orf72-linked ALS/FTD [129, 130]. Both groups used transgenic fly lines expressing G_4C_2 repeats, leading to RNA foci and DPR expression. By measuring the degree of

eye degeneration, these studies identified members of the NPC and nucleocytoplasmic machinery as modifiers of toxicity. Moreover, they validated their results using induced pluripotent stem-cell-derived neurons (iPSN) from patients with C9orf72-related disease. While in one of these studies they identified RNA export dysfunctions [129], in the other they focused on protein transport and detected RanGap1 and Ran mislocalization, together with defects in transport of a fluorescent reporter [130]. Most importantly, both studies presented the common finding that toxicity of RNA transcripts or DPRs of the hexanucleotide expansion, can be rescued by altering expression of specific NCT-related cellular proteins. Notably, two further screens in *Drosophila* and in *Saccharomyces cerevisiae* indicated a role of NCT in C9orf72 expansion toxicity [131, 132]. Lastly, it was reported that the poly-dipeptide PR leads to toxicity by clogging the nuclear pores [133].

Perturbations in NCT have been observed in HD as well. PolyQ expanded HTT protein aggregates lead to mislocalization of Nup62, Nup88, and RanGAP1; decrease in nuclear Ran protein, and change the localization of reporter proteins between the nucleus and cytosol [134]. Moreover, an independent HD study detected mislocalization of RanGap1 and Lamin B1 (a structural component of the nuclear lamina), impairment of mRNA export, and mislocalization of the mRNA export factor Gle1 [135]. It is important to mention that the findings from these two studies were performed using a wide variety of systems, such as primary neuronal cells, iPSNs, mouse models of HD, and postmortem patient material.

Finally, the most recent studies connecting NCT dysfunction to protein aggregation put TDP-43 and tau aggregates in the picture. Regarding TDP-43, analysis of the interactome of detergent-insoluble TDP-43 aggregates revealed an enrichment of components of the NPC and the NCT machinery. Moreover, nuclear pore pathology was validated in several cell types, as well as in ALS patient's material [137]. As for tau, it was shown that Nups with FG domains mislocalize from the nuclear membrane and associate with cytoplasmic tau aggregates. Moreover, nuclei isolated from AD brains were more permeable to large fluorescently tagged dextrans, demonstrating alterations in the NPC diffusion barrier or the nuclear membrane. In addition, AD patient brains presented lower nuclear to cytoplasmic ratio of Ran-GTP [138].

In summary, a potential unifying mechanism in NDs is that protein aggregates

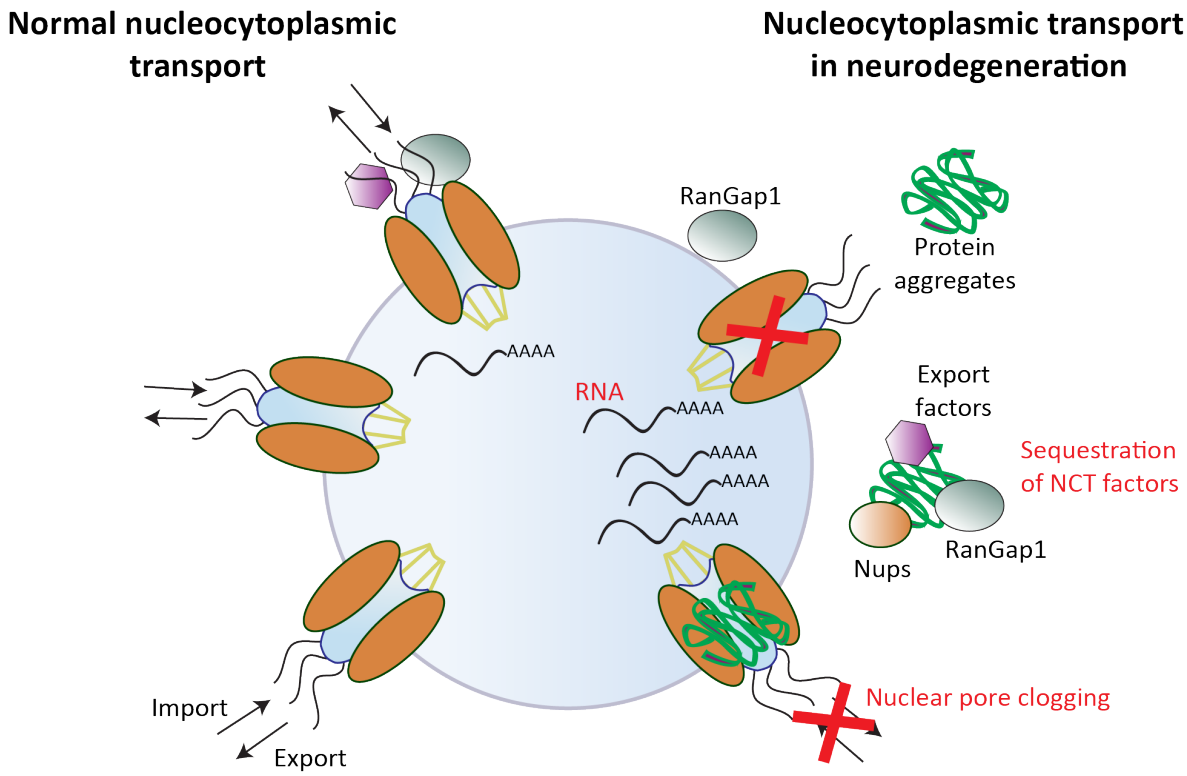

Figure 2.2: **Nucleocytoplasmic transport impairment in NDs.** Misfolded protein aggregates have been shown to lead to mislocalization of several nucleocytoplasmic components, such as export factors, Nups and RanGap1. Moreover, obstruction of the nuclear pores by the aggregates, as well as deficient export of mRNA have been detected. Modified from [136].

or oligomers may sequester Nups, or other components of the NCT machinery, in a non-functional manner (Fig.2.2). Since Nups can be very long-lived proteins and individual subcomplexes are exchanged slowly over time, this can be especially detrimental to post-mitotic cells such as neurons [128]. Intriguingly, it is yet an open question whether common NCT pathways are disrupted by different protein aggregates, and if therapeutic intervention to restore NCT, could reduce disease progression across various NDs.

2.2.3 Trophic signaling dysregulation

Another commonality among several neurodegenerative diseases is the dysregulation of neurotrophic factors and their receptors. The Neurotrophin (NTF) family of proteins forms a class of functionally and structurally related proteins that regulate

growth, differentiation and survival of central and peripheral neurons. The mammalian NTF family comprises nerve growth factor (NGF), Brain-derived neurotrophic factor (BDNF), neurotrophin 3 (NT-3) and neurotrophin 4/5 (NT-4/5). NTFs are initially synthetized as pre-proproteins, cleavage of the signal peptide converts them into pro-NTF, and further processing into mature NTF which are secreted from the cell. All of these proteins act through two distinct receptor types: Trk receptor tyrosine kinase family and neurotrophin receptor p75. In fact, different neurotrophins show binding specificity for particular Trk receptors: NGF binds preferentially to tropomyosin receptor kinase A (TrkA), BDNF and NT4 to TrkB, and neurotrophin 3 (NT3) to TrkC. The p75 receptor can bind to each neurotrophin as well as to the pro-NTFs, recruits signaling adaptors and modulates Trk signaling [139].

Neurotrophin binding induces dimerization and autophosphorylation of Trk receptors at multiple tyrosine residues, leading to the recruitment of different intracellular signalling components and the activation of downstream pathways. Trk signaling occurs through three principal tyrosine kinase-mediated pathways: the MAPK–ERK pathway, the PI3K–AKT pathway and the phospholipase Cγ1 (PLCγ1)–PKC pathway. The effects elicited through these signaling pathways predominantly promote cell survival and differentiation. In contrast, ligand binding to p75 is generally thought to induce death signals. For example, concomitant binding of pro-NGF to receptor sortilin and p75, selectively promotes cell death [140]. However, binding of mature NTFs to p75 can both promote cell death or increase cell survival, since its signaling pathways are complex and the endpoint depends on several factors [139, 141, 142].

Dysregulation of NTFs has been reported in several neurodegenerative diseases. In Alzheimer's disease, increased levels of pro-NGF were detected throughout the human brain, while decreased levels were detected only in the basal forebrain [143, 144, 145]. Moreover, a loss of the NGF receptor TrkA, but not of p75, was identified in the basal forebrain and cortex of AD brains [146]. Importantly, in absence of NGF signaling, cholinergic neurons (which are affected in AD) show shrinkage, reduction in fiber density and downregulation of transmitter-associated enzymes (Choline acetyltransferase (Chat) and Acetylcholinesterase (AChE)), resulting in a decrease of cholinergic transmission [147]. Apart from the NGF and TrkA downregulation observed in AD, binding of Aβ to p75 lead to apoptosis in cultured cells [148, 149]. Furthermore, BDNF and TrkB expression are also downregulated in cortex and hip-

pocampus in AD [150, 151], even at pre-clinical stages [152]. Accordingly, enthorinal administration of BDNF in rodent and primate models of AD was neuroprotective [153].

Moreover, a decrease in NGF, BDNF [154, 155], and Glial cell-derived neurotrophic factor (GDNF) [156] has been shown in the substantia nigra of PD patients. However, infusion of GDNF in PD patients brains did not ameliorate clinical symptoms in clinical trials [157, 158].

BDNF and TrkB mRNA and/or protein levels are reduced in cortex, striatum and hippocampus of HD patients as well as in animals models [159, 160, 161]. NT-3 mRNA levels are as well greatly reduced in HD patients [159]. Beyond these reductions, BDNF-TrkB signaling is disrupted in HD: mutant HTT impaired axonal transport of BDNF [162, 163] and retrograde transport of TrkB receptors in striatal dendrites [164]. Remarkably, TrkB receptors failed to properly engage postsynaptic signaling mechanisms in HD mouse models and this dysfunction could be corrected by inhibition of p75 or its downstream target PTEN [165].

Imbalances in neurotrophin signaling in neurodegeneration have been presented as an attractive therapeutic target. However, the use of NTFs themselfs as therapy has mostly failed, among other reasons, due to their short half-lives, inability to penetrate tissue barriers, and activation of multiple receptors (where p75 activity can counteract the benefit of Trk activity) [166]. Therefore, current strategies are focusing on the generation of small molecules that target specific neurotrophin receptors [142].

2.3 Animal models of neurodegenerative diseases

Animal models of NDs have been briefly mentioned in section 1.1.2 and will be further introduced here with a focus on mouse models. Generation of animal models of NDs has been based on discovered mutated genes and genetic risk variants of disease. These genetic guideposts, along with the identification of hallmark aggregating proteins, have provided valuable insight into the pathophysiology and mechanisms of neurodegenerative diseases. However, most individuals suffer from so called sporadic forms of these disorders (*i.e.* have no known genetic cause) and the genetic form of the disease does not always perfectly phenocopy the sporadic form. Already this

discrepancy between models and affected humans, indicates that current models might not be as perfect as desired. Therefore, conclusions taken out of animal studies should not be overestimated [167, 168, 80].

AD is characterized by three hallmark pathologies: senile plaques (Aβ plaques), neurofibrillary tangles, and hippocampal and cortical neurodegeneration [169]. Nevertheless, current mouse models do not reproduce the whole complexity of the pathology. On one hand, there are mice that model amyloid deposition with Aβ aggregate accumulation in senile plaques. These mice express AD-linked human mutations in *APP*, *PSEN1*, and *PSEN2*. *APP* mutants either increase total Aβ or increase the relative production of the more aggregation-prone Aβ42, this second case happening more commonly. Moreover, co-expression of *PSEN1/2* mutants with an *APP* transgene drastically accelerates amyloid deposition. Interestingly, these mice present abnormal dystrophic neurites, astrocytosis, microgliosis, and behavioral deficits such as memory impairment [170, 171].

Alternatively, mice in which Aβ deposition is driven in absence of APP overexpression, including knock-in models, show plaques and gliosis, but subtle behavioral abnormalities [172, 173]. Unfortunately, the biggest inconveniences of APP models are the lack of tau pathology, robust neurodegeneration, and neurotransmitter abnormalities. Differences in neuroinflammatory responses and differences in brain aging between mice and humans that might influence disease progression might explain why APP transgenic mice do not fully recapitulate AD pathology. In accordance, genetic ablation of endogenous tau in mice expressing human tau enhances tangle formation [174], suggesting that endogenous mouse tau may interfere with the ability of human tau to form tangles. Furthermore, another study investigated whether Aβ species produced in mice are enough to drive full AD pathology in non-genetically manipulated human neurons. To this aim, they generated a chimeric model by xenografting human cortical precursor cells into the brains of newborn mice, which integrated into the mouse host tissue. This chimeric model presented numerous Aβ plaques and Aβ-associated neuroinflammation in the human transplant and, importantly, the transplanted neurons showed remarkable signs of neurodegeneration that were not detected in the mouse host brain or in transplanted PSC derived mouse neurons. Thus, human neurons can respond to Aβ pathology differently than their murine counterparts *in vivo* [175].

On the other hand, genetically based models of tau pathology, unlike Aβ models, exhibit overt neurodegeneration. However, these models are largely based on transgenic overexpression of mutations that cause FTD-MAPT and it is not yet known how relevant they are for AD tauopathy. Possibly, the hTau BAC mouse, which exhibits more moderate tau pathology and neurodegeneration may model AD tauopathy better [176]. Moreover, tau pathology could be enhanced by expressing both mutant human tau and APP in multiple transgenic mice [177, 178], or by injection of aggregated Aβ into a tau transgenic model [179]. Nevertheless, the mechanisms of tau-driven neurodegeneration remain elusive and, it is uncertain, if synergistic interactions between the two pathologies in mice are relevant to human disease [80].

PD is characterized by progressive loss of dopamine (DA) neurons in the substantia nigra pars compacta and the presence of misfolded α-synuclein in Lewy bodies and neurites [4]. Drug-induced mouse models of PD, such as the 6-hydroxydopamine (6-OHDA) and 1-methyl-4-phenyl-1,2,3,6-tetrahydropyridine (MPTP) models, have been widely used and lead to the key sysmptomatic treatment of PD, namely L-dopa in combination with carbidopa. Unfortunately, trials to identify neuroprotective therapies using these models have been futile [180]. However, the PD drug-induced models are acute, rapid and do not model the molecular pathology of PD. They kill DA neurons by mechanisms that may not be reflective of PD and produce a DA-loss phenotype without any progressing evolution of pathology [167].

Alternatively, genetically-based mouse models of PD have been generated. Most of them constitutively overexpress human WT α-syn (modelling *SNCA* multiplication), or human mutant A53T or A30P α-syn (modelling missense *SNCA* mutations) under a variety of different promoters. Despite accumulation of α-syn aggregates in the brain, as well as motor and non-motor deficits, most models' disadvantage is the lack of DA neurons loss [167]. Surprisingly, only one BAC model overexpressing human WT α-syn reported DA neuron loss [181]. Moreover, conditional overexpression of mutant α-syn also lead to DA neuron degeneration [182].

To study other genetic forms of PD, several mouse models have been generated, including transgenic models based on overexpression of LRRK2 mutants, and deletion models of Parkin, PINK1 and DJ-1. Similarly as in α-syn models, these mice

present only partial PD phenotypes and provide conflicting results in terms of DA neurodegeneration [183]. In conclusion, in line with the AD models situation, PD mouse models do not faithfully reproduce the predominantly sporadic human disease and there is room for improved models.

Regarding ALS, patients exhibit loss of upper and lower motor neurons, leading to fatal paralysis with respiratory failure. FTD is characterized by progressive degeneration of the frontal and temporal lobes leading to dementia. Despite different clinical manifestation, motor neuron degeneration and cognitive deficits can be concomitant in patients [6]. Indeed, ubiquitinated TDP-43 inclusions were discovered to be a common pathological hallmark in both ALS and FTD sporadic cases [46]. To date, the mostly studied ALS models have been transgenic mice overespressing various SOD1 mutations [184]. SOD1 mice develope cortical and spinal motor neurons loss, denervation of the muscular junctions, aggregates of misfolded SOD1, and progressive paralysis with reduced lifespan. Importantly, SOD1 mice have greatly contributed to the identification of the non-cell autonomous component of ALS. It is been demonstrated that glial cells surrounding the motor neurons contribute to their selective destruction [185, 186, 187]. However, SOD1 models do not develop TDP-43 pathology. Therefore, they represent good models for the minority of SOD1 genetic cases of ALS, while mostly occurring cases, sporadic and with TDP-43 pathology, are not represented.

To investigate sporadic disease, a wide variety of TDP-43 mouse models have been developed [188, 184]. These animals replicate partial disease phenotypes, not the full ALS human phenotype. Moreover, important caveats for TDP-43 models are the differences in RNAs bound by TDP-43 among different species, as well as distinct RNA processing alterations elicited by TDP-43 between mice and humans. To complicate things further, cell functionality might be highly dependent on well-balanced levels of TDP-43, with modest changes in expression being detrimental for cells [189].

Currently, ALS and FTD research focuses on understanding disease mechanisms linked to C9orf72. While two BAC models of hexanucleotide expanded C9orf72 developed RNA foci and RAN proteins, they did not show the neurodegenerative or behavioral features of ALS/FTD [190, 191]. In contrast, a recent mouse model presented decreased survival, paralysis, muscle denervation, motor neuron loss, anxiety-like behavior, and cortical and hippocampal neurodegeneration, RNA foci, and RAN

proteins [192]. These mice may be especially promising as a preclinical model in light of recent advances in therapy development based on antisense oligonucleotides (ASOs) [193]. In fact, ASO treatment against spinal muscular atrophy, a rare and often fatal genetic disease affecting muscle strength and movement, has recently been approved by the U.S. Food and Drug Administration [194]. Interestingly, administration of ASOs in preclinical models of C9orf72 ALS/FTD has already shown promising results [195] and further ASO testing in other models might be crucial for therapy development.

Finally, mouse models of HD aim to model progressive deterioration of cognitive and motor functions, and the selective loss of GABAergic MSNs, as well as glutamatergic cortical neurons that project to the striatum [39]. The R6/2 [76] and N-171-82Q [196] mouse models develop acute HD-like phenotypes, since they express a truncated N-terminal form of human mutant HTT. However, several compounds that proved effective in R6/2 mice, did not have beneficial effects on patients [197, 198]. These results rose the concerns that truncated models could have the drawbacks of loosing the natural genomic and protein context of the polyglutamine expansion, leading to altered regulation, post-translational modifications and protein interactions [199]. To overcome these concerns, full-length models, such as the YAC128 [200], the BACHD [113] and the zQ175 [201, 202] were generated. Although the predictive value in therapy development of the zQ175 model is still being investigated, the results obtained with the truncated models suggest that confirmation in more than one model will be necessary for robust conclusions in preclinical trials.

Overall, there is currently still room for improvement in the mouse models for neurodegenerative diseases. Thus far, mice have had poor predictive value in the development of symptomatic therapies and especially in the development of disease-modifying therapies. However, even if other animal species, such as non-human primates, would be better suited to model the aging component in NDs, the costs and logistics of performing large-scale therapeutic trials in non-human primates are tremendous. Moreover, mice models can be of great advantage to study basic research questions regarding the development of the diseases, as to which misfolded protein species are toxic and when, and why specific cell populations are particularly vulnerable, potentially leading to novel therapeutic targets.

2.4 Artificial β-sheet proteins as a model for amyloid-like aggregation in neurodegeneration

The generation of a combinatorial library of *de novo* protein sequences that have been rationally designed to form β-sheet secondary structures, has provided the neurodegeneration field with an alternative tool to study mechanisms of amyloid-like toxicity [203]. The sequence of these synthetic proteins consists of six β-strands (seven residues each) containing a pattern of alternating polar and nonpolar aminoacids, respectively linked by four-residue linkers (Fig.2.3 A). Moreover, transmission electron microscopy revealed that these proteins self-assemble into fibrils (Fig.2.3 B) and can bind the amyloid dye Congo red, similarly to natural amyloid proteins in neurodegenerative diseases [203].

Three of the *de novo* sequences, numbers 4, 17, and 23 in the library, have been further employed in other studies, and referred to as β4, β17, and β23. A study in 2011, overexpressed myc-tagged versions of the three artificial β-sheet proteins in Hek293T cells. First, they observed that β4, β17, and β23 proteins formed aggregates that could be labeled by the amyloid dye NIAD-4. Second, they detected time-dependent β-sheet-induced cell death, while overexpression of a control α-helix forming protein did not affect cell survival. Moreover, β-sheet proteins impaired cytoplasmic stress response. Finally, proteins involved in key cellular pathways were identified as interactors of the β-sheet proteins by quantitative proteomics [81]. Interestingly, this study was followed by a report in 2016, in which it was described that cytosolic, but not nuclear aggregation of artificial β-sheet proteins, impairs nucleocytoplasmic transport of mRNA and proteins [204].

Artificial β-sheet proteins do not possess a biological function and therefore allow us to study cytotoxicity mechanisms related to protein aggregation in a gain of function situation. Since the function of endogenous proteins is not compromised, as might occur with HTT in HD, or α-Synuclein in PD, research can be targeted at characterizing the cellular consequences of protein aggregation. Therefore, during this thesis, we aimed at exploiting the potential of artificial β-sheet proteins further to study neurodegeneration in a context more related to disease, such as primary neurons and a mouse model.

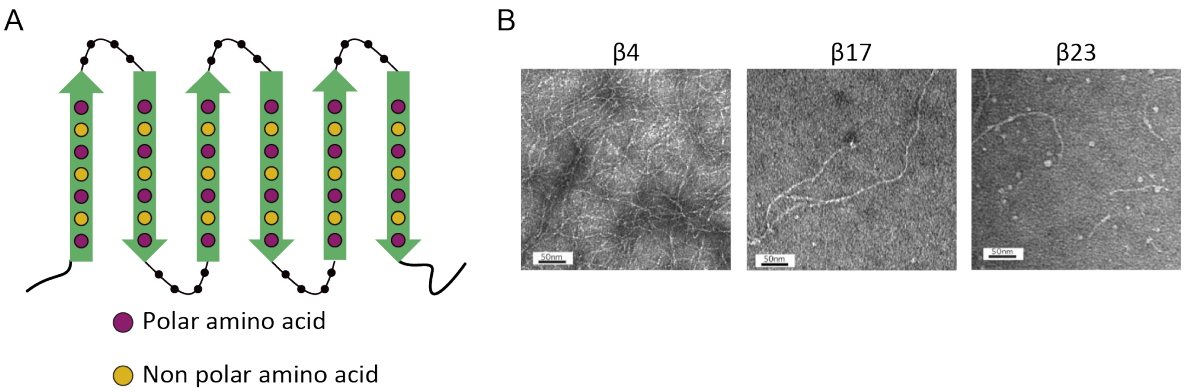

Figure 2.3: **Artificial amyloid-like aggregating β-sheet proteins.** (A) The sequence of artificial β-sheet proteins is composed of alternating polar and nonpolar aminoacids, forming six β-strands. (B) Transmission electron microscope images depicting that the artificial proteins self-assemble into amyloid-like fibrils. Adapted from [203].

2.5 Aims of the thesis

In order to uncover common mechanisms of toxicity in neurodegenerative diseases, here I have utilized synthetic β-sheet proteins with three main aims:

• Analyzing the effects of aggregation of synthetic β-sheet proteins in neurons cultured *in vitro*.

• Identifying β-sheet protein interactors and testing their potential role in common mechanisms of cell toxicity due to protein misfolding.

• Studying the synthetic β-sheet protein's aggregation effects *in vivo* by: generating and characterizing a reversible transgenic β23 mouse model of neurodegeneration.

3 Materials and Methods

3.1 Materials

3.1.1 Chemicals, reagents and kits

All chemicals, reagents, and kits were purchased from Merck, Sigma-Aldrich, Roth, Roche, Thermo-Scientific,Bio-rad, Takara Bio, Qiagen, and Machery-Nagel.

3.1.2 Buffers

PBS
137 mM NaCl
2.7 mM KCl
4.3 mM Na_2HPO_4*$7H_2O$
1.4 mM KH_2PO_4

TE
10 mM Tris Base pH=8
1 mM EDTA

50x TAE
2 M Tris acetate
50 mM EDTA

Western Blot buffers

Cell lysis buffer
50 mM Tris-HCl pH=7.4
150 mM NaCl
2 mM EDTA
1% Triton X-100

+ cOmplete EDTA-free protease inhibitor cocktail tablet
+ PhosSTOP phosphatase inhibitor cocktail tablet

10X Tranfer buffer
30.3 g Tris Base
144 g Glycine
Fill to 1 L with MilliQ dH_2O

To prepare 1 L of the working solution 1x Transfer buffer, mix the following reagents: 100 ml 10x transfer buffer + 200 ml Methanol + 700 ml MilliQ dH_2O.

20X TBS-T
400 ml of 1 M Tris Base pH=8
600 ml of 5 M NaCl
20 ml Tween 20

To prepare 1 L of the working solution 1x TBS-T, take 50 ml of 20X TBS-T and add 950 ml of MilliQ dH_2O.

6X Sample loading buffer
0.125 M Tris-HCl pH=6.8
20% Glycerol
4% SDS
2% β-mercaptoethanol
0.02% Bromphenolblue

4% stacking gel (mix for one gel)
3.05 ml dH_2O
1.3 ml 0.5 M Tris pH=6.8, 0.4% SDS
0.65 ml 30% Acrylamyde/Bis solution
50 μl APS 10%
5 μl TEMED

12% resolving gel (mix for one gel)
3.5 ml dH_2O
2.6 ml 1.5 M Tris pH=8.8, 0.4% SDS
4 ml 30% Acrylamyde/Bis solution
50 μl APS 10%
5 μl TEMED

5X Running buffer
154.5 g Tris base
721 g Glycine
50 g SDS
MilliQ dH_2O up to 10 L

Hash stripping buffer
20 mL SDS 10%
12.5 ml 0.5 M Tris-HCl, pH=6.8
67.5 ml dH_2O
0.8 ml β-mercaptoethanol

Cell culture solutions and buffers

Primary neuronal culture

Borate buffer
3.1 g Boric acid
4.75 g Borax
Add to 1 L dH_2O
Adjust to pH=8.5
Filter sterile with a 0.22 μm Bottle-top vacuum filter system (Corning)

Dissection medium
HBSS (Thermo Fisher)
+ 1% Pen/Strep (Invitrogen)
+ 10 mM Hepes (Biomol)
+ 10 mM $MgSO_4$

Culture medium
Neurobasal (Thermo Scientific)
+ 1% Pen/Strep (Invitrogen)
+ 1% L-Glutamine (Thermo Fisher)
+ 2% B27 supplement 50X (Thermo Fisher)

Hek293T culture for lentiviral production

Culture medium
DMEM Glutamax (+ 4.5 g/L D-Glucose, - Pyruvate)
+ 10% FBS (Sigma)
+ 1% G418 (Gibco)
+ 1% NEAA (Thermo Fisher)
+ 1% Hepes (Biomol)

TBS-5
50 mM Tris-HCl pH=7.8
130 mM NaCl
10 mM KCl
5 mM $MgCl_2$

Filter sterile with a 0.22 μm Bottle-top vacuum filter system

Culture medium for CRISPR/Cas9 lentivirus production
2 ml DMEM
+ 10% FBS (Sigma)
+ 1% L-Glutamine
+ 10,000 units of Penicillin
+ 10 mg/ml of Streptomycin

Interactome analysis buffers

Lysis buffer for Immunoprecipitation (IP)
0.25% NP40
5% Glycerol
50 mM Tris HCl
150 mM NaCl
DNAseI (5 μl/ml)
RNAseI (0.5 μl/ml)
+ cOmplete EDTA-free protease inhibitor cocktail tablet (Roche)

Beat digestion buffer
8 M Urea
40 mM Hepes pH=8
Endoproteinase LysC
10 mM DTT

Trypsin digestion buffer
Trypsin
50 mM Ammonium bicarbonate
55 mM Chloroacetamid

MTT solubilizer

50 g SDS 10%
225 ml Dimethylformamide 45%

Adjust to pH=4.5 with acetic acid
Fill up to 500 ml with water

Immunostaining on brain sections buffers

Blocking buffer
0.2% BSA
5% Donkey serum

0.2% L-Lysine
0.2% Glycine
in PBS

Primary antibody solution
2% BSA
0.3% Triton 100-X
0.01% Sodium azide
in PBS

Secondary antibody solution
0.3% Triton 100-X
3% Donkey serum
0.01% Sodium azide
in PBS

Mowiol
6 g Glycerol
2.4 g Mowiol 4-88
stirr for 1 h
Add 6 ml dH_2O
Stirr for 2 h
12ml Tris-HCl 0.2 M pH=8.4
Heat up solution to 50°C in agitation until Mowiol 4-88 is completely dissolved.
Add antifading agent: 0.5% Propyl-galatete and stirr for 4 hs.
Centrifuge at 7500xg for 30 min to remove undissolved solids.
Aliquot and store at -20°C.

3.1.3 Plasmids and Crispr sgRNA

Plasmids				
ID	**Insert**	**Backbone**	**Resistance**	**Source**
ID1	mCherry	mCherry-N1	Kan	Clontech
ID2	mycβ23mCherry	mCherry-N1	Kan	Hartl lab
ID30	mycβ4mCherry	mCherry-N1	Kan	Hartl lab
	αS-829	pcDNA3.1	Amp	Hartl lab
	mycβ4	pcDNA3.1	Amp	Hartl lab
	mycβ23	pcDNA3.1	Amp	Hartl lab
ID21	mycβ23-frt1-IRES-frt-mCherry	pTRE3G	Amp	Cloned
ID22	mycβ23-frt2-IRES-frt-mCherry	pTRE3G	Amp	Cloned
ID25	none	pTRE3G	Amp	Clontech
ID53	Tet-On 3G (tTa)	pCMV-Tet3G	Amp	Clontech
ID58	myc-b23-mCherry	pTRE3G	Amp	Cloned
Lentiviral plasmids				
ID	**Insert**	**Backbone**	**Resistance**	**Source**
ID32	myc-mCherry	pENTR1A-164	Kan	Cloned
ID33	mycβ4-mCherry	pENTR1A-164	Kan	Cloned
ID34	mycβ17-mCherry	pENTR1A-164	Kan	Cloned
ID35	mycβ23-mCherry	pENTR1A-164	Kan	Cloned
ID66	none	pVsVg	Amp	D.Edbauer
ID67	none	pSPAX2	Amp	D.Edbauer
ID74	none	pFhSynW2	Amp	D.Edbauer
	none	pLenticrisprv2	Amp	D.Hornburg (Plasmid ♯52961)
	none	pMD2.G	Amp	D.Hornburg (Addgene Plasmid ♯12259)
ID68	mycmCherry	pFhSynW2	Amp	Cloned

ID74	mycβ4-mCherry	pFhSynW2	Amp	Cloned
ID75	mycβ17-mCherry	pFhSynW2	Amp	Cloned
ID76	mycβ23-mCherry	pFhSynW2	Amp	Cloned
ID97	Flag-Girdin-eGFP	pFhSynW2	Amp	Cloned
	Flag-GirdinFL	pFhSynW2	Amp	Cloned
ID98	Flag-eGFP	pFhSynW2	Amp	Cloned
ID99	myc-β23L63P-frt1-IRES-frt-mCherry	pFhSynW2	Amp	Cloned
ID100	myc-β23-frt1-IRES-frt-mCherry	pFhSynW2	Amp	Cloned

Table 3.1: Plasmids

Gene name	sgRNA 1	sgRNA 2	sgRNA 3
Aimp1	AGGTTTCTCTGCCGATTCTG	GGAGCAGAAGGGTGCAGAGG	GCTAAAGCAAGAGCTGATTC
Aldh1b1	GTCGGGCAGTCAGCATCCTG	GCAGGATGGATGCCTCAGAG	GAAACCCCGCCTCTTTGATG
Ap3m1	GTTAGACAATGGATTCCCAC	TGATCTCTCCCTCTCTTTCA	TGATCCCGTGACCAAGGTAC
Bag6	GCTGTCAGGCTCCTCCATAG	GCATCCCTTCCGAGAAACAG	GGGAAAGGTTATTCACCTGG
Ccdc88a	GTCATGAACTGCTCCAGAAG	GACTAACCTGGATGAGTATG	GTATGTGGCTTTAGTGGATG
Clcn3	CGGGACTGGCATCAGGTAAG	GCATCTGCCTCAGTGCATTG	GTATTTGCTCCATATGCCTG
Dnm2	GCGGACACCATGGGCAACCG	GTGACAATTCCTGATCCTCG	GGTCAAGTTCAACACTGAGG
Dyrk1a	GGTCACTGTACTGGTGTGAG	GCTGGATCACGGAAGGTTTG	GAAGACACCAACAGGGCCAG
Ehd3	TGAACATTGTGACAGCTGGG	AGTGATGCAGGGAGATGTGG	AGCAAAATCATACCCTGTGG
Hcfc1	AGTTCCGGTTAAGGATGCAG	TGGTTCATCCCAGCTGTGAG	TGGACATAGCTTCTCCCTTG
Lrrc7	GCCAATGAGCTTCCGTTTGG	AGCAGCGGCATGGCACCAGG	TGGAGGTTGGCAGACTTGAG
Ppp2r5d	GAAGAAGGATAAGGTGAGCG	AGCAGCTCAAGCAAGGATGG	CGTTCTTTCTTGACAATCTG
Sec61b	GGCGTTGGACCCGGCTGCAG	CGGGATCCACTGTTCGGCAG	GACTTACACTTTGAGCCCTG
Sncb	GGGCCTGTCCATGGCCAAGG	AGGAAGCAAGACCAGTGGAG	GAGCAGGCATCGCATCTGGG
Stau2	TGGGGTTTGCCATTTTATCG	GAAGGTAAGGTTACAAAGAG	AGGTAGTATAACTCCAACTG
Stmn2	GTGTAGATGTTGATGTTGCG	TGTTCCTTCCACAGACATGG	GTTTCCTCCCCAGTCTCAAG
Stmn3	GGTAGGGCTCGGGAGCCTAG	TGGTAGATGGTGTTCGGGTG	GGCCTCTGGCCAGAGCTTCG
Tpr	GCTTCTAGAAGTGGCCACAG	GGAGTACCCATGACATCCCG	GAGCGCTGCTGATGACTCAG
Usp14	CGGAGCTCACCAGAGTAGAG	TGGGCTTTGAACACCATTGG	GCAATTCCATCTGATAAAAG
BDNF control	GGATGTCGCCCTGGCTGAAG	AGATGACGTTGAAGCTTACG	GGATTCCGGCTTAAAGTTTG
Negative control	CTAAGGTTAAGTCGCCCTCG		

Table 3.2: Crispr sgRNA

3.1.4 Primary antibodies

Primary antibodies			
Antigen	**Host**	**Company**	**Reference**
mCherry	Goat	Sicgen (Origene)	AB0040-200
mCherry	Rabbit	Abcam	ab167453
myc 9E10	Mouse	Thermo Fisher	13-2500
myc	Rabbit	Cell signaling technology	2272
MAP2	Chicken	Novus	NB300-213
Cas9 (7A9-3A3)	Mouse	Cell signaling technology	14697
DDK (Flag)	Mouse	Origene	TA-50011-100
Akt	Rabbit	Cell signaling technology	9272
Phospho-Akt (Ser473)	Rabbit	Cell signaling technology	4060
Erk1/2	Rabbit	Cell signaling technology	9102
Phospho-Erk1/2	Rabbit	Cell signaling technology	4376
Tubulin	Mouse	Sigma	T9026
RanGap1	Mouse	Santa Cruz	sc-28322
Nup153	Mouse	Abcam	ab24700

Table 3.3: Primary antibodies

3.1.5 Secondary antibodies

Donkey serum and all secondary antibodies used for immunostainings were purchased from Jackson Immunoresearch Laboratories. Secondary antibodies were used at 1:250 or 1:300 dilution.

3.1.6 Mouse lines

Mouse lines		
Line name	**Official name**	**Comments**
β23-frt1	TRE3G:mycb23frt1-IRES-frt-mCherry	Unrecombined line. By crossing it to a tTa driver line, double transgenic mice express the artificial β-sheet protein β23 [203] with the point mutation L63P and the fluorescent protein mCherry as separately translated proteins.
β23-frt2	TRE3G:mycb23frt2-IRES-frt-mCherry	Second βb23 transgenic line. By crossing it to a tTa driver line, double transgenic mice express the artificial β23 protein [203] and the fluorescent protein mCherry as separately translated proteins. This line was generated but not used for experiments.
CamKIIa-tTA	B6;CBA-Tg(Camk2a-tTA)1Mmay/J	Tet-Off tTa driver line [205].
Flpe	Tg(ACTFLPe)9205Dym	Flippase line used to generate the recombined line. Originally purchased from Jax lab, reference MGI:2448985 [206].
β23-frt1-mCherry	TRE3G:mycb23frt1-mCherry	Recombined line. By crossing it to a tTa driver line, double transgenic mice express the artificial β-sheet protein β23 [203] with the point mutation L63P and the fluorescent protein mCherry as a fused proteins.

Table 3.4: Mouse lines

3.1.7 Genotyping primers

Primers			
ID	**Name**	**Sequence 5'→3'**	**PCR**
14	b23-1-For	TTTCCGTACCACTTCCTACCCTCGT	b23-1, Recom
15	b23-1-Rev	GCCTGCAAAGGGTCGCTACAGAC	b23-1
16	b23-2-For	GGGCCTCGGTACACATGCTTTAC	b23-2
17	b23-2-Rev	CAAGTAGTCGGGGATGTCGGC	b23-2, Recom
23	CamK-wt-For	CAAATGTTGCTTGTCTGGTG	Camk
24	CamK-wt-Rev	GTCAGTCGAGTGCACAGTTT	Camk
25	CamK-tg-For	CGCTGTGGGGCATTTTACTTTAG	Camk
26	CamK-tg-Rev	CATGTCCAGATCGAAATCGTC	Camk
55	NEFH-wt-For	CTAGGCCACAGAATTGAAAGATCT	Camk
56	NEFH-wt-Rev	GTAGGTGGAAATTCTAGCATCATCC	Camk
57	NEFH-tg-For	CTCGCGCACCTGCTGAAT	Camk
58	NEFH-tg-Rev	CAGTACAGGGTAGGCTGCTC	Camk
35	Flp-For	CTAATGTTGTGGGAAATTGGAGC	Flpe
36	Flp-Rev	CTCGAGGATAACTTGTTTATTGC	Flpe

Table 3.5: Genotyping primers

3.2 Methods

3.2.1 Agarose gel electrophoresis

Agarose gels were prepared by dissolving agarose in 1X TAE buffer, ususally to 1% concentration. If DNA fragments to separate were over 10 Kb, 2% gels were prepared. The mix was boiled in a microwave for 3-5 min until agarose was fully dissolved. After cooling down, Ethidium bromide (Roth) was added to a concentration of 0.5 μg/μl. Then, the solution was poured into a plastic tray for polymerization at RT. DNA was separated on the gel based on size by electrophoresis, at a voltage of 100 – 180 V. DNA was visualised by UV light using a Gel Doc XR+ machine (Biorad).

3.2.2 Plasmid DNA generation

All enzymes were purchased from New England Biolabs, except for Pfu polymerase, which was purchased from Promega. All primers and sequencing reactions were purchased from Eurofins genomics.

Cloning

DNA plasmids were cloned either via classic restriction and ligation, or using the Infusion cloning kit (Takara bio). Initially, the backbone vector was restricted overnight with two different restriction enzymes. Then, loading buffer was added to the reaction mix. To only isolate the restricted vector and discard the undesired DNA fragments, the mix was run on a 1-2% agarose gel and the band of restricted vector was excised. GeneRuler 1 kb was used to check for the correct band size. After excision, vector DNA was extracted and purified using the NucleoSpin gel and PCR clean-up kit. Finally, DNA concentration was measured with a Nanodrop (Peqlab, Nanodrop 1000) and the software NanoDrop 1000 3.7.1 (Thermo Scientific).

PCR with Pfu polymerase was used to amplify the insert DNA. PCR products were run on a 1% agarose gel and bands were excised. Then, DNA was extracted and purified as mentioned above. If classic cloning was used, the insert was restricted overnight with the same restriction enzymes used to restrict the vector. Next, restricted DNA insert was purified using the Nucleospin kit. Finally, 50 ng of purified backbone

vector were ligated with 250-500ng of purified insert, according to 1:5 or 1:10 ratio vector:insert. The ligation reaction was performed overnight at 16°C using T4 ligation enzyme. Alternatively, if Infusion cloning was used, the restriction step was skipped and ligation was performed following the manufacturer's instructions.

Transformation of DH5α electrocompetent cells

Homemade electrocompetent DH5α E.coli bacterial cells were used for transformation via eletroporation. 100-500 ng of DNA were added to 50 μl of bacteria. The mix was transferred to a prechilled cuvette (Gene Pulser Cuvettes, 0.2 cm electrodes, Bio-Rad) and electroporation was performed with two pulses of 25 μF (Bio-Rad, Puls Controller). Next, 250 μl of LB medium were added to the cells and the whole volume was transferred to a round-bottom 14 ml Falcon tube. After 1 h incubation at 37°C and 225 rpm, transformed cells were streaked on either Amp or Kan-containing agar plates and incubated overnight at 37°C.

Isolation of plasmid DNA

Plasmid DNA was isolated from single bacterial colonies. First, bacteria were expanded overnight at 37°C in 300 ml LB medium containing either 100 μg/ml of Amp or 30 μg/ml of Kan. Afterwards, DNA isolation was performed according to the manufacturer's instructions with the Nucleobond kit. DNA was resuspended in TE buffer to a working concentration of 1 μg/μl. Finally, plasmid samples were sent for sequencing and results were aligned with the expected sequence using the Megalign software, included in the Lasergene core suite software.

3.2.3 CRISPR/Cas9 design and cloning

Construct design and generation was modified from the Zhang lab protocol provided under https://www.addgene.org/crispr/zhang. Oligos were designed for BsmBI golden gate cloning. Suitable guides were selected via the chopchop online tool (https://chopchop.rc.fas.harvard.edu/). The retrieved 20 bp sequences were inserted (without PAM) into 5'-GT CGTCTC C CACC G– 20 bp –GTTT C GAGACG TG-3'.

The resulting sequences and the respective reverse complements were ordered.

For oligo annealing 1 μl (100 μM) of forward and reverse oligos were added to 98 μl TE buffer and incubated for 5 min at 95°C. Afterwards, the mix was cooled down for 2 h to RT. Annealed oligos were stored at -20°C.

For golden gate cloning reaction, 50 ng of vector lentiCRISPRv2 were mixed with 2 μl T4 ligase buffer (Promega), 1 μl T4 DNA ligase (Promega), 1 μl 10 U/μl BsmBI (NEB) and 1 μl of the annealed oligos from a 1:10 dilution in dH_2O. dH_2O was added to a final volume of 20 μl. The reaction proceeded in a Thermocycler (Bio-Rad) and the PCR cycles were: 1) 5min at 37°C, 2) 10 min at 16°C, 3) 5 min at 55°C, 4) 5 min at 80°C. Step 1 and 2 were repeated 10 times. The reaction mix was either stored at 4°C or directly used for transformation.

RecA-deficient (recA1) bacteria electrocompetent DH10b were transformed as above with 1 μl of the golden gate cloning reaction product and streaked on Amp plates. Single colonies were selected and expanded. Plasmid DNA was isolated by miniprep and sequenced using the U6 primer.

3.2.4 Generation of an inducible stable cell line

The Tet-On 3G Inducible Expression System (Clontech, Cat.No. 631168) was used to generate an inducible double-stable cell line expressing mycβ23mCherry. First, a stable cell line expressing the Tet-On 3G transactivator was created. To do so, Hek293T cells were seeded on a 30 cm dish and transfected with 2 μg of plasmid pCMV-Tet3G (ID53) when near confluent. After 48 hrs, cells were split into 4 x 10 cm dishes. After an additional 48 hs, G418 (Gibco) was added at 500 μg/ml. Medium with fresh G418 was replaced every 2-4 days for 2 weeks. Next, a total of 24 individual colonies were transferred into separate wells of a 24-well plate using cloning cylinders (Sigma). Clones were furhter cultured in a maintenance concentration of G418 100 μg/ml. When confluent, cells from each well were split into three wells of a 6-well plate for testing and maintenance. One well was used for maintenance, and the other two were transfected with 5 μg of pTRE3G-Luc. After 4 hs, the culture medium of one well was replaced with fresh medium containing 500 ng/ml Dox (Sigma), the other well received Dox-free fresh medium. Finally, after 24 hs, luciferase activity was measured

and the fold induction calculated (+Dox RLU/-Dox RLU). The clone with the highest fold induction (clone 11, in this case) was selected for expansion, which was done in maintenance concentration of G418 100 μg/ml, and a stock of the pCMV-Tet3G stable cell line was cryopreserved.

Subsequently, Tet3G-expressing cells were cultured in a single well of a 6-well plate and always kept in G418 100 μg/ml. When near confluent, the well was cotransfected with 2 μg of plasmid ID58 (pTRE3G-mycβ23mCherry) and 100 ng hygromycin linear selection marker. After 48 hs, cells were split into 4 x 10 cm dishes. After an additional 48 hs, hygromycin was added at 100 μg/ml. Medium was replaced with fresh complete medium plus hygromycin every 2-4 days for two weeks. As before, a total of 24 individual colonies were transferred into separate wells of a 24-well plate using cloning cylinders. Clones were cultured in maintenance concentrations of G418 and hygromycin, 100 μg/ml and 50 μg/ml, respectively. When confluent, cells from each well were split into three wells of a 6-well plate for testing and maintenance. 500 ng/ml Dox was added to one of the wells and mCherry fluorescence and aggregate presence was assessed at the fluorescent microscope after 48 hs. The clone with the highest mCherry intensity (clone 5, in this case) was selected for expansion and a stock of the double-stable cell line mycβ23mCherry was cryopreserved.

Cryopreservation was performed using cryovials (Nunc) containing cells in 50% DMEM, 40% FBS, 10% DMSO. Cryovials were placed at -80°C in freezing containers (Nalgene) containing isopropanol. For long-term storage, cryovials were transferred to liquid nitrogen tanks.

3.2.5 Lentivirus production in Hek293T cells

Hek293T cells for lentiviral packaging were purchased (Lenti-X 293T cell line, Takara) and expanded in Hek293T culture medium for lentiviral production (see 3.1.2). Then, a cellular stock of passage 3-4 Hek293T cells was generated by cryopreserving vials containing approximately four millions cells in 50% DMEM, 40% FBS, 10% DMSO. Stock was stored in liquid nitrogen.

To produce a lentiviral batch, one vial of Hek293T cells was thawed at 37°C. Cells were transferred into 5 ml of Hek293T culture medium and centrifuged for 5 min at

800xg. The cell pellet was resuspended in 10 ml of Hek293T culture medium and cultured in a T75 cm^2 flask (Falcon). Next day, medium was completely exchanged. Following day, when cells had usually reached 80% confluency, they were trypsinized and passaged to a T175 cm^2 flask (Falcon). One day later, cells were trypsinized and passaged to a three-layered 525 cm^2 (Falcon). Subsequently, one day later, cells were trypsinized and four T75 cm^2 flasks containing 5.7 million cells each were seeded. At this point, G418 was removed from the culture medium composition. Next day in the evening, the three of the flasks were transfected for virus production. Transfection reaction mix was prepared according to the following table:

Transfection mix for 3xT75 cm^2	
Mix A	
Reagent	**Quantity**
LTR-vector (pFhSynW2)	18.6 μg
pSPAX2	11 μg
pVsVg	6.4 μg
DMEM without FBS	1500 μl
Mix B	
Reagent	**Quantity**
TransIT-Lenti transfection reagent (Mirus)	108 μl
DMEM without FBS	1500 μl
Add mix A to mix B	

Table 3.6: Transfection mix for lentiviral production

The transfection mix was incubated for 20 min at RT and, meanwhile, cell medium was exchanged. Then, 1 ml transfection mix was added to each flask, leaving the transfection overnight. In the morning on the following day, cells were checked for fluorescence (only if the LTR vector contained a fluorescent protein sequence), washed once with prewarmed PBS and fresh medium was added. After 48 hs, culture medium containing the viral particles was collected, pooling the three flasks into one Falcon tube. To remove cells debris, centrifugation for 10 min at 1200xg was performed. Then, the supernatant was filtered through 0.45 μm pore size filters using 50ml syringes, and transferred to Utra-clear centrifuge tubes (Beckman). Finally, cell medium was

centrifuged at 100,000xg for 2 h with a centrifuge Avanti JXN-30, rotor JS-24.38 (Beckman). Supernatant was discarded and the lentivirus pellet resuspended in 100 μl TBS-5 buffer. After aliquoting, virus was stored at -80°C.

Lentivirus production for CRISPR/Cas9 expression

For lentivirus production 1.2*10^6 Hek293T cells were seeded per well into 6-well plates and grown in culture medium for Crispr/Cas9 lentivirus production. Six hours later, cells were transfected with Lipofectamine2000. Transfection reaction mix was prepared according to the following table:

Transfection mix in 6-well plates	
Mix A	
Reagent	**Quantity**
OptiMEM	100 μl
pMD2.G	1 μg
psPAX2	1.5 μg
pLentiCRSPRv2	2.2 μg
Mix B	
Reagent	**Quantity**
Lipofectamine2000	10 μl
OptiMEM	100 μl
Add mix A to mix B	

Table 3.7: Transfection mix for Crispr/Cas9 lentiviral expresssion

Solution A and B were combined, incubated 30 min at RT, and added to the cells. 16 hours later, medium was removed and 3 mL fresh cell medium with 30% FBS was added. Cell medium containing virus was harvested after 24 h and stored at -80°C.

In order to concentrate and rebuffer the viruses in neuron compatible medium they were precipitated according to Kuttner *et. al* (2009). [207]. In short, virus aliquots were thawed and centrifuged for 5 min at 16,000xg and 4°C. The supernatant was mixed 1:1 with precipitation buffer (for 500 μl supernatant: 170 μl of 50% PEG600 (final 8.5%) , 75 μl of 4M NaCl (final 0.3M), 255 μl PBS) and incubated at 4°C for 4 h. Samples were gently agitated every 20 min. Next, samples were centrifuged for 10

min at 7,000xg and 4°C. The supernatant was discarded and 100 μl of neuronal culture medium was added to the pellet containing the virus. All steps for lentivirus production for Crispr/Cas9 expression were performed by Daniel Hornburg and Martin Dodel.

3.2.6 Primary neuronal culture

Coating

The surface of culture wells was coated previous to neuronal seeding to facilitate attachment and growth. First, sterile Poly-D-lysine 1 mg/ml in borate buffer solution was used for 2-4 h. After 3-4 times PBS washing, laminin 5 μg/ml in PBS solution was added for further 2-4 h. Finally, one more PBS washing was done before cell seeding. If neurons were to be used for immunocytochemistry, they were seeded onto 13 mm glass coverslips placed in 24-well plates. Coverslips were sterilized overnight at 180°C and were coated as above.

Neuronal dissociation protocol

Primary cortical or hippocampal neurons were dissociated from E15.5 or E17.5 CD-1 wt embryos. First, pregnant CD-1 females were sacrificed by cervical dislocation and the uterus was placed in prechilled PBS. Then, the uterus was transferred into ice cold dissection medium and embryos were dissected out of it. Next, embryos were decapitated and heads transferred into fresh dissection medium. Afterwards, whole brains were dissected out of the skull and neocortices were excised out. Finally, meninges were removed and cortex or hippocampus were dissected and placed in prewarmed Trypsin (Gibco) with 1% DNAseI 0.05% for 20 min at 37°C. Next, trypsin activity was stopped by adding Neurobasal supplemented with 0.05% FBS. The medium was discarded and prewarmed cell culture medium was added to the tissue. After homogenization by pipetting, cells were pelleted at 130xg for 5 min and resuspended in prewarmed culture medium. After cell counting using a Neubauer chamber (Brand), dissociated primary neurons were seeded on 96, 24, 12 or 6 well-plates (Costar). Cortical neuron seeding density was 100,000 cells/cm^2 and hippocampal neuron seeding density was 80,000 cells/cm^2. Neuronal cultures were maintained at 37°C, 5% CO_2.

3.2.7 Neuronal transfection with calcium phosphate

Primary neurons were transfected at 10 Days in vitro (DIV) with a modified protocol from Jiang and Chen [208]. Briefly, DNA was mixed with dH_2O and $CaCl_2$ was added dropwise to the solution. This mix was added dropwise to a second tube containing 2x HBS and incubated at RT for 30-45 min. Next, coverslips were transferred into a new culture plate, containing prewarmed fresh neuronal culture medium. Subsequently, 30 μl of transfection mix was added dropwise to each well and incubated for 3.5 h. Then, cells were washed once with culture medium that had previously been acidifed in 10% CO_2, and incubated for 30 min in the acidified medium at 37°C, 5% CO_2. Finally, coverslips were transferred back to their original culture medium.

3.2.8 Lentiviral transduction

Virus were thawed and immediately added to freshly prepared neuronal culture medium. A fifth of the culture medium was removed and the equivalent volume of virus-containing medium was added to neurons. Usually, 1 μl/cm^2 of virus was added, but this amount was at times adjusted to match protein expression levels among different constructs.

3.2.9 BDNF treatment of primary hippocampal neurons

E17 primary hippocampal neurons were cultured in 12 well plates. At 10+3 and 10+4 DIV, respectively, recombinant human BDNF (hBDNF) (R and D Systems) was administered to neurons. To do so, cell medium was removed, and cells were washed once with warmed-up PBS. Then, hBDNF diluted in warmed-up neurobasal medium without additives was added to the neurons in concentrations of 0, 5 ,15, 25, and 50 ng/ml. Cells were incubated for 30min at 37°C, 5% CO_2. After incubation, cells were washed once with PBS and lysed in 200 μl lysis buffer. Lysates were stored at -20°C for further use.

3.2.10 Western blot

First, cell culture medium was removed and cells washed twice with ice-cold PBS. For cell lysis, 100 μl/cm^2 prechilled cell lysis buffer was added to cells and incubated for 20 min at 4°C. Cell scrapers (Starstedt) were used to facilitate cell detachment and lysate collection. Lysates were stored at -20°C until further use.

To perform the western blot, samples were centrifuged for 10min at 4,000xg and 4°C to separate the soluble cell lysate from cell debris. Supernatants were collected in prechilled Eppendorf tubes. Next, equal amounts of the cell lysates were transferred to another Eppendorf tube containing 6x sample loading buffer. Tubes containing sample and loading buffer were boiled for 5min at 95°C on a heating block (Eppendorf). Acrylamyde gels were handcasted using Bio-Rad glassplates and consisted of a 12% resolving gel and a 4% stacking gel. When solidified, gels were placed into the running chamber containing 1X running buffer. After boiling, samples were loaded on the gel and protein standards (Bio-Rad) were included in one well for protein size reference. If there were wells with no sample, 5 μl of sample loading buffer were added to prevent samples from running unevenly. First, gels were run for 20 min at 100 V and, afterwards, at 120 V until the front run out.

After running, stacking gel was removed and the resolving part was soaked in 1X transfer buffer for 10 min. Meanwhile, mini trans-blot filter paper (Bio-Rad) was soaked as well in 1X transfer buffer. PVDF membrane (Thermo Fisher) was activated in methanol, washed twice in MilliQ dH_2O, and equilibrated in 1X transfer buffer. To transfer proteins from the gel to the PVDF membrane, filter papers, PVDF membrane, and gel were assembled into a so called sandwich and transference was performed using a Trans-Blot Turbo transfer system (Bio-Rad). Transference parameters were 25 V, 2.5 A for 40-50 min.

Next, membrane was blocked using 3% BSA, 5% dried milk (Roth) in TBS-T for 1 h at RT on a shaker. After rinsing twice with 1x TBS-T, primary antibody was added and incubated for 2 days overnight at 4°C on a shaker. Primary antibodies were diluted 1:1000 in 3% BSA in TBS-T, 0.01% Sodium azide (SA). Then, membranes were washed three times for 10 min in 1X TBS-T and secondary antibody was added. Secondary antibodies were diluted 1:5000 in 5% dried milk in TBS-T and applied for

2 h at RT on a shaker. Finally, membranes were washed three times for 10 min in 1x TBS-T, ECL detection reagent (GE Healthcare) was added on the membrane, and substrate reaction detection was performed using a Peqlab Fusion Fx7.

Immunoprecipitation for interactome analysis

Cortical neurons were washed three times with ice-cold PBS and 250 μl of prechilled lysis buffer were added per well. Lysates were incubated for 10 min at 4°C, collected in prechilled Eppendorfs and stored at -20°C. For the mCherry immunoprecipitations, we used the Thermo Scientific Pierce Protein G Agarose (10 ul/100 ug IgG). First, to block non-specific binding, serum samples containing IgG were incubated with Protein G agarose for 1 hour. Then, the neuronal lysates were loaded to the IgG-protein G Agarose and incubated for 4 h. Non-IgG and non-antigen components were discarded from the sample by washing (0.1% NP40, 5% Glycerol, 50 mM Tris HCl, 150 mM NaCl). Next, for the beat digestion, we used beat digestion buffer. Later, samples were incubated for 1 hour with Trypsin digestion buffer (Trypsin, 50 mM ABC, 55 mM CAA) and washed with quenching buffer (2 M Urea, 50 mM thiourea). Trypsin was added for overnight digestion. Finally, ACN and TFA were added to stop the reaction.

3.2.11 Immunocytochemistry

Cell culture medium was removed and cells washed once with ice-cold PBS. Fixation was performed by adding 4% PFA in PBS for 20 min. Next, cells were washed once more with PBS and stored in PBS at 4°C until further use.

After cell fixation, remaining free groups of PFA were blocked with 50mM Ammoniumchloride in PBS for 10 min at RT. Cells were rinsed once with PBS and permeabilized with 0.25% Triton X-100 in PBS for 5 min. After permeabilization, cells were washed three times for 5 min each with PBS. Then, blocking was performed for 30 min at RT. Blocking solution contained 2% BSA (w/v)(Roth) and 4% donkey serum (v/v) in PBS. After the blocking step, coverslips were transferred one by one to a light-protected humid chamber and placed on parafilm. Immediately after, each coverslip was covered with 50 μl of diluted primary antibody in blocking solution. After 1 h incubation in primary antibody, cells were washed three times for 5 min

each with PBS. Then, each coverslip was covered with 50 μl of 1:250 diluted secondary antibody in blocking solution. Secondary antibody solution contained 1:2000 diluted Dapi to stain cell nucleus. Finally, coverslips were washed three times for 5 min each with PBS, dipped in dH_2O and mounted on menzer glass slides using Dako fluorescence mounting medium. Slides were stored in darkness overnight at RT for the mounting medium to dry, followed by storage at 4°C for further use.

Neuronal morphology analysis

Coverslips were immunostained against mCherry and imaged with a 40x objective. Maximum intensity projections were analyzed. First, cell morphologies were semi-automatically traced with the Simple Neurite Tracer plug-in of ImageJ. Importantly, cell morphologies were traced in a blinded way. Then, complexity of the traced neurons was quantified with the Sholl analysis plug-in of ImageJ. To that aim, a custom-made ImageJ macro was created to automatically do the Sholl analysis in batch (by Daniel del Toro Ruiz).

3.2.12 MTT cell viability assay

MTT reagent was purchased from Sigma-Aldrich. MTT assays were performed on cells cultured in 96-well plates. First, cell medium was exchanged for 100 μl of fresh medium. Then, 20 μl of 5 mg/ml MTT in PBS were added to each well. The plate was placed back in the incubator for 2-4 h at 37°C, 5% CO_2 for the cells to metabolize MTT (yellow) into formazan crystals (purple). Subsequently, 100 μl solubilizer solution were added to each well to dissolve the crystals. The plate was incubated overnight at 37°C, 5% CO_2. Finally, absorbance was measured at 570 nm. Each condition was measured in triplicates and absorbance values averaged for each experiment. A condition with only medium was included in all experiments. The average absorbance value for the medium condition was subtracted from all conditions in the experiment.

3.2.13 Generation of the TRE3G:mycβ23frt-IRES-frt-mCherry mouse line

To generate inducible transgenic mice expressing β23, a Tetracycline (Tet)-responsive expression system was used. Two mouse lines with two different frt were

generated. In one line, referred as β23frt1, the frt sequence before the IRES was placed in frame to code for the following aminoacid sequence: KFLFSRKYRNF. In the other line, referred as β23frt2, the frt sequence before the IRES was placed in frame to code for the following aminoacid sequence: SSYSLESIGT. For both lines, the frt after the IRES corresponded to frt1.

Plasmid DNA generation was done in several steps. First, IRES-frt-mCherry insert sequence was restricted out of plasmid ID16 with EagI and MluI restriction enzymes. pTRE3G vector (Clontech) was obtained and linearized with EagI and MluI as well. Then, insert was ligated into the vector and DNA was sequenced (Step1). Next, mycβ23frt1/2 insert sequence was amplified by PCR from plasmids ID17 and ID18, adding an ApaI restriction site at 5'end and an EagI restriction site at 3'end. This second insert was restricted with EagI first, followed by ApaI restriction. The plasmid generated in step 1, was restricted with EagI first, followed by ApaI as well. Subsequently, restricted mycβ23frt1/2 inserts were ligated into the linearized vector from step1 and DNA was sequenced (step2). The final vectors were purified with endotoxin free (EF) maxi prep kit. The vector containing TRE3G:mycβ23frt1-IRES-frt-mCherry was termed ID21. The vector containing TRE3G:mycβ23frt2-IRES-frt-mCherry was termed ID22.

The DNA fragments to be used for pronuclear injection were obtained after XhoI and SapI restriction of ID21 and ID22. The fragments were extracted from an agarose gel using JetSorb gel extraction kit (Genomed) and subsequently filtered using PVDF 0.45 μm Ultrafree MC GV filters (Millipore). Purity of the DNA was checked by gel electrophoresis. Final DNA was given to the transgenic service at a concentration of 50-100 ng/μl. The transgenic service conducted the pronuclear injections and provided us with several mouse founders. Then, tail biopsies of these founders were used to detect transgene integration by PCRs b23-1 and b23-2. Out of these founders, only one showed germline transmission and expression of the transgene from ID21 (β23-frt1 1056). In addition, one showed germline transmission and expression of the transgene from ID22 (β23-frt2 1401). For this thesis, all work with the β23 transgenic mouse was performed with the β23-frt1 1056 line. Of note, it has been detected that mice of the 1056 line express a mutated form of the β23 protein, β23L63P, in which the last lysine aminoacid in the transgene sequence was exchanged by a proline.

3.2.14 Mouse colony maintenance

Mice were housed at the animal facility of the Max Planck Institute of Biochemistry (Martinsried, Germany) under Specific-pathogen-free (SPF) conditions and with *ad libitum* access to food and water. Mice were maintained accordingly to local animal welfare guidelines (Regierung von Oberbayern). Female and male mice were used for the experiments.

All mice used in this thesis were heterozygous. β23 mice were kept in a C57BL/6NRj genetic background. To induce β23 expression in the forebrain, mice were crossed to CamKIIα:tTa mice, which were obtained from the Jackson Laboratory, and originally published by Mayford *et. al* (1996). CamKIIα:tTa mice were kept in a mixed CBAxC57BL/6NRj background. Therefore, β23;CamKIIα:tTa mice were in a 25%CBA, 75%C57BL/6NRj genetic background.

To induce β23 expression in the whole CNS, mice were crossed to NEFH:tTa mice, which were obtained from the Jackson Laboratory, and originally published by Walker *et. al* (2015). NEFH:tTa mice were backcrossed onto C57BL/6NRj genetic background for at least four generations. Therefore, β23;NEFH:tTa mice were in a pure C57BL/6NRj genetic background.

Mice which express the construct mycβ23frt1-IRES-frt-mCherry, therefore leading to separate translation of β and mCherry, are referred to as unrecombined. To excise out the IRES cassette, β23-frt1 line was crossed to a Flippase line (FLPe), obtained from the Jackson Laboratory. The progeny of these mice were genotyped to detect presence of the construct mycβ23frtmCherry, and absence of mycβ23frt1-IRES-frt-mCherry. Mice in which recombination had worked, were further kept and maintained in C57BL/6NRj background. Therefore, mice which expressed mycβ23frtmCherry as a fusion protein are referred to as recombined.

Doxycyclin administration

β23;CamKIIα:tTa mice were administered doxycycline from embryonic day 0 until postnatal day 21. Females were given 2mg/ml doxycycline in the drinking water during the whole pregnancy and until pups were weaned. The antibiotic was

dissolved in 5% sucrose water and kept in dark drinking bottles to prevent light exposure. Mice had *ad libitum* access to drinking and bottles were exchanged once a week.

β23;NEFH:tTa mice were administered doxycycline from embryonic day 0 until postnatal day 21. Females were given 200 mg/kg doxycycline in food pellets (Snniff) during the whole pregnancy and until pups were weaned. Mice had *ad libitum* access to food and pellets were exchanged once a week.

3.2.15 Mouse getnoyping protocols

A tail biopsy of 1-2 mm of each mouse was lysed in 100 μl of 50 mM NaOH for three cycles of 15min at 95°C, vortexing in between each cycle. Next, 10 μl of 1.5M Tris-HCl pH=8.8 were added for neutralization. DNA containing-solution from lysed tails was used for genotyping by polymerase chain reaction (PCR). A PCR master mix was prepared on ice (47-49 μl) and mixed with the respective DNA samples (1-3 μl). PCRs were performed in a Thermocycler (BioRad) and products were run on 1% agarose gels.

The PCR protocols are depicted in the following tables (Tables 3.8, 3.9, 3.10, 3.11, 3.12). All unrecombined mice were genotyped twice using two different PCR protocols: b23-1 and b23-2. All recombined mice were genotyped using the Recom PCR protocol. Genotyping to identify CamKIIα:tTa-positive mice was performed using the CamK PCR protocol. Genotyping to identify NEFH:tTa-positive mice was also performed using the CamK PCR protocol. Flippase-positive mice were identified using the Flp PCR protocol.

b23-1 PCR protocol			
Step	**Temperature (°C)**	**Time**	**Go to**
1	95	5 min	
2	95	1 min	
3	62	30 s	
4	72	1 min	Go to step 2, 34x
5	72	5 min	
6	12	forever	
PCR product 618 bp			

Table 3.8: b23-1 PCR protocol

b23-2 PCR protocol			
Step	**Temperature (°C)**	**Time**	**Go to**
1	95	5 min	
2	95	1 min	
3	60	30 s	
4	72	1 min	Go to step 2, 34x
5	72	5 min	
6	12	forever	
PCR product 427 bp			

Table 3.9: b23-2 PCR protocol

Recom PCR protocol			
Step	**Temperature (°C)**	**Time**	**Go to**
1	95	5 min	
2	95	1 min	
3	60	1 min	
4	72	1 min	Go to step 2, 34x
5	72	5 min	
6	12	forever	
PCR product 600 bp			

Table 3.10: Recom PCR protocol

CamK PCR protocol			
Step	**Temperature (°C)**	**Time**	**Go to**
1	94	3 min	
2	94	30 s	
3	57	1 min	
4	72	1 min	Go to step 2, 34x
5	72	2 min	
6	12	forever	
Two PCR products: 450 bp (transgene) and 200 bp (wt positive control)			

Table 3.11: CamK PCR protocol

Flp PCR protocol			
Step	**Temperature (°C)**	**Time**	**Go to**
1	94	1 min	
2	94	1 min	
3	60	1 min	
4	72	1 min	Go to step 2, 34x
5	72	1 min	
6	12	forever	
PCR product ∼500 bp			

Table 3.12: Flp PCR protocol

3.2.16 Histology

Transcardial perfusion

Mice were anesthetized first with isofluorane (cp-pharma) and then with ketamine/xylazine in saline (16% ketamine (Medistar), 8% xylazine (Medistar)). They were first perfused using a Minipuls 3 peristaltic pump (Gilson) with ice-cold PBS for 3-4 min, followed by 6-8 min of ice-cold, freshly prepared 4% PFA. Brains were extracted and post-fixed for 24-48 h in 4% PFA at 4°C. For storage, brains were placed in 0.05% sodium azide in PBS at 4°C. Of note, after perfusion, brains ought not to be embedded, since this inhibits myc staining to detect β23. In our hands, agarose and gelatin/albumin embedding prevented myc antibodies from binding. Other embedding materials have not been used.

Immunostaining of brain sections

Serial 50-70 μm-thick brain sections were obtained with a Vibratome VT1000S (Leica). For storage, sections were kept in 0.05% sodium azide in PBS at 4°C. For immunostainings, sections were first washed in PBS. Then, they were permeabilized in 0.5% Triton X-100 in PBS for 30min on a shaker. Next, sections were washed in PBS and blocked for 1.5 h at RT on a shaker. After washing in PBS, sections were incubated three days in primary antibody solution at 4°C on a shaker. Next, sections were washed three times in PBS for 10 min, and incubated overnight at 4°C on a shaker in secondary antibody solution. Both primary and secondary antibodies were usually diluted 1:300. Dapi was used to stain cell nucleus, added to the secondary antibody solution in 1:2000 dilution from a 1 mg/ml stock. After the secondary antibody incubation, sections were washed 3 times for 10 min in PBS and mounted in mowiol mounting medium. Mounted sections were left to dry overnight at RT and stored at 4°C for further use.

Antigen retrieval was needed for some antibodies and it was mandatory to detect myc in brain sections. For that purpose, before the staining protocol, sections were incubated for 30 min at 95°C in 10 mM Sodium citrate, 0.05% tween 20 in PBS. After cooling down, sections were washed in PBS. Permeabilization and further staining procedure as mentioned above was performed.

3.2.17 Data presentation and statistical analysis

Images were obtained with a Leica SP8 confocal microscope and processed with the ImageJ software. Data are presented as mean ± SD and significant levels are indicated with asterisks, corresponding to $* \ p < 0.05$, $* * \ p < 0.01$, $* * * \ p < 0.001$, $* * * * \ p < 0.0001$. The software GraphPad Prism 6 was used for graphical presentation and statistical analysis. Adobe Illustrator CS6 was used for figure assembly.

4 Results

4.1 Artificial β-sheet proteins are toxic in primary neurons

We analyzed artificial β-sheet protein aggregation and cytotoxicity in primary neurons. To this aim, we first overexpressed mCherry-tagged β-sheet proteins in primary cortical neurons by transfection (note that β-sheet proteins were also myc-tagged in all our experiments throughout this thesis, even if not explicitly mentioned), including mCherry overexpression as a control. Thereby, we could already detect aggregation of mCherry-tagged artificial β-sheet proteins one day after transfection (Fig.4.1 A, B). Moreover, to gain insight into the toxicity effects in a time-dependent manner, we analyzed neuronal death on day one and day three after transfection (10+1 DIV and 10+3 DIV). Quantification of cell death via cleaved caspase-3 staining, revealed that β4mCherry and β23mCherry caused significantly more neuronal death than overexpression of mCherry, which was not toxic. In addition, neuronal death driven by β4mCherry and β23mCherry overexpression increased in a time-dependent manner (Fig.4.1 C, D).

To further characterize cytotoxicity effects caused by artificial β-sheet protein aggregation, we analyzed neuronal morphology in transfected hippocampal neurons. In these experiments, we chose hippocampal over cortical neurons because of their rather homogeneous morphology and we quantified neuronal complexity by Sholl analysis. This software is an ImageJ pluggin that sets concentric circles around the soma and quantifies the number of intersections to these circles. As depicted in Fig.4.2, hippocampal neurons expressing β4mCherry and β23mCherry were less complex than mCherry expressing neurons.

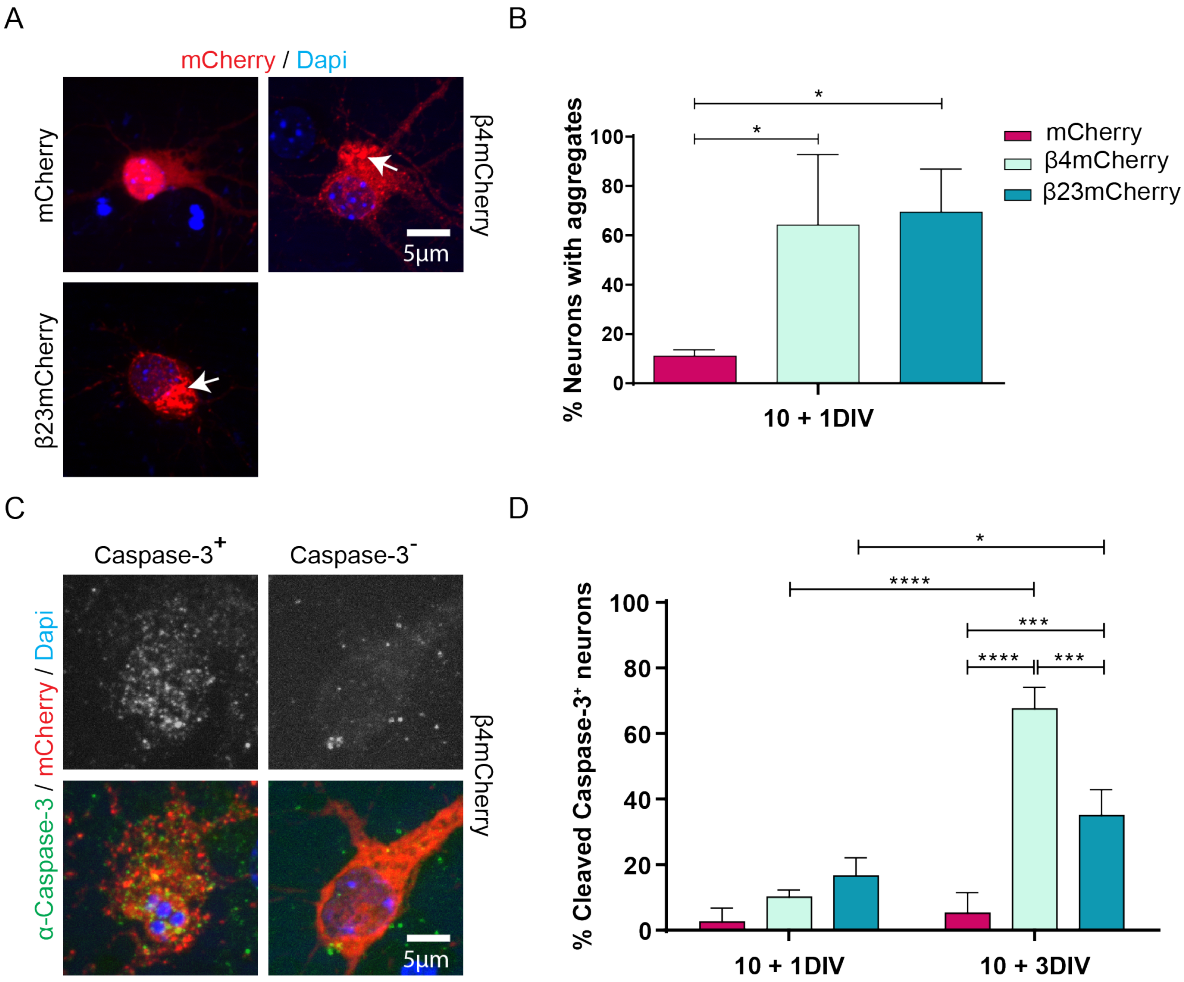

Figure 4.1: **β-sheet aggregation and toxicity in transfected neurons.** (A) E15.5 cortical neurons transfected with either mCherry, which was diffuse throughout the nucleus and cytoplasm, β4mCherry or β23mCherry, both of which formed cytoplasmic aggregates (arrows), time point 10+1 DIV. (B) Quantification of transfected neurons with aggregates. N=3 independent experiments, 25-45 cells/condition/experiment, One-way ANOVA + Dunett's multiple comparison test. (C) Representative images of an immunostaining against cleaved Caspase-3, time point 10+3 DIV. Top row depicts the cleaved Caspase-3 channel in positive (left) and negative (right) neurons. Bottow row depicts the merge of immunostained cleaved Caspase-3 with mCherry fluorescence and the nuclear marker Dapi (notice the apoptotic nucleus in the left cells). (D) Quantification of transfected cleaved Caspase-3 positive neurons. N=3 independent experiments, 25-45 cells/condition/experiment, Two-way ANOVA + Tukey's multiple comparison test.

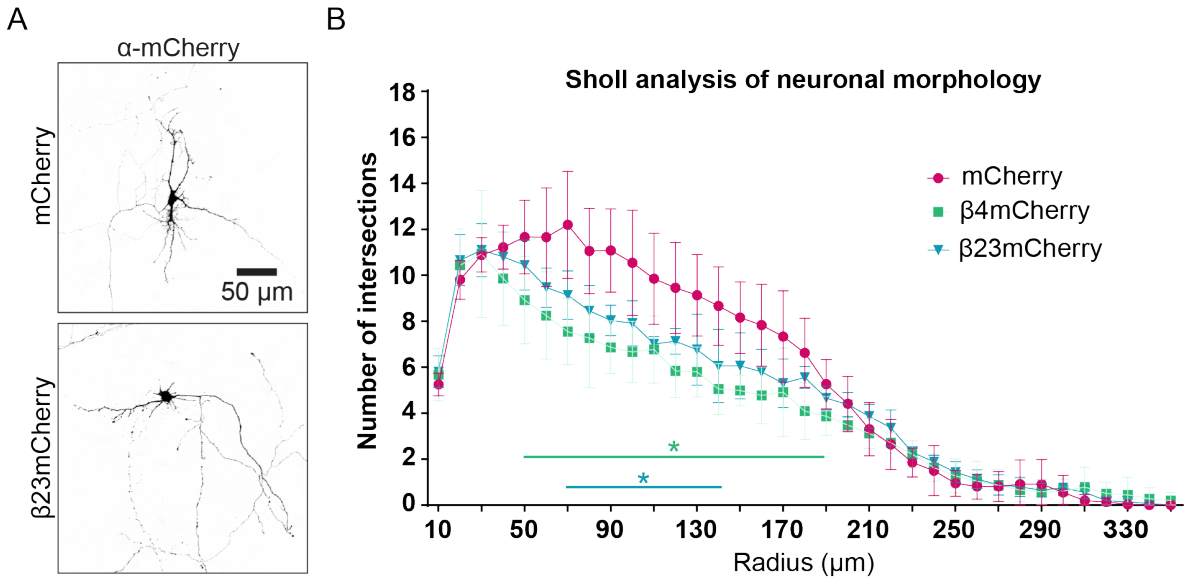

Figure 4.2: **Sholl analysis in transfected hippocampal neurons.** (A) Images of the morphology of E17.5 transfected primary hippocampal neurons, exemplifying the reduced complexity observed in β-sheet-expressing neurons compared to mCherry positive neurons, time point 10+2 DIV. (B) Quantification of neuronal morphology by semiautomated Sholl analysis, time point 10+2 DIV. N=3 independent experiments, 10-30 cells/condition/experiment, Two-way ANOVA + Tukey's multiple comparison test.

Since at the start of this thesis the effects of β-sheet proteins had been characterized in Hek293T cells [81], we decided to complement our studies in neurons with further experiments in Hek293T cells. For this purpose, we generated a β23mCherry inducible stable cell line by making use of the Tet-ON inducible system. Therefore, upon addition of Dox to the cell media, β23mCherry expression was induced. With this new inducible Hek293T line, we detected β23mCherry aggregates as soon as one day after induction, and observed more aggregates accumulating over time (Fig.4.3 A). In addition, using the MTT toxicity assay, we quantified cell viability at different time-points after induction. These assays showed that β23mCherry expression caused significant reduction in cell viability by three days after induction, compared to uninduced cells (Fig.4.3 B).

Surprisingly, this decrease in viability that we observed, although significant, was rather modest in comparison to the reported toxicity effects caused by β23 electroporation in Hek293T cells [81][204]. However, previous studies made use of

β-sheet constructs without an mCherry tag. Thus we decided to investigate ourselves the effects of the β-sheet proteins without the mCherry tag, which will be referred to as untagged proteins for the rest of the thesis (note that they still contained the myc tag) .

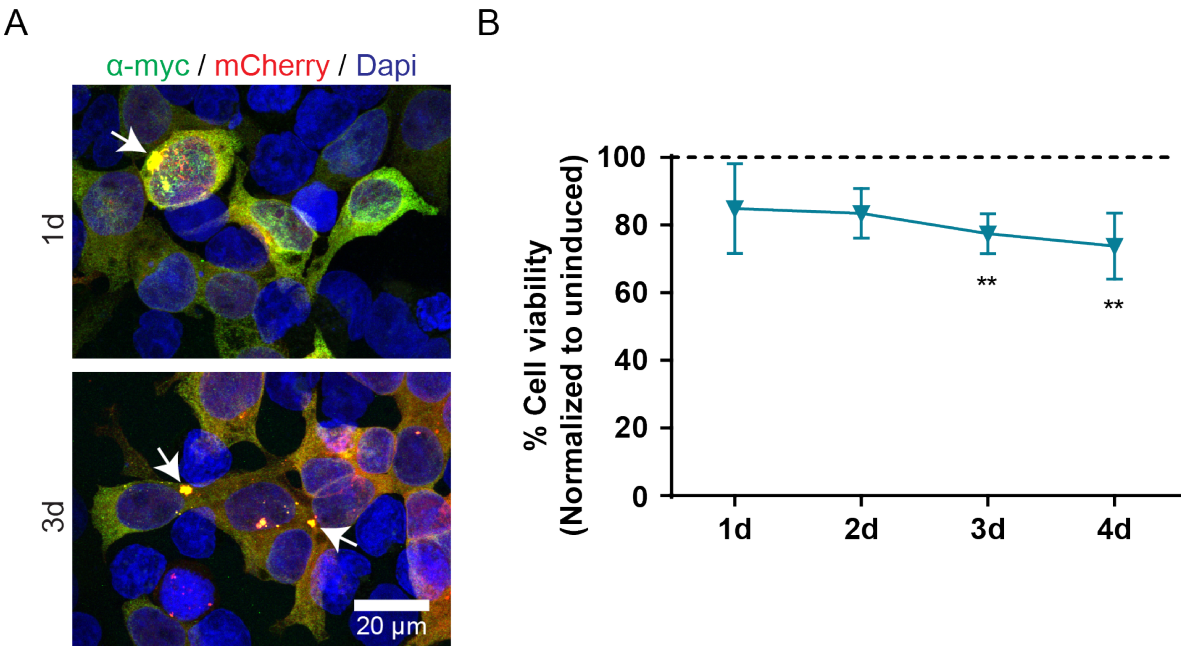

Figure 4.3: **β23mCherry toxicity in an inducible stable cell line.** (A) Images of Hek293T cells with aggregates (arrows) one and three days after expression induction with Dox. (B) Quantification of cell viability overtime after expression induction, measured by MTT assay . Viability values of induced cells were normalized to viability values of uninduced cells. N=4 independent experiments, One-way ANOVA + Bonferroni multiple comparison test.

In the following experiments, we studied the effects on viability of untagged β4 and β23 in Hek293T cells and in primary cortical neurons. In Hek293T cells, we transfected β4, β23, and non-aggregating protein α-S824 as a control. In parallel, we transfected the mCherry-tagged proteins as well, using mCherry as a control. Three days after transfection we performed MTT assay to quantify cell viability and detected no decrease neither in untagged, nor in mCherry-tagged β-sheet expressing Hek293 cells (Fig.4.4 A).

In addition, we quantified untagged β-sheet protein driven cell death in transfected cortical neurons via cleaved Caspase-3 staining. In these experiments, despite extensive

protein aggregation, only expression of untagged β4, but not β23, lead to significant cell death in comparison to the control (Fig.4.4 B). Moreover, β4 induced neuronal toxicity was lower as compared to β4mCherry driven neuronal death (Fig.4.1 D). However, we did not quantify and compare the expression levels of the different β-sheet proteins. Transfection rates in neurons are very low [208], which made β-sheet detection by western blot impossible in our hands.

At this point, mCherry-tagged β-sheet proteins had shown the most robust toxicity in transfected neurons in our experiments. Given that we aimed to focus on the neuronal effects of β-sheet protein aggregation, we proceeded to further confirm the toxicity of mCherry-tagged proteins in these cells at a population level. For this purpose, we transduced primary cortical neurons at 10 DIV with lentivirus (LV) and analyzed cell viability at different time points. Moreover, since we achieved high transduction rates, we performed western blots to control for protein expression levels.

We observed increasing fluorescence starting from two days after transduction (10+2 DIV) and β-sheet protein aggregation from 10+4 DIV (Fig.4.5 A). Therefore, we performed western blots at 10+3 DIV. Furthermore, cell viability was measured at 10+3, 10+4, 10+6, 10+10, and 10+14 DIV via MTT assay. β4mCherry and β23mCherry led drastically to neuronal death over time, while mCherry expression did not impair neuronal survival even fourteen days after transduction (Fig.4.5 B). Notably, western blot quantification showed no significant expression level differences among mCherry, β4mCherry, and β23mCherry (Fig.4.5 C, D). Therefore, we confirmed that mCherry-tagged β-sheet protein expression resulted in neuronal survival impairment both in transfected and LV-transduced primary neurons.

Overall, we confirmed that artificial proteins β4mCherry and β23mCherry formed aggregates and lead to neuronal death in a time-dependent manner in primary neurons.

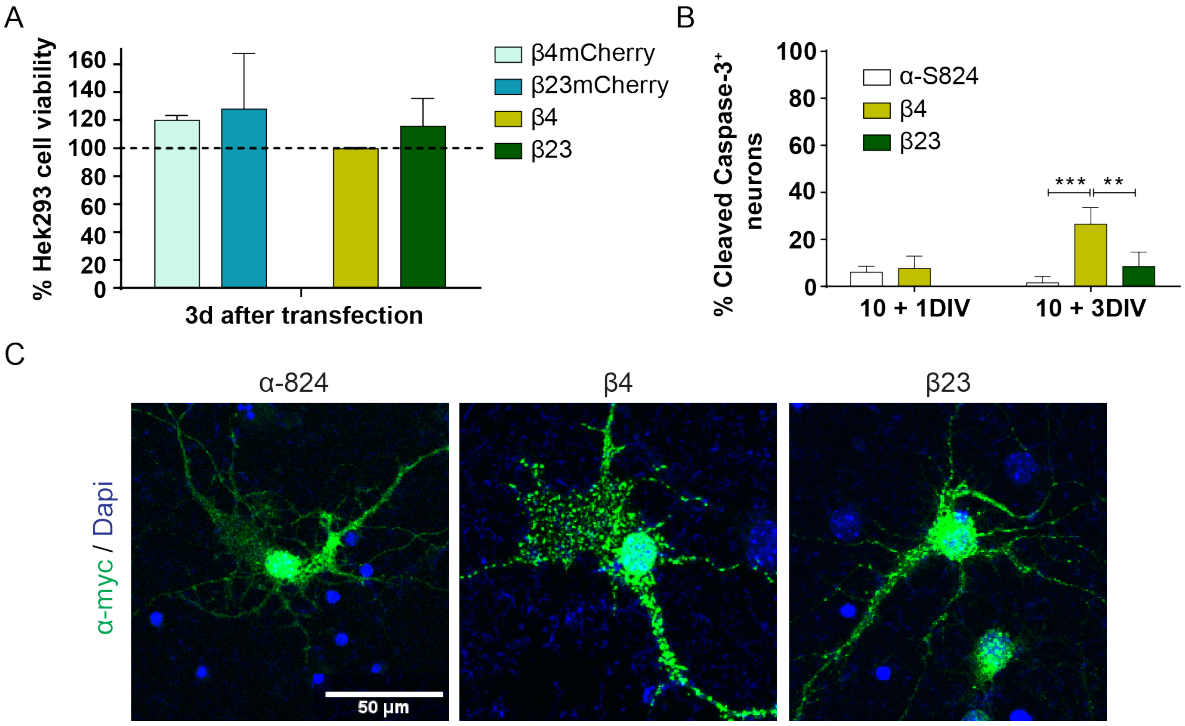

Figure 4.4: **β-sheet toxicity of non-mCherry-tagged constructs.** (A) Quantification of cell viability in transfecetd Hek293T cells measured by MTT assay. N=2 independent experiments. (B) Quantification of transfected cleaved Caspase-3 positive neurons expressing either control protein α-S824 or untagged β-sheets. E15.5 cortical neurons. N=3 independent experiments, 25-50 cells/condition/experiment, Two-way ANOVA + Tukey's multiple comparison test. (C) Images of transfected primary cortical neurons. Cells expressing β4 and β23 presented multiple aggregates both in the nucleus and cytoplasm.

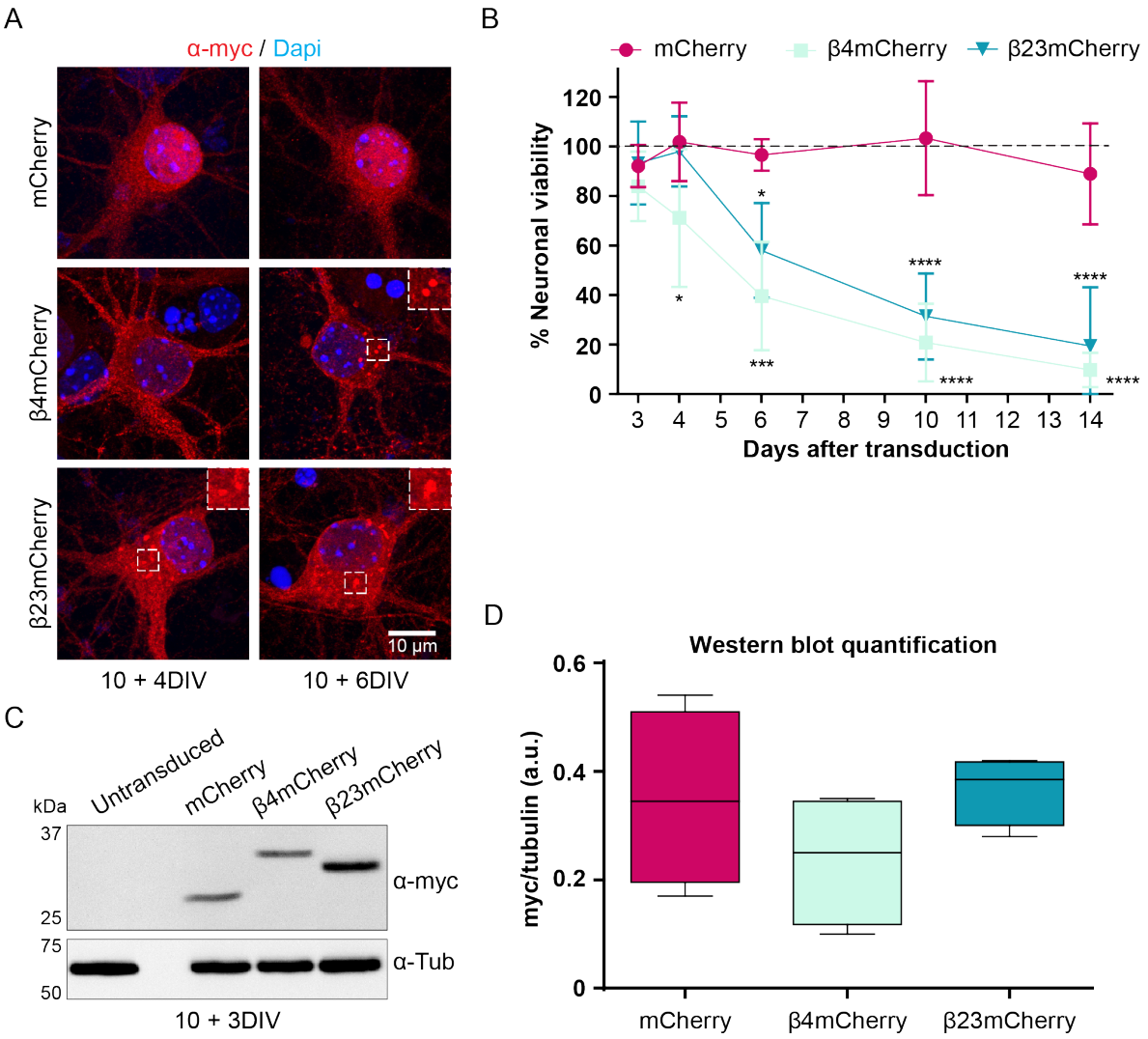

Figure 4.5: **β-sheet toxicity in transduced neurons.** (A) Images of LV-transduced E15.5 cortical neurons with aggregates (insets). (B) Quantification of neuronal viability over time after transduction. Viability values were normalized to untransduced neurons. N=4 independent experiments, Two-way ANOVA + Tukey's multiple comparison test. (C) Representative Western blot of neuronal lysates. (D) Western blot quantification showed no difference in expression between mCherry and β-sheet proteins in transduced neurons, time point 10+3 DIV. N=4 independent experiments, One-way ANOVA + Tukey's multiple comparison test.

4.2 Interactome analysis of β-sheet proteins in primary neurons

Previous studies have shown that several proteins aberrantly interact and coaggregate with naturally aggregating proteins, contributing to their toxicity mechanisms [125, 118]. Since we aimed to find out which molecular players were involved in β-sheet-mediated neuronal death in primary cultures, we performed interactome analysis. Thereby, we focused on the identification of protein candidates which were potentially involved in common mechanisms of cell toxicity due to protein misfolding.

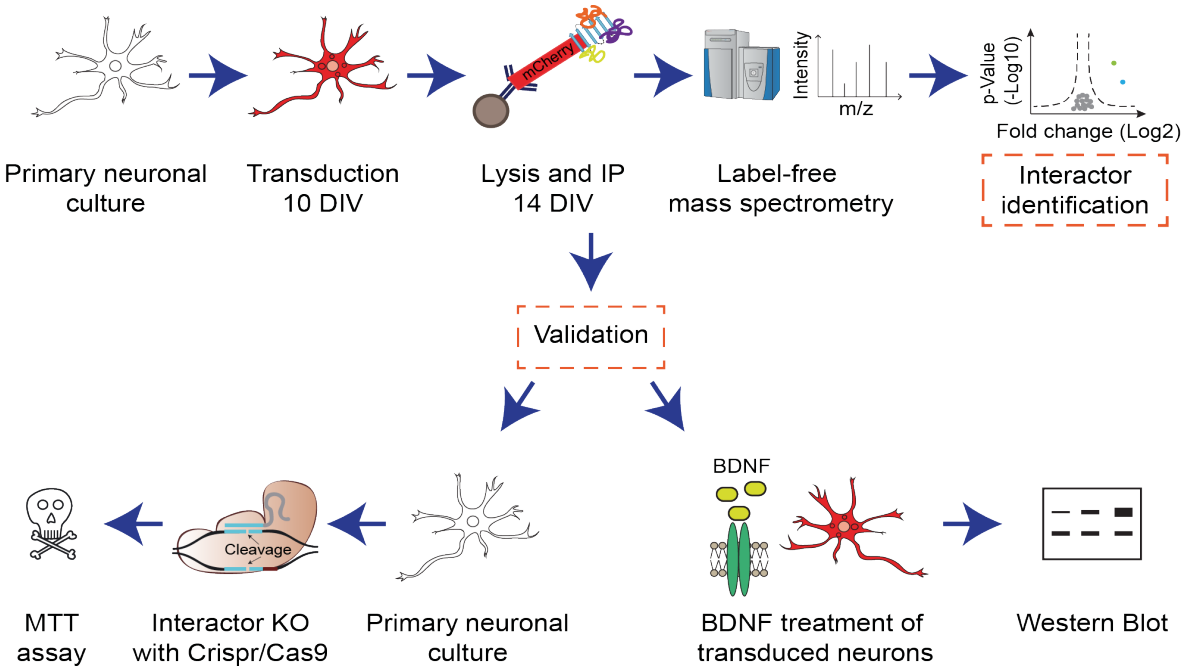

Figure 4.6: **Interactome analysis of β-sheet proteins.** Schematic representation of the process of interactome identification and further candidate validation approaches.

To identify the β-sheet interactomes we transduced E15 primary cortical neurons at 10 DIV (these viruses were kindly provided by Alexandra Lepier from the LMU viral vector facility). At an early stage of toxicity, 10+4 DIV, we lysed the cells and did an immunoprecipitation (IP) against mCherry. After further lysate processing, we used label-free mass spectrometry to identify the interactomes of β4mCherry, β17mCherry and β23mCherry. As before, we used mCherry expressing neurons as control and for normalization. Of note, all immunoprecipitations and mass spectometry analyses were performed by Daniel Hornburg. Figure 4.6 schematically summarizes the procedures

for interactome identification and further experiments based on the identified protein interactors.

We identified ninety-eight different proteins which interacted significantly with the β-sheet proteins in comparison to mCherry. Table 4.1 lists all these interactors, including the enrichment for each of the β-sheet proteins and the corresponding p-value. Moreover, the list has been sorted from highest to lowest enrichment for β23mCherry, and color-coded depicting highest enrichment in green and lowest in red.

Interestingly, we identified several common interactor proteins, as well as proteins specifically interacting with some of the β-sheet proteins (Fig.4.7 A). In addition, we analyzed the content of intrinsically disordered regions (IDR) of the significant interactors versus all proteins detected. IDRs are polypeptide segments having low aminoacid sequence complexity, that do not fold into a stable tertiary structure, and often act as critical hubs in protein interaction networks [209]. Proteins with high IDR content are prone to interaction and coaggregation [210]. Consistently, we detected an enrichment of low complexity aminoacid sequences in the population of β-sheet protein interactors (Fig.4.7 B).

Furthermore, gene ontology (GO) annotation [211] of the interactors revealed that these proteins are involved in a wide variety of cellular functions. Annotation enrichment classification [212] particularly highlighted their involvement in kinase signaling, cell morphology, cellular transport, and synaptic transmission (Fig. 4.7 C).

Finally, we also quantified the total proteomes of mCherry and β-sheet protein-expressing primary neurons. Importantly, we detected that the protein levels of almost all β-sheet interactors were unchanged in comparison to their expression levels in mCherry-expressing neurons. Therefore, their interaction with the β-sheet proteins was not caused by an augmentation in protein availability. Notably, artificial β-sheet protein expression lead to changes in the expression levels of some proteins, which we detected to be mostly in response to β23mCherry expression. Most of these proteins were related to metabolic processes (Table 4.2). Interestingly, we measured a downregulation of Sorl1 receptor, which has previously been genetically linked to AD [213, 214]. Moreover, other interesting changes in protein expression which we detected were the upregulation of the presynaptic protein synaptophysin, and the upregulation

of Ubl5, a protein linked to extended lifespan in *C.elegans* [215].

Interactome results		mCherry vs B23mCherry		mCherry vs B4mCherry		mCherry vs B17mCherry	
Gene names	Protein names	p-value (-log10)	Fold change (log2)	p-value (-log10)	Fold change (log2)	p-value (-log10)	Fold change (log2)
Ap3m1	AP-3 complex subunit mu-1	1.63	-6.50	1.67	-6.68	0.86	-4.71
Mapk15	Mitogen-activated protein kinase 15	3.39	-6.14	0.00	0.00	0.00	0.00
Ddn	Dendrin	3.23	-5.95	0.00	0.00	0.00	0.00
C2cd2l	C2 domain-containing protein 2-like	2.52	-5.78	1.83	-2.23	1.49	-1.52
Hcfc1	Host cell factor 1	2.41	-5.61	0.81	-1.63	1.43	-1.75
Znf532	Zinc finger protein 532	3.45	-5.06	0.00	0.00	2.30	-2.17
Tpd52l2	Tumor protein D54	2.49	-5.02	1.95	-2.26	1.62	-1.85
Iqsec3	IQ motif and SEC7 domain-containing protein 3	2.77	-4.60	0.00	0.00	0.00	0.00
Nfrkb	Nuclear factor related to kappa-B-binding protein	3.32	-4.48	2.75	-3.14	1.67	-2.85
Ccdc88a	Girdin	2.55	-4.38	1.14	-1.40	3.24	-3.66
Tab1	TGF-beta-activated kinase 1 and MAP3K7-binding protein 1	3.39	-4.31	3.00	-3.38	3.99	-4.21
Nyap1	Neuronal tyrosine-phosphorylated phosphoinositide-3-kinase adapter 1	2.95	-4.28	0.00	0.00	0.00	0.00
Magi2	Membrane-associated guanylate kinase	3.57	-4.28	0.00	0.00	0.00	0.00
Fry	Protein furry homolog	2.13	-4.15	2.32	-2.67	3.43	-3.90
Sestd1	SEC14 domain and spectrin repeat-containing protein 1	4.96	-3.96	5.33	-3.35	3.12	-3.05
Tab2	TGF-beta-activated kinase 1 and MAP3K7-binding protein 2	2.10	-3.89	0.00	0.00	3.61	-4.31
Mpst	3-mercaptopyruvate sulfurtransferase	4.68	-3.69	4.73	-3.59	4.61	-3.68
Mark4	MAP/microtubule affinity-regulating kinase 4	4.00	-3.63	3.43	-3.37	4.27	-3.24
Map3k7	Mitogen-activated protein kinase kinase kinase 7	3.40	-3.57	2.44	-3.06	3.64	-3.83
Myo9a	Unconventional myosin-IXa	2.27	-3.49	0.00	0.00	0.00	0.00
Nacad	NAC-alpha domain-containing protein 1	2.35	-3.48	0.00	0.00	0.00	0.00
Lrrc49	Leucine-rich repeat-containing protein 49	2.24	-3.44	0.00	0.00	0.00	0.00
Csnk2a2	Casein kinase II subunit alpha	3.83	-3.41	3.14	-3.13	3.08	-3.20
Dzank1	Double zinc ribbon and ankyrin repeat-containing protein 1	1.85	-3.37	0.67	1.01	0.62	-0.56
Aimp1	Aminoacyl tRNA synthase complex-interacting multifunctional protein 1	2.70	-3.31	0.00	0.00	0.00	0.00
Emsy	Protein EMSY	2.86	-3.31	0.00	0.00	0.00	0.00
Hectd4	HECT domain E3 ubiquitin protein ligase 4	1.20	-3.29	1.71	-4.08	1.21	-3.18
Ank\$1b	Ankyrin repeat and sterile alpha motif domain-containing protein 1B	2.80	-3.22	0.00	0.00	0.00	0.00
Dnmt3a	DNA (cytosine-5)-methyltransferase 3A	2.01	-3.14	1.96	-2.96	3.21	-3.61
Lrrc7	Leucine-rich repeat-containing protein 7	1.17	-3.07	1.51	-3.22	0.00	0.00
Sipa1l1	Signal-induced proliferation-associated 1-like protein 1	1.41	-3.02	0.00	0.00	0.69	-1.72
Lzts1	Leucine zipper putative tumor suppressor 1	2.83	-2.89	0.00	0.00	0.00	0.00
Pafah1b2	Platelet-activating factor acetylhydrolase IB subunit beta	0.97	-2.88	0.70	-2.68	1.03	-3.00
Bag6	Large proline-rich protein BAG6	1.09	-2.82	0.51	-1.58	1.61	-3.33
Iqsec1	IQ motif and SEC7 domain-containing protein 1	1.97	-2.68	1.64	-2.34	1.58	-2.03
Magi3	Membrane-associated guanylate kinase	2.47	-2.62	0.00	0.00	0.00	0.00
Elp4	Elongator complex protein 4	3.48	-2.62	2.99	-2.20	3.24	-2.40
Dnm2	Dynamin-2	0.98	-2.59	0.83	-2.35	0.80	-2.41
Mtch1	Mitochondrial carrier homolog 1	1.05	-2.48	1.09	-2.55	1.24	-2.86
Cep170b	Centrosomal protein of 170 kDa protein B	0.71	-2.47	0.90	-2.53	1.35	-3.52
Kif21a	Kinesin-like protein KIF21A	2.50	-2.47	0.00	0.00	0.00	0.00
Sugt1	Suppressor of G2 allele of SKP1 homolog	2.18	-2.36	1.31	-1.91	2.57	-3.48
Sec24b	SEC24 Homolog B	1.11	-2.34	0.00	0.00	0.79	-1.88
Agfg1	Arf-GAP domain and FG repeat-containing protein 1	0.98	-2.33	1.09	-2.41	1.09	-2.38
Dusp3	Dual specificity protein phosphatase 3	1.59	-2.29	1.57	-2.28	1.53	-2.29
Hist1h2a	Histone H2A type 1	1.29	-2.28	0.52	-1.98	1.72	-2.68
Stmn2	Stathmin-2;Stathmin	1.52	-2.19	1.17	-2.23	1.87	-2.33
Gcat	2-amino-3-ketobutyrate coenzyme A ligase, mitochondrial	2.39	-2.18	0.00	0.00	0.00	0.00
Stau2	Double-stranded RNA-binding protein Staufen homolog 2	1.91	-2.16	0.09	-0.14	0.11	0.06
Lxn	Latexin	1.15	-2.12	0.00	0.00	3.00	-2.98
Arpc5	Actin-related protein 2/3 complex subunit 5	0.82	-2.08	1.12	-2.69	1.18	-2.73
Slc39a7	Zinc transporter SLC39A7	1.13	-2.03	0.00	0.00	1.18	-2.06
Madd	MAP kinase-activating death domain protein	1.22	-2.02	0.09	-0.27	0.61	-1.05
Snrk	SNF-related serine/threonine-protein kinase	1.66	-1.99	0.63	1.23	1.66	-0.49
Dtna	Dystrobrevin alpha;Dystrobrevin	1.32	-1.98	1.42	-1.96	1.67	-2.26
Thy1	Thy-1 membrane glycoprotein	1.63	-1.95	0.00	0.00	0.00	0.00
Cdc42bpa	Serine/threonine-protein kinase MRCK alpha	1.33	-1.95	1.78	-2.36	1.74	-2.22
Rgs7	Regulator of G-protein signaling 7	1.28	-1.95	0.00	0.00	0.00	0.00
Chd8	Chromodomain-helicase-DNA-binding protein 8	1.56	-1.90	0.81	-2.02	0.00	0.00
Stmn3	Stathmin-3;Stathmin	1.39	-1.84	0.00	0.00	0.60	-1.27
Myl1;Myl3	Myosin light chain 1/3, skeletal muscle isoform;Myosin light chain 3	1.06	-1.82	3.01	-3.39	0.00	0.00
Mfn2	Mitofusin-2	1.78	-1.82	0.92	-1.52	2.33	-2.16
Gng2	Guanine nucleotide-binding protein G(I)/G(S)/G(O) subunit gamma-2	0.40	-1.76	1.16	-3.87	0.43	-1.78

Interactome results		mCherry vs B23mCherry		mCherry vs B4mCherry		mCherry vs B17mCherry	
Gene names	Protein names	p-value (-log10)	Fold change (log2)	p-value (-log10)	Fold change (log2)	p-value (-log10)	Fold change (log2)
Usp14	Ubiquitin carboxyl-terminal hydrolase 14;Ubiquitin carboxyl-terminal hydrolase	1.32	-1.71	2.46	-2.11	3.33	-2.72
Ogt	UDP-N-acetylglucosamine–peptide N-acetylglucosaminyltransferase 110 kDa subunit	2.30	-1.70	1.99	-0.51	2.51	-0.80
Grip1	Glutamate receptor-interacting protein 1	2.47	-1.59	1.66	-0.48	3.91	-1.84
Hecw1	E3 ubiquitin-protein ligase HECW1	1.32	-1.30	0.14	-0.19	2.02	-2.13
Ubl4a;Ubl4	Ubiquitin-like protein 4A	0.79	-1.22	0.58	-1.06	1.39	-2.04
Crmp1	Dihydropyrimidinase-related protein 1	3.58	-1.22	2.46	-1.20	3.55	-1.64
Arrb1	Beta-arrestin-1	0.57	-0.94	0.05	0.05	1.83	-1.85
Sec61b	Protein transport protein Sec61 subunit beta	0.00	0.00	2.09	-3.67	0.00	0.00
Fam65a	Protein FAM65A	0.00	0.00	0.00	0.00	3.24	-2.15
Aldh1b1	Aldehyde dehydrogenase X, mitochondrial	0.00	0.00	1.33	-3.38	0.00	0.00
Clcn3	H(+)/Cl(-) exchange transporter 3	0.00	0.00	2.92	-2.09	0.00	0.00
Ehd3	EH domain-containing protein 3	0.00	0.00	1.99	-2.74	0.00	0.00
Rdh14	Retinol dehydrogenase 14	0.00	0.00	0.00	0.00	1.89	-2.63
Gapvd1	GTPase-activating protein and VPS9 domain-containing protein 1	0.00	0.00	0.00	0.00	3.66	-2.93
Chordc1	Cysteine and histidine-rich domain-containing protein 1	0.00	0.00	0.00	0.00	1.74	-3.02
Ppp2r5d	Serine/threonine-protein phosphatase 2A 56 kDa regulatory subunit delta isoform	0.00	0.00	1.03	-2.21	1.09	-2.32
Utrn	Utrophin	0.00	0.00	0.00	0.00	1.99	-3.75
Wnk2	Serine/threonine-protein kinase WNK2	0.00	0.00	1.27	-2.05	1.39	-2.32
Flii	Protein flightless-1 homolog	0.00	0.00	2.43	-2.18	0.00	0.00
Ndufb10	NADH dehydrogenase [ubiquinone] 1 beta subcomplex subunit 10	0.00	0.00	3.85	-3.46	0.00	0.00
Agpat1	1-acyl-sn-glycerol-3-phosphate acyltransferase alpha	0.00	0.00	1.48	-2.14	1.23	-2.22
Nup153	Nucleoporin 153	0.00	0.00	2.68	-2.15	0.00	0.00
Tpr	Nucleoprotein TPR	0.00	0.00	1.59	-3.66	0.00	0.00
Ddx19a;Ddx19b	ATP-dependent RNA helicase DDX19A	0.00	0.00	0.56	-2.78	0.82	-3.38
Mvd	Diphosphomevalonate decarboxylase	0.00	0.00	2.32	-2.29	0.00	0.00
Dyrk1a	Dual specificity tyrosine-phosphorylation-regulated kinase 1A	0.00	0.00	3.78	-1.68	0.00	0.00
Nme1	Nucleoside diphosphate kinase A	0.00	0.00	0.00	0.00	4.11	-3.86
Scamp3	Secretory carrier-associated membrane protein 3	0.00	0.00	0.83	-1.57	2.31	-2.12
Csnk1d	Casein kinase I isoform delta	0.00	0.00	0.00	0.00	3.01	-2.39
Oxa1l	Mitochondrial inner membrane protein OXA1L	0.00	0.00	2.03	-2.39	3.48	-3.38
Sncb	Beta-synuclein	0.00	0.00	1.31	-3.15	0.00	0.00
Ccar2	Cell cycle and apoptosis regulator protein 2	0.13	0.08	0.16	0.09	2.40	-1.47

Table 4.1: **Interactome of β-sheet proteins.** List of significantly enriched interactors. Color code ranges from dark red for no enrichment to dark green for highest enrichment. The cutoff value for enrichment was set at log2$\leq$-1, which equals to at least a two-fold enrichment. The value for significance was (-log10)$\geq$1.3, which equals to a p value$\leq$0.05.

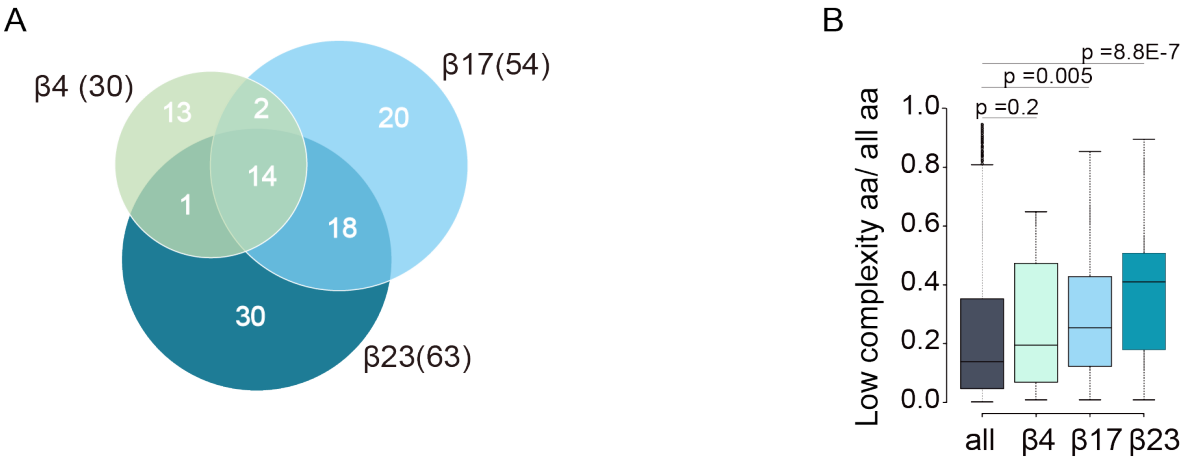
A
β4 (30)
β17(54)
β23(63)
13
2
20
14
1
18
30
B
p =8.8E-7
p =0.005
p =0.2
Low complexity aa/ all aa
1.0
0.8
0.6
0.4
0.2
0.0
all
β4
β17
β23

C

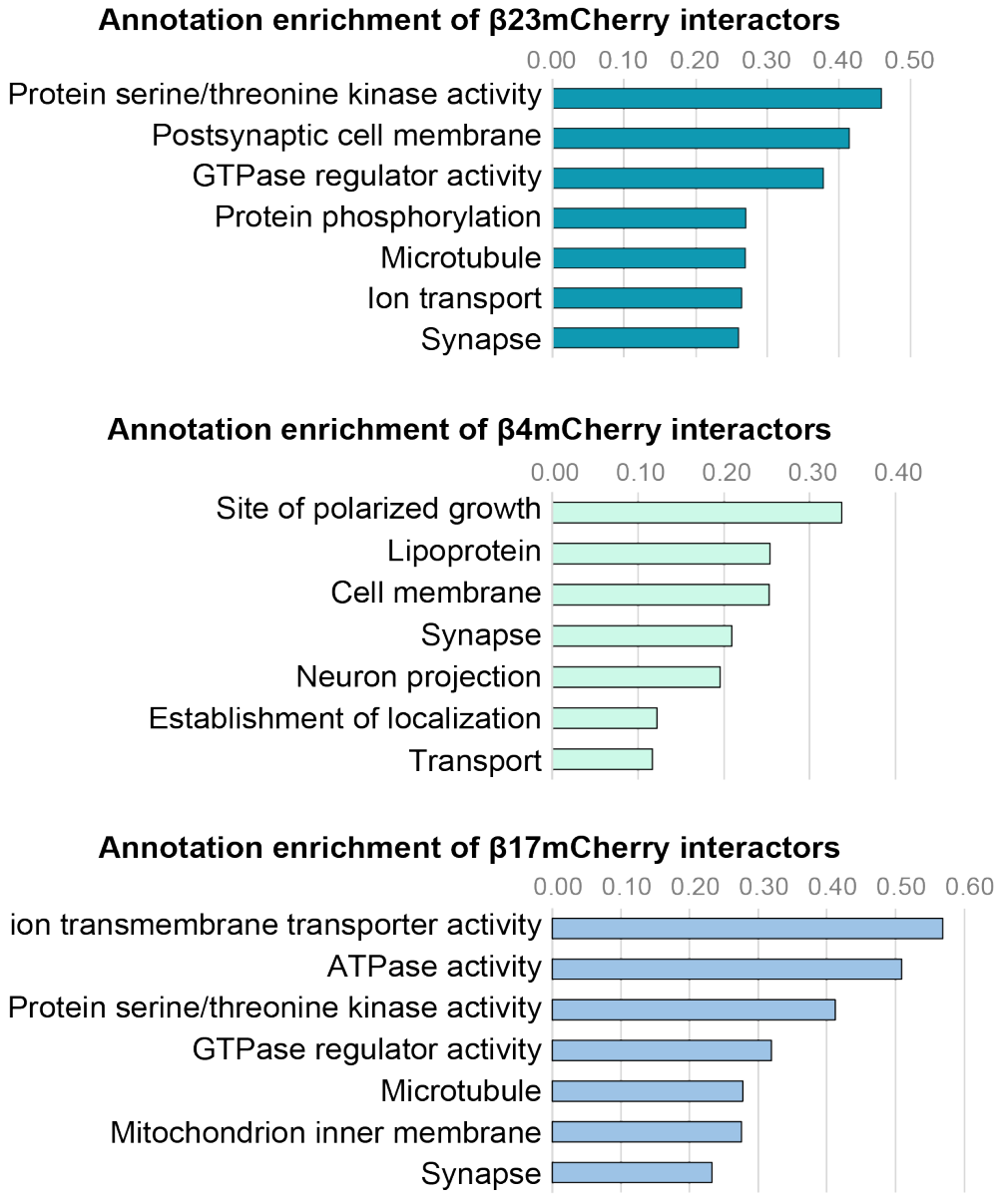
Annotation enrichment of β23mCherry interactors
0.00 0.10 0.20 0.30 0.40 0.50
Protein serine/threonine kinase activity
Postsynaptic cell membrane
GTPase regulator activity
Protein phosphorylation
Microtubule
Ion transport
Synapse
Annotation enrichment of β4mCherry interactors
0.00 0.10 0.20 0.30 0.40
Site of polarized growth
Lipoprotein
Cell membrane
Synapse
Neuron projection
Establishment of localization
Transport
Annotation enrichment of β17mCherry interactors
0.00 0.10 0.20 0.30 0.40 0.50 0.60
Metal ion transmembrane transporter activity
ATPase activity
Protein serine/threonine kinase activity
GTPase regulator activity
Microtubule
Mitochondrion inner membrane
Synapse

Figure 4.7 *(previous page)*: **Interactome charachterization.** (A) Venn diagram depicting the number of interactors identified for each β-sheet protein. These interactors were significantly enriched in the β-sheet protein samples in comparison to the mCherry samples. N=4 independent experiments. (B) Measurements of low complexity aminoacid sequence content in β-sheet interactor proteins in comparison to all identified proteins. Two-sample Wilcoxon test. (C) Annotation enrichment for β-sheet interactors. These annotations represent a combination of gene ontology (GO) [216] and Kyoto Encyclopedia of Genes and Genomes (KEGG) enrichments [217].

Proteome results: proteins with altered expression levels		mCherry vs B23mCherry		mCherry vs B4mCherry		mCherry vs B17mCherry	
Gene names	Protein names	p-value (-log10)	Fold change (log2)	p-value (-log10)	Fold change (log2)	p-value (-log10)	Fold change (log2)
Sorl1	Sortilin-related receptor	1.76	4.56	0.78	0.32	0.52	1.36
Rpia	Ribose-5-phosphate isomerase	1.29	2.81	0.19	0.80	1.04	2.41
Epha5	Ephrin type-A receptor 5	5.70	2.69	1.71	0.35	1.30	0.42
Oplah	5-oxoprolinase	2.44	2.63	0.82	1.40	0.22	0.12
Kcnd2	Potassium voltage-gated channel subfamily D member 2	1.88	2.43	1.25	-0.40	0.63	-0.26
Mpdu1	Mannose-P-dolichol utilization defect 1 protein	1.83	2.41	0.35	0.24	0.15	0.14
Hist1h2a	Histone H2A type 1	3.51	2.15	0.13	-0.21	0.20	0.41
Dnajc16	DnaJ homolog subfamily C member 16	2.51	1.92	0.06	0.12	0.02	-0.03
Nkiras2	NF-kappa-B inhibitor-interacting Ras-like protein 2	3.43	1.81	0.70	1.08	0.05	-0.03
Plxnb1	Plexin-B1	3.23	1.66	0.41	0.14	0.62	0.22
Sec61b	Protein transport protein Sec61 subunit beta	0.89	1.47	0.51	0.30	0.14	0.10
Igfbp5	Insulin-like growth factor-binding protein 5	0.00	0.00	4.07	-2.29	0.00	0.00
Pcyt1b	Choline-phosphate cytidylyltransferase B	1.21	-0.23	6.08	3.01	0.64	1.14
Tab1	TGF-beta-activated kinase 1 and MAP3K7-binding protein 1	1.23	-0.90	0.27	-0.39	0.58	-0.55
Lxn	Latexin	0.50	-1.04	0.50	-1.03	0.58	-1.17
Scpep1	Retinoid-inducible serine carboxypeptidase	2.64	-1.78	0.00	0.00	0.00	0.00
Slc39a7	Zinc transporter SLC39A7	1.57	-1.84	1.07	-1.33	1.44	-1.72
Taco1	Translational activator of cytochrome c oxidase 1	2.54	-1.86	0.00	0.00	0.00	0.00
Tenm3	Teneurin-3	2.01	-2.19	0.00	0.00	0.00	0.00
Snrpc	U1 small nuclear ribonucleoprotein C	3.29	-2.37	0.00	0.00	0.00	0.00
Celf5	CUGBP Elav-Like Family Member 5	2.86	-2.61	0.00	0.00	1.43	-1.71
Ubl5	Ubiquitin-like protein 5	1.72	-2.96	1.66	-2.87	1.43	-2.50
Syp	synaptophysin	4.91	-5.13	0.00	0.00	0.00	0.00

Table 4.2: **Changes in proteome with β-sheet protein overexpression.** List of proteins the expression of which was changed in β-sheet *vs* mCherry expressing neurons. Color code ranges from dark red for highest downregulation in expression to dark green for highest upregulation. The cutoff value for enrichment was set at log2$\leq \pm 1$, which equals to at least a two-fold enrichment. The value for significance was (-log10)$\geq$1.3, which equals to a p value$\leq$0.05.

4.3 Artificial β-sheet proteins interact with essential cellular proteins

Interaction with β-sheet proteins might prevent other proteins from fulfilling their endogenous functions, perhaps leading to similar loss of function effects as a protein KO. To investigate this possibility, we selected 19 interactors for further experimental validation (Table 4.3). Our main candidate selection criteria were: reported links to neurodegeneration, the candidate's role in critical pathways for NDs, and their novelty.

We made use of a Crispr/Cas9 screening approach for validation, thereby determining which candidates were necessary for neuronal survival. To that aim, we transduced WT primary cortical neurons with lentivirus to coexpress the single guide RNA (sgRNA) and Cas9 [218]. For each selected candidate, we used three different sgRNAs for reproducibility and to rule out possible off-target effects. In our initial preliminary experiments, we transduced at 2 DIV, which caused an unexpected proliferation of what looked like progenitors from the cortical hem. Therefore, we decided to transduce at 10 DIV when cells are more mature, by which the proliferation was prevented (data not shown). Two weeks after transduction with the sgRNA/Cas9 virus, time to enable protein candidate degradation [219], we analyzed neuronal viability by MTT assay. We normalized neuronal survival to a negative control condition, in which neurons were transduced with a LV expressing Cas9 and a sgRNA which did not target any genomic sequence. In addition, BDNF KO was used as a positive control for neuronal death in all experiments.

We detected that KO of several candidates led to a significant reduction in neuronal survival, as shown both in a heat map and a bar graph in Figure 4.8 B, C. The KO of candidates Ccdc88a, Aimp1, and Stmn2 led to the strongest effect in viability, since all three guides caused significant neuronal death. Also remarkable were the KOs of candidates Ap3m1, Hcfc1, Aldh1b, Stmn3, and Clcn3, which also led to significant reductions in neuronal viability with one or two guides. Overall, these data suggested that β-sheet proteins interacted with essential cellular proteins, possibly disturbing their correct function.

Gene names	Involved in	Link to neurodegeneration	Interactor of
Ap3m1	Trafficking to lysosomes	None, but autophagy impairment has been linked to several diseases, including AD, PD, and HD [220].	Common
Hcfc1	Transcription coactivator activity, cell cycle control	Downregulated in dopaminergic neurons in PD model [221]. β-sheet interactor in Hek293 cells [81].	Common
Ccdc88a	Guanidine exchange factor activity, involved in controling cell migration, survival, autophagy, cell polarity, endocytosis	An autosomal recessive mutation causes progressive encephalopathy with odema (PEHO) like syndrome in humans [222]. β-sheet interactor in Hek293T cells [81].	Common
Aimp1	Transcription	Enriched in insoluble fraction of brain proteome in MCI and symptomatic cases of AD [123]. Axon degeneration in motor neurons in Aimp1-KO mice [223]. Aimp1 causes neurodegenerative disease with infantile onset in humans [224].	β23
Lrrc7	Component of the post-synaptic density (PSD) of excitatory synapses. Required for normal synaptic spine architecture and function	Upregulated in frontal cortex of ALS patients [225]. Link to multiple sclerosis [226].	β23 and β4
Bag6	Chaperone	KO in mice is lethal, defects in apoptosis and proliferation in the brain [227]. Bag6 rescues PrP-induced apoptosis in cell culture [228].	Common
Dnm2	GTPase, associated with microtubulli, implicated in endocytosis and cell motility	Autosomal dominant mutations lead to neuromuscular disease [229].	Common
Stmn2, Stmn3	Neuronal growth, microtubule regulatory protein	Reduced protein levels in neocortex in AD patients [230]. Downregulated in Down's syndrome [231]. Genetic risk factor associated to prion disease [232].	Common
Stau2	Microtubule-dependent transport of neuronal RNA	Transcriptionally downregulated in AD, PD, HD, and ALS [233].	β23
Usp14	Ubiquitin hydrolase, regeneration of ubiquitin at the proteasome	Neuron-specific Usp14 transgenic rescues the phenotype of an ataxia model [234].	Common
Sec61b	Protein translocation at the ER membrane	Sec61a contributes to polyQ toxicity in Drosophila [235].	β4
Aldh1b1	Mitochondrial protein, oxidation of aldehydes	Aldh1a and Aldh2 linked to PD [236] [237].	β4
Clcn3	Voltage gated Chloride channel	Its deficiency leads to phenotypes similar to human neuronal ceroid lipofuscinosis [238].	β4
Ehd3	Endocytic transport	Regulates BACE1 transport, link to AD [239].	β4
Ppp2r5d	Protein phosphatase regulatory subunit	Knockout mice develop tauopathy and show sensorymotor defects [240].	β4 and β17
Dyrk1a	Protein phosphorilation	Risk factor for AD [241].	β4
Tpr	Nuclear pore complex, basket protein	Involved in nuclear export of N-terminal Htt [242].	β4
Sncb	Synaptic transmission	Associated with hippocampal axon pathology in both PD and dementia with Lewy bodies, not found in Lewy bodies [243].	β4

Table 4.3: Candidate selection

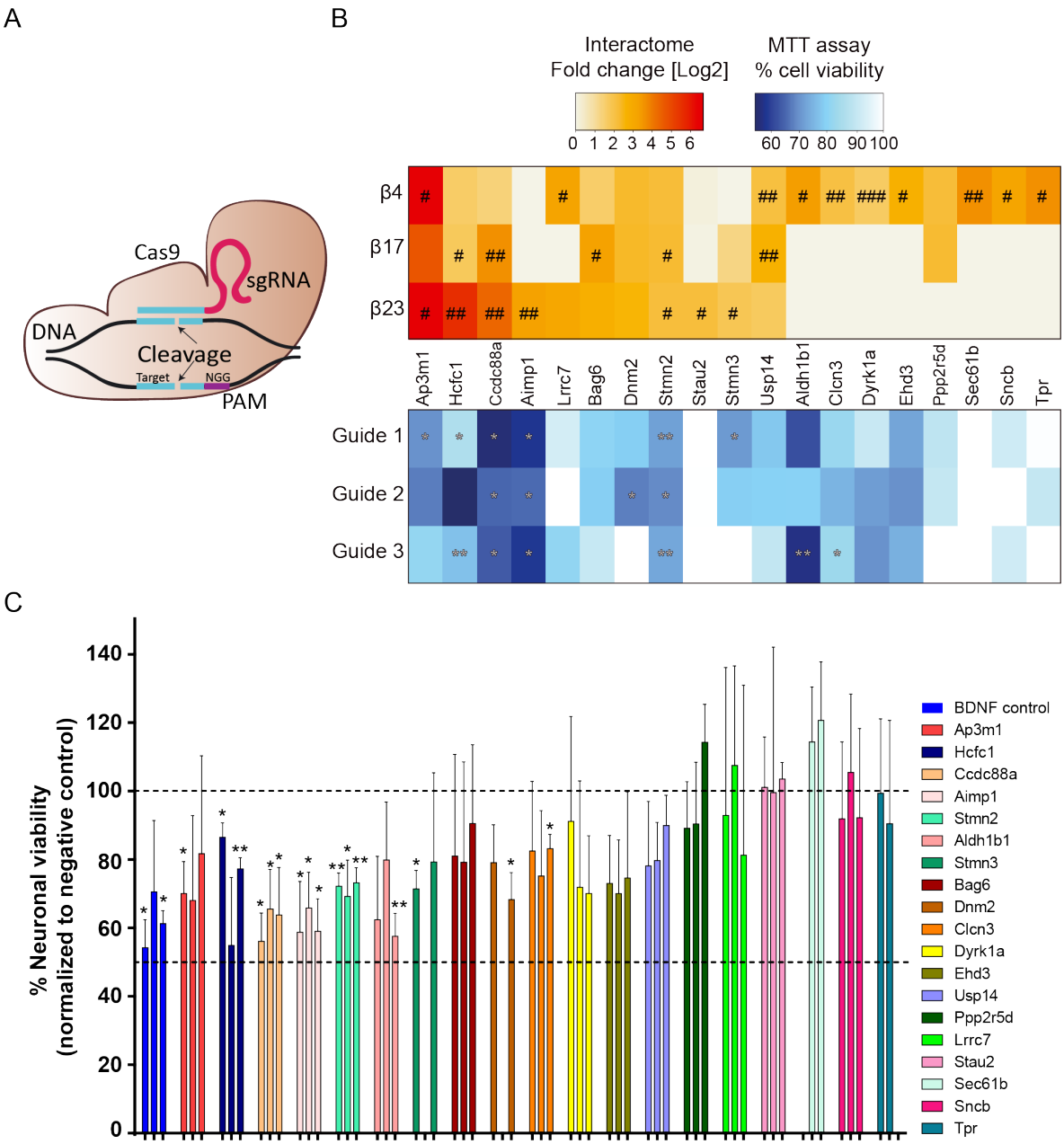
A
Cas9
sgRNA
DNA
Cleavage
Target
NGG
PAM
B
Interactome
Fold change [Log2]
0 1 2 3 4 5 6
MTT assay
% cell viability
60 70 80 90 100
β4
β17
β23
Ap3m1
Hcfc1
Ccdc88a
Aimp1
Lrrc7
Bag6
Dnm2
Stmn2
Stau2
Stmn3
Usp14
Aldh1b1
Clcn3
Dyrk1a
Ehd3
Ppp2r5d
Sec61b
Sncb
Tpr
Guide 1
Guide 2
Guide 3
C
% Neuronal viability
(normalized to negative control)
0
20
40
60
80
100
120
140
BDNF control
Ap3m1
Hcfc1
Ccdc88a
Aimp1
Stmn2
Aldh1b1
Stmn3
Bag6
Dnm2
Clcn3
Dyrk1a
Ehd3
Usp14
Ppp2r5d
Lrrc7
Stau2
Sec61b
Sncb
Tpr

Figure 4.8 *(previous page)*: **Knock-out of specific β-sheet protein interactors in cortical neurons.** (A) Schematic representation of the used Crispr/Cas9 system. The Cas9 protein, which contains two nuclease domains, introduces double-stranded breaks (DSB), at sites defined by the sgRNA. Cas9 also requires that a short conserved sequence, known as Protospacer adjacent motif (PAM), follows immediately 3' of the target complementary sequence. DSBs can be repaired by the cellular non-homologous end joining (NHEJ) pathway, resulting in insertions and/or deletions which disrupt the targeted locus. (B) Heatmaps displaying the enrichment of selected candidates in the interactome (grey-red) and the cell viability results in MTT assays after Crisr/Casp9 KO of the candidate (white-blue) in E15.5 cortical neurons. For the viability results: N=3 independent experiments, Unpaired t-test + Welch's correction. ♯ p-value < 0.05, ♯♯ p-value < 0.01, ♯♯♯ p-value < 0.001. (C) Bar graph representation of the cell viability results in MTT assays after Crisr/Casp9 KO of the candidate. Same data as white-blue heatmap, with the addition of the BDNF control.

4.3.1 Ccdc88a (girdin) overexpression does not rescue β-sheet toxicity in primary neurons

One essential protein interacting with the β-sheet proteins in cortical neurons and in Hek293T cells [204] was Ccdc88a, also known as girdin. Girdin is an actin-binding protein which can be phosphorylated by Akt [244], and is ubiquitously expressed in mammalian cells. Moreover, girdin acts as a guanidine exchange factor (GEF) and integrates signals from various ligand-activated receptor types, such as receptor tyrosine kinases and GPCRs [245]. This integrative position involves girdin in a variety of cellular functions, including: cell migration, survival, autophagy, cell polarity, and endocytosis [246, 247]. Most interesting, girdin KO mice die at P25, and a homozygous frameshift mutation in the girdin gene creating a TAG stop codon causes progressive encephalopathy with odema (PEHO) like syndrome in humans [222]. Thus, we hypothesized that girdin's loss of function by its interaction with the β-sheet proteins might contribute to neuronal cytotoxicity. That being the case, girdin overexpression could improve neuronal viability.

To test this, we coexpressed a GFP-tagged C-terminal fragment of mouse girdin (aminoacids 1122 to 1871) with either β4mCherry or β23mCherry using lentivirus. GFP coexpressed with the β-sheet proteins was used as a control, and we analyzed neuronal viability by MTT assay 10 and 14 days after transduction. Moreover, we thought that girdin expression levels could play a role in rescuing toxicity and we therefore used three different amounts of girdin virus to try to rescue toxicity: 0.25, 0.5, and 1 μl/well. However, girdin overexpression did not rescue neuronal viability in any condition (Fig.4.9 A).

To test if the use of the C-terminal fragment was not enough to rescue toxicity because of the lack of girdin's microtubule binding domain, which is at the N-terminus, we included a condition in which we coexpressed full-length girdin. However, neither the fragment nor the full-length protein improved neuronal viability in our experimental conditions (Fig.4.9 A).

Furthermore, we also checked the expression levels of mCherry, β4mCherry, and β23mCherry by Western blot. Coexpression of these proteins with GFP resulted in a slight reduction in their expression. However, coexpression with the highest amount

of C-terminal fragment girdin resulted in stronger expression reduction (Fig.4.9 B), especially of mCherry and β4mCherry. Hence the trend towards improved cell viability observed in the β4mCherry expressing neurons (Fig.4.9 A), was probably due to its lower expression levels.

A plausible explanation for the downregulation in expression that we detected might be that both β-sheets and girdin were expressed under the same promoter (human Synapsin1a promoter), most likely leading to a competition for transcription factors between the two constructs, and the consequent reductions in expression.

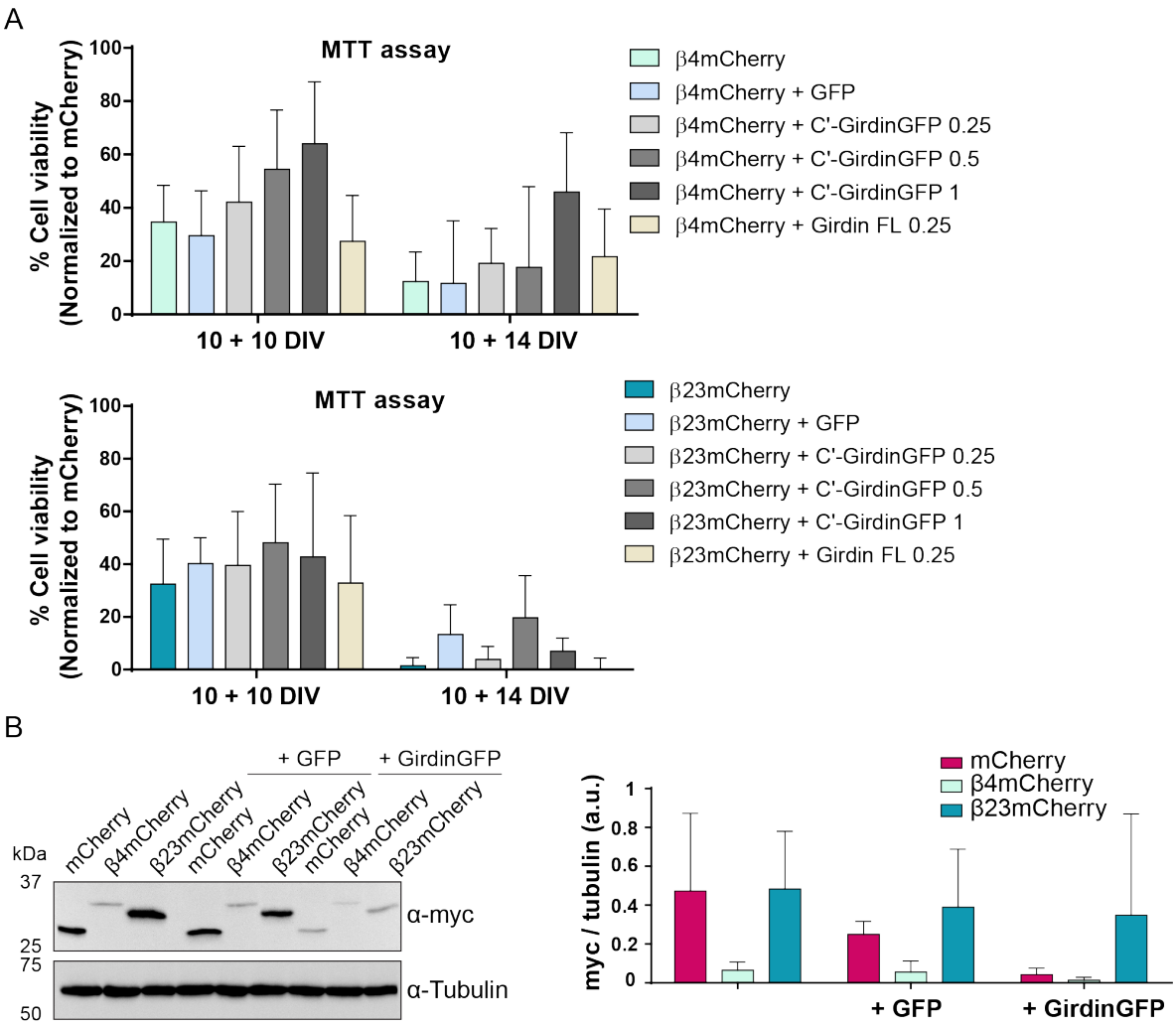

Figure 4.9: **Neuronal death caused by β-sheets is not prevented by Girdin overexpression.** (A) Neuronal viability measured by MTT assay. Neither overexpression of the C-terminal fragment of girdin (C'), nor the full-length (FL) girdin improved viability in presence of β4mCherry or β23mCherry. N=4. (B) Representative Western blot image and quantification of three experiments revealed that coexpression of girdin with mCherry or the β-sheet proteins resulted in their downregulation, respectively. E15.5 cortical neurons. N=3, time point 10+4 DIV.

4.4 Artificial β-sheet proteins might impair survival signaling

In our interactome data set in primary cortical neurons, one prominently enriched GO term was "Protein serine/threonine kinase activity" (Fig.4.7 C). Thus, we hypothesized that one of the mechanisms by which β-sheet proteins cause cytotoxicity is impairing kinase signaling. Consequently, as a secondary validation approach, we analyzed kinase-mediated survival signaling in β-sheet protein presence. In particular, we studied BDNF signaling and focused on Akt and Erk 1/2 phosphorylation as an indication of neuronal survival signaling activation.

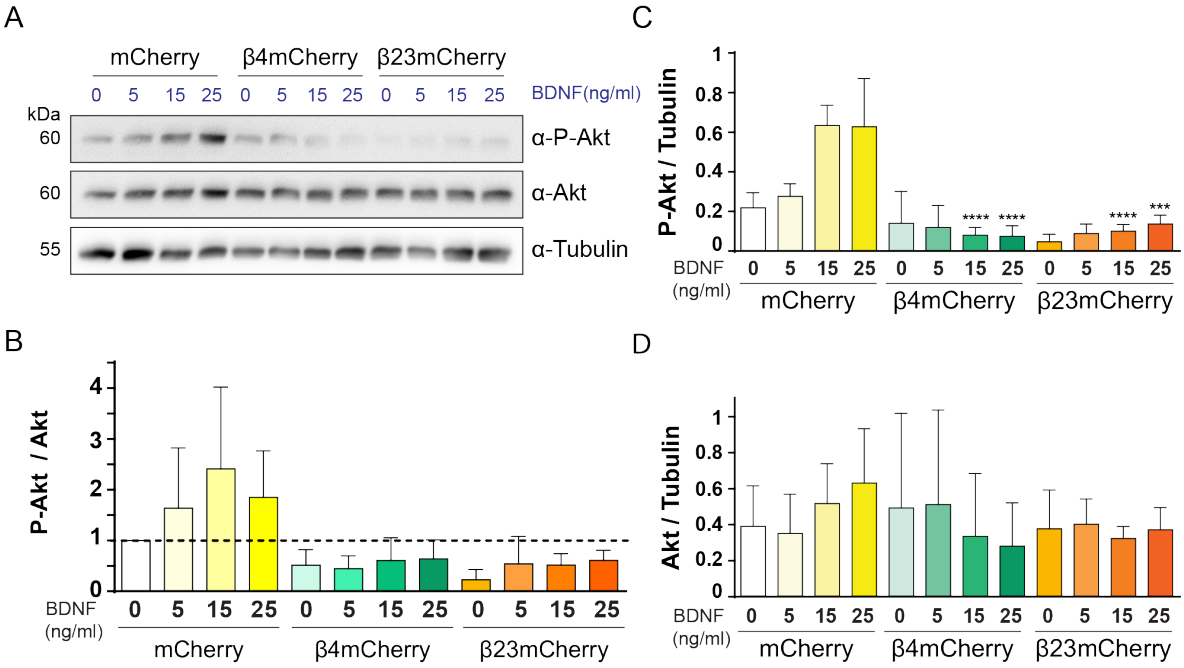

Figure 4.10: **Akt signaling is impaired by β-sheet protein expression.** (A) Representative image of a Western blot suggesting less P-Akt in β4mCherry and β23mCherry expressing neurons. 10+4 DIV LV-transduced E17.5 hippocampal neurons were treated with different concentrations of recombinant hBDNF for 30min and lysed afterwards. (B), (C), and (D) Quantifications of Western blot signals using ImageJ. N=3, One-way ANOVA + Tukey's multiple comparison test. Significance indicated in (C) refers to the difference in P-Akt levels among β4mCherry and β23mCherry expressing neurons to the respective counterpart condition in mCherry expressing neurons.

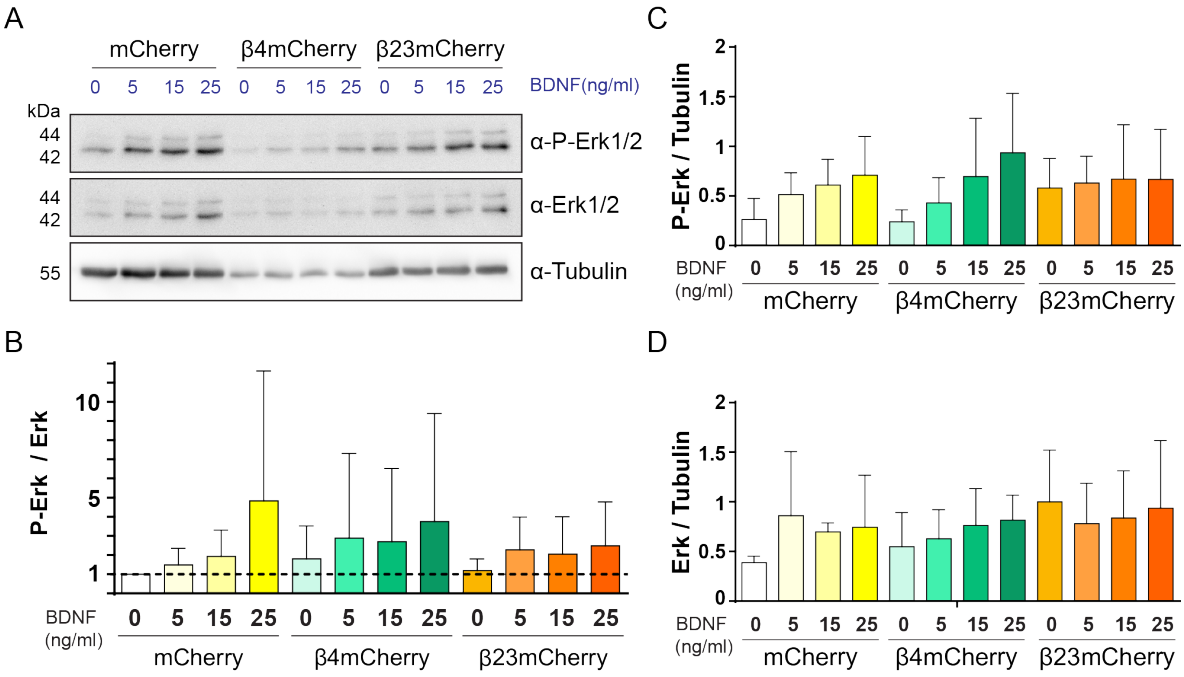

Figure 4.11: **Erk signaling might not be impaired by β-sheet protein expression.** (A) Image of a Western blot against P-Erk1/2 and Erk1/2. 10+4 DIV LV-transduced E17.5 hippocampal neurons were treated with different concentrations of recombinant hBDNF for 30min and lysed afterwards. (B), (C), and (D) Quantifications of Western blot signals using ImageJ. N=4, One-way ANOVA did not show any statistical differences.

Our experimental approach consisted of, first, transducing primary hippocampal neurons at 10 DIV. Four days after transduction, we applied a range of human BDNF (hBDNF) concentrations to the cells ranging from 0 to 25 ng/ml, for 30min. Then, we lysed the neurons and performed western blots. We first blotted against phosphorylated Akt or Erk1/2 (P-Akt, P-Erk1/2), stripped the membranes, and blotted against the non-phosphorylated proteins for signal normalization. In addition, as a loading control, we used tubulin.

Interestingly, we observed a trend towards a reduction in the ratio of P-Akt/Akt in β-sheet protein presence (Fig.4.10 A,B), although it was not significant to mCherry control. When normalizing P-Akt to Tubulin, the reduction in phosphorylated Akt in β-sheet protein presence in comparison to mCherry was very prominent. Moreover, we detected a BDNF dose-dependent effect in the control condition, but not in β-sheet protein expressing neurons (Fig.4.10 C). Alternatively, no significant differences in Akt levels were detected (Fig.4.10 D).

Conversely, no difference neither in P-Erk/Erk, nor in P-Erk levels, was detected between mCherry and β-sheet protein expressing neurons (Fig.4.11), suggesting a specific reduction in pro-survival P-Akt, but not P-Erk signaling. Nevertheless, the results we obtained for Erk signaling were highly variable and further experiments would be necessary.

Overall, our interactome analysis in primary neurons allowed us to identify both single proteins and pathways which might be affected in the presence of amyloid-like aggregating proteins.

4.5 Novel β23 transgenic mouse model

4.5.1 Broad β23 expression in the forebrain

In order to study gain of function toxicity caused by protein aggregation *in vivo*, we generated a novel transgenic mouse model with β23 expression. We generated a construct which consisted of the myc-tagged β23, separated from mCherry by an Frt-flanked IRES sequence. Thereby, mycβ23 and mCherry were expressed in the same cell, but translated separately. Mice in which mycβ23 and mCherry were expressed as separate proteins will be further referred to as unrecombined. In addition, the presence of Frt sites gave an additional possibility of excision of the IRES sequence, resulting in a mycβ23mCherry fusion construct. Therefore, mice in which mycβ23mCherry was expressed as a fused protein will be further referred to as recombined.

Moreover, the β23 transgene was placed under control of a tetracycline-inducible promoter (pTRE3G) consisting of 7 repeats of a 19 bp tet operator sequence located upstream of a minimal CMV promoter (Figure 4.12). This tetracycline inducible system allowed for temporal controlled β-sheet protein expression. Specifically, we made use of the Tet-OFF system to control expression: in absence of Doxycycline (Dox, a derivative of tetracycline which is a preferred effector [248]), the tTa protein can bind to the promoter and expression is activated. However, in presence of Dox, tTa cannot bind the promoter and expression is prevented [249]. Another widely used strategy in mouse genetics is the Tet-ON system, in which the reverse tTa protein (rtTa) is capable of binding the operator only if bound by a tetracycline [250].

To induce expression in the brain, specifically in the forebrain, we crossed our β23 mice to the broadly used CamkIIα:tTa line [205], whithout administering Dox to the mice. These mice will be further referred to as CamK;β23. Then we analyzed the brains of double transgenic mice and controls to identify the expression pattern of the new mouse line. To that aim, we performed immunostainings a the age of 4.5-5 months. As observed via mCherry staining, expression was as expected restricted to the forebrain (Fig.4.13 A). Moreover, if we focused on regions which are especially important in NDs, we observed that in the neocortex mCherry-positive cells were detectable in all layers. In the hippocampus, we detected expression only in the CA1 (Fig.4.13 A'), but not in CA3 or the dentate gyrus. Moreover, conspicuous mCherry expression was detected in the striatum (Fig.4.13 A").

Subsequently, to make sure that β23 was expressed as well, we coimmunostained for myc and mCherry. We could clearly identify several mycβ23 positive cells in the neocortex of double transgenic mice. On the contrary, neither myc nor mCherry expression were detected in single transgenic β23+ mice, demonstrating the absence of leakyness in expression (Fig.4.13 B). Of note, co-staining revealed many more mCherry-positive cells than double myc and mCherry-positive cells. In addition, we did not detect clear myc staining neither in the hippocampus nor in the striatum. Although cells should be positive for both stainings, these differences in expression patterns may be explained by differential penetrance of the antibodies, or by non-stoichiometric expression of β23 and mCherry. Finally, due to the CamkIIα-driven expression, we expected expression of our transgene only in neurons, but not in glia. To analyze if that was the case, we stained against mCherry and the neuronal marker NeuN. Thereby, we did not detect any mCherry positive, NeuN negative cell, confirming the solely neuronal expression (Fig.4.14).

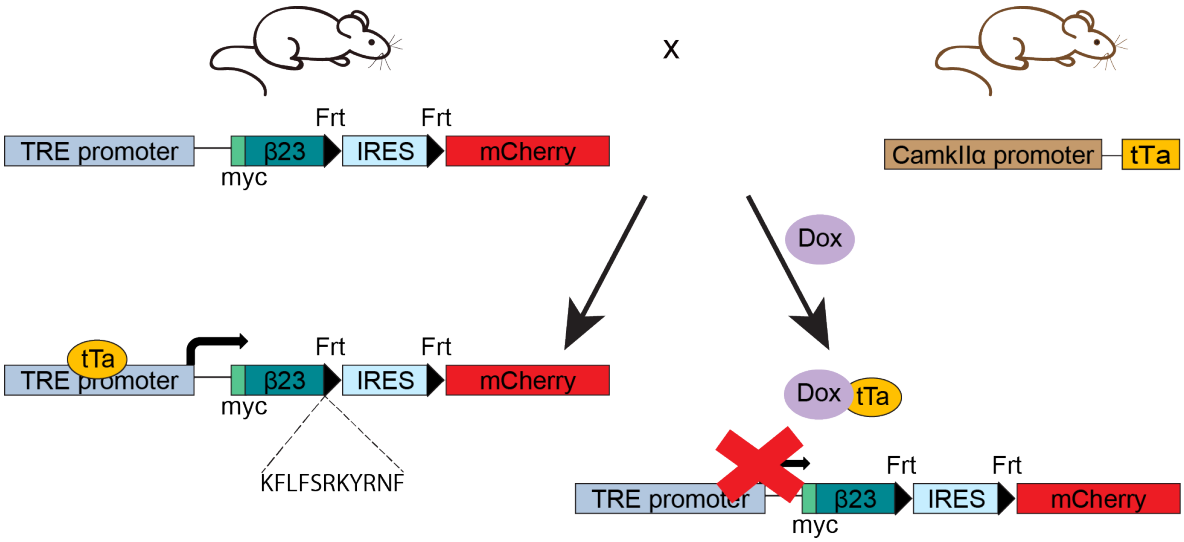

Figure 4.12: **β23 expression strategy.** Schematics depicting the transgene contained by the β23 mice. Of note, the Frt DNA sequence is in frame with the rest of the peptide and translates into the aminoacid sequence highlighted by the dashed lines. To induce β23 expression, mice need to be crossed to tTa mice (CamkIIα:tTa mice in this case). In absence of Dox, the tTa protein can bind to the TRE promoter and expression is induced, whereas administering Dox to mice prevents tTa binding and β23 expression is repressed.

A

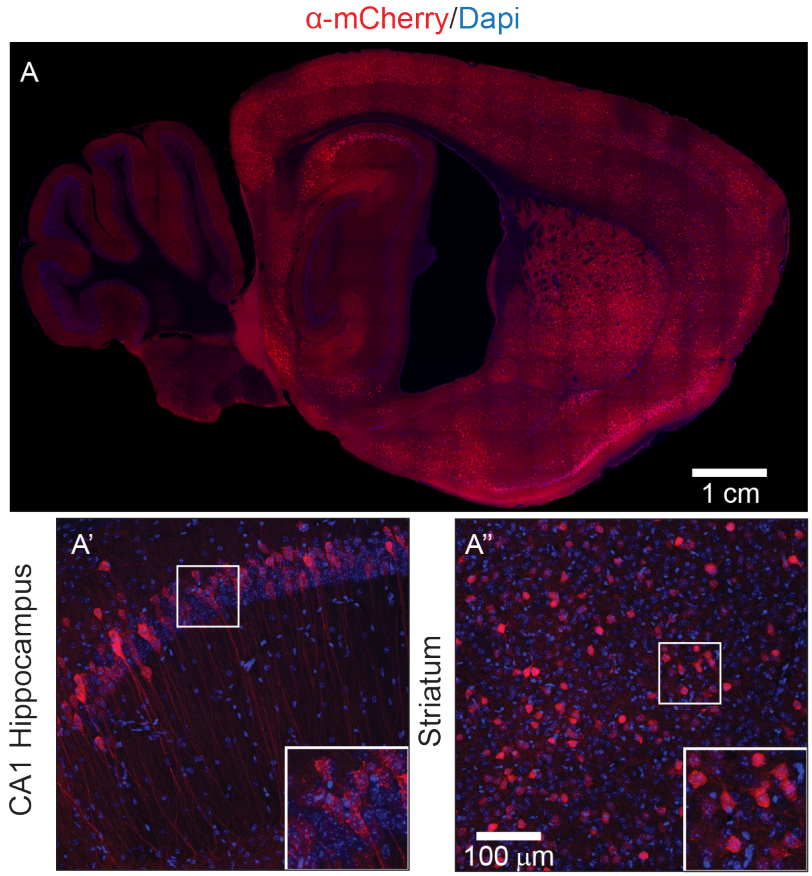
α-mCherry/Dapi
A
1 cm
A'
A''
CA1 Hippocampus
Striatum
100 µm

B

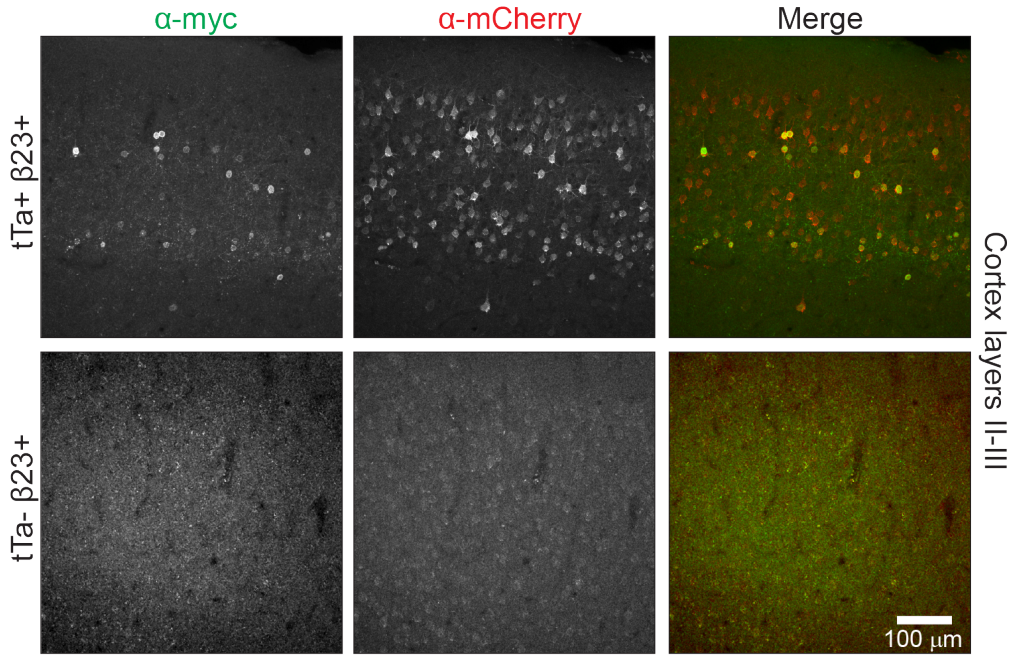
α-myc
α-mCherry
Merge
tTa+ β23+
tTa- β23+
Cortex layers II-III
100 µm

Figure 4.13 *(previous page)*: **β23 expression pattern in CamK;β23 unrecombined mice is restricted to forebrain.**(A) Immunostaining showing mCherry expression in the brain of unrecombined double transgenic mice at 20 weeks of age. (B) Co-staining against myc and mCherry in the cortex of a double transgenic mouse and a single transgenic β23+ control. No staining was visible in the control, indicating no leakyness in β23 expression.

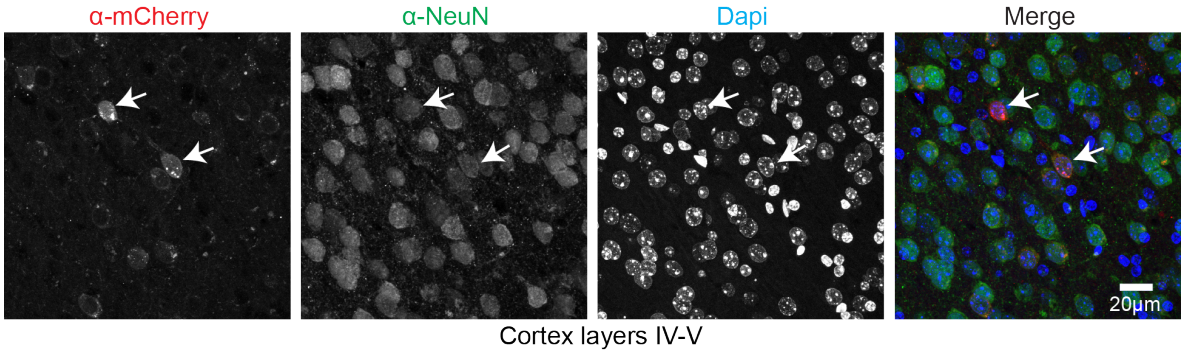

Figure 4.14: **β23 is expressed only in neurons.** Immunostaining depicting colocalization of mCherry positive cells with neuronal marker NeuN (arrows) in the cortex of a double transgenic CamK;β23 mouse of 40 weeks of age. Different cortical regions of at least three mice were visually inspected.

4.6 β23 causes brain atrophy in CamK;β23 mice

Observing the brains of positive double transgenic CamK;β23 mice and their littermates at macroscopic level, we detected that they differed in size (Fig.4.15 A). We therefore measured the brain weight at different ages. At the early age of one month, CamK;β23 unrecombined mice had slightly smaller brains than their littermate controls. Indeed, the difference was significant only between non-transgenic and double transgenic mice. With increasing age, the differences in brain weight of double transgenic CamK;β23 mice compared to all other three genotypes became more pronounced (Fig.4.15 B). Although brains from non-transgenic, β23 single transgenic, and CamkIIα:tTa single transgenic mice kept on growing with age, that was not the case for the brains of CamK;β23 unrecombined mice. With regard to the animal's body weight, we detected no differences among genotypes at any measured age (Fig.4.15 C).

Notably, a previous report showed that expression of the tTa protein induced neurotoxicity in the granule cell layer of the dentate gyrus in the CamkIIα:tTa model. They reported that the degree of toxicity varied among several genetic backgrounds and was strong in mice on at least 50% CBA background. Moreover, while mice on C57BL/6 background were protected, they performed poorly in memory tests [251]. For our experiments, we purchased the CamkIIα:tTa mouse line from the Jackson laboratory on 50% CBA, 50% C57BL/6 background and kept it on this background. Since our β23 line was pure C57BL/6, offspring from crossing the two lines were 25% CBA, 75% C57BL/6. By lowering the CBA background without removing it completely, we aimed at circumventing both the toxicity and the poor behavior performance. Nevertheless, our brain weight data indicated that tTa single transgenic mice might not be completely free of tTa-induced neurotoxicity because their brain weights were slightly lower when compared to non-transgenic and β23 single transgenic controls (Fig.4.15 B).

Besides measuring brain weight, we quantified the cortex width of double transgenic CamK;β23 mice at five months of age. We compared it to the cortex width of tTa single transgenic mice and found that double transgenic mice had a significantly thinner cortex (Fig. 4.15 D, E).

Moreover, the paper mentioned above reported that Dox treatment during development of the mice, would prevent dentate gyrus degeneration [251]. Therefore, we administered Dox in sucrose water (2mg/ml Dox concentration) to mice from E0 until weaning for testing. Then, we measured the brain weight of these mice at 20 weeks and 95-105 weeks of age (22-24 months). In agreement with literature, our brain-weight data indicated that Dox treatment prevented the reduction in brain weight in single-transgenic tTa mice. However, we also detected no decrease in brain weight in CamK;β23 expressing mice (Fig.4.15 F), suggesting that β23 does not cause gross morphological defects when its expression under the CamkIIα promoter is restricted to post-developmental age. Possibly, these results might be attributed to constantly lower expression levels after Dox treatment, since we observed that mCherry fluorescence was not as strong in Dox treated brains as compared to brains of non-Dox mice. Altogether, these results suggest that β23 expression could lead to brain atrophy in an age-dependent manner and in an expression level-dependent manner, although β23 may exert strongest effects during embryonic development.

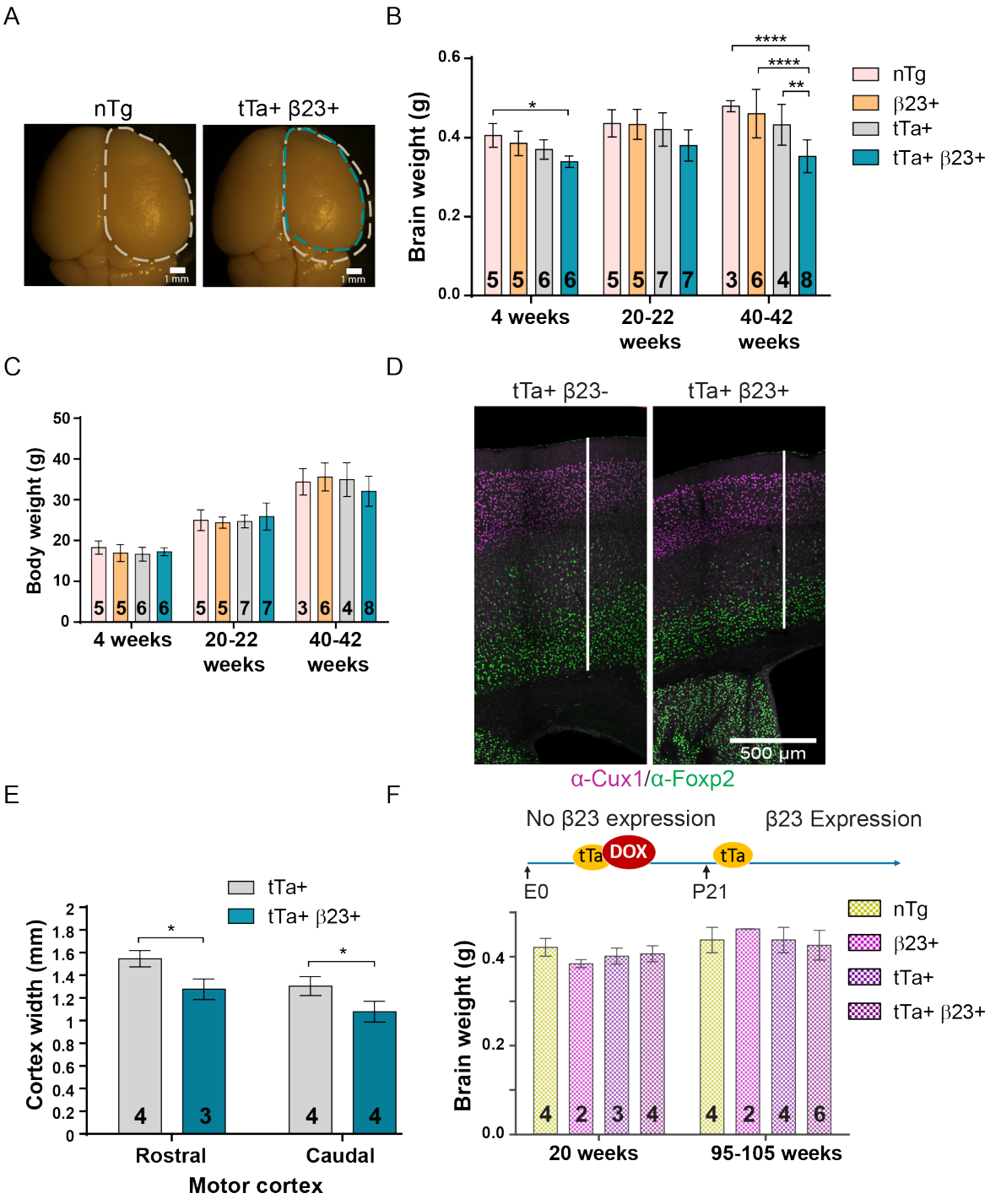
A
nTg
tTa+ β23+
1 mm
1 mm
B
Brain weight (g)
0.6
0.4
0.2
0.0
*
****
****
**
5 5 6 6
5 5 7 7
3 6 4 8
4 weeks
20-22 weeks
40-42 weeks
nTg
β23+
tTa+
tTa+ β23+
C
Body weight (g)
50
40
30
20
10
0
5 5 6 6
5 5 7 7
3 6 4 8
4 weeks
20-22 weeks
40-42 weeks
D
tTa+ β23-
tTa+ β23+
500 µm
α-Cux1/α-Foxp2
E
tTa+
tTa+ β23+
Cortex width (mm)
2
1.8
1.6
1.4
1.2
1
0.8
0.6
0.4
0.2
0
*
*
4 3 4 4
Rostral
Caudal
Motor cortex
F
No β23 expression
β23 Expression
tTa
DOX
tTa
E0
P21
Brain weight (g)
0.4
0.2
0.0
4 2 3 4
4 2 4 6
20 weeks
95-105 weeks
nTg
β23+
tTa+
tTa+ β23+

Figure 4.15 *(previous page)*: **CamK;β23 unrecombined mice present brain atrophy.** (A) Images of perfused brains of a non-transgenic control mouse and littermate double transgenic CamK;β23 mouse, both females of 20 weeks of age. Dashed lines outline the forebrains of the non-transgenic brain (white) and the double transgenic brain (blue). (B) Quantification of brain weight at different ages. All female mice. Numbers on the bars indicate the number of animals. Statistics: Two-way ANOVA + Tukey's post-test. (C) Body weight quantification of the same mice as in B. (D) Image depicting the difference in cortex width. Cux1 was used as upper cortical layer marker and Foxp2 as a marker for lower cortical layers. Foxp2 staining suggests a reduction in lower layer width, which may be due to reduced neuronal numbers. (E) Cortex width measurements in two brain sections. Measurements of the motor cortex were performed. All female mice of 22 weeks of age. (F) Brain weight quantification of unrecombined mice that received Dox from E0 to P21. Both female and male mice pooled together.

4.7 CamK;β23mCherry recombined mice do not show brain atrophy

By crossing our β23 mouse line to a flippase mouse line, we induced recombination of the frt sites in the construct, and the IRES was excised. Thereby, β23 and mCherry were expressed as a fusion protein after crossing this recombined line to CamkIIα:tTa (Fig.4.16 A). Indeed, when we did an immunoprecipitation (IP) against mCherry, using forebrain lysate, and blotted against myc, we detected one clear band at approximately 37kDa, the size of the fusion protein (Fig.4.16 B). These results were confirmed by blotting against mCherry. On the other hand, unrecombined β23 would have run at 10kDa [81], which we did not detect. Moreover, we did not detect any signal in single transgenic mice, further indicating that our line is not leaky, as shown above in Figure 4.13 B.

Immunostaining against mCherry revealed β23mCherry expression restricted to the forebrain (Fig.4.16 C), as observed in the unrecombined line. Although the restricted expression pattern given by CamkIIα:tTa-driven expression was conserved, we did not detect β23mCherry in the CA1 region of the hippocampus in the recombined line. In addition, comparison of cortical expression between unrecombined and recombined mice, showed strong β23mCherry expression in neural processes, while mCherry is stronger in the soma in the unrecombined mouse (Figure 4.16 D). Furthermore, β23mCherry aggregates were readily detected in the recombined line and β23mCherry localized also throughout the cell soma (Fig.4.16 E). Finally, we measured the brain weight of recombined mice at 40-42 weeks of age and compared the results to the brain weight of unrecombined mice. Surprisingly, recombined mice did not present brain atrophy (Fig.4.16 F), suggesting that β23 and β23mCherry lead to different effects in brain architecture.

Overall, we detected the progressive effect on brain atrophy only in CamK;β23 unrecombined, non-Dox treated mice (Fig. 4.15 B). Based on these results, we decided to focus on these mice for further histological and behavioral characterization. Therefore, following findings are from experiments with mice which did not receive Dox during development, and expressed β23 and mCherry as two separate proteins.

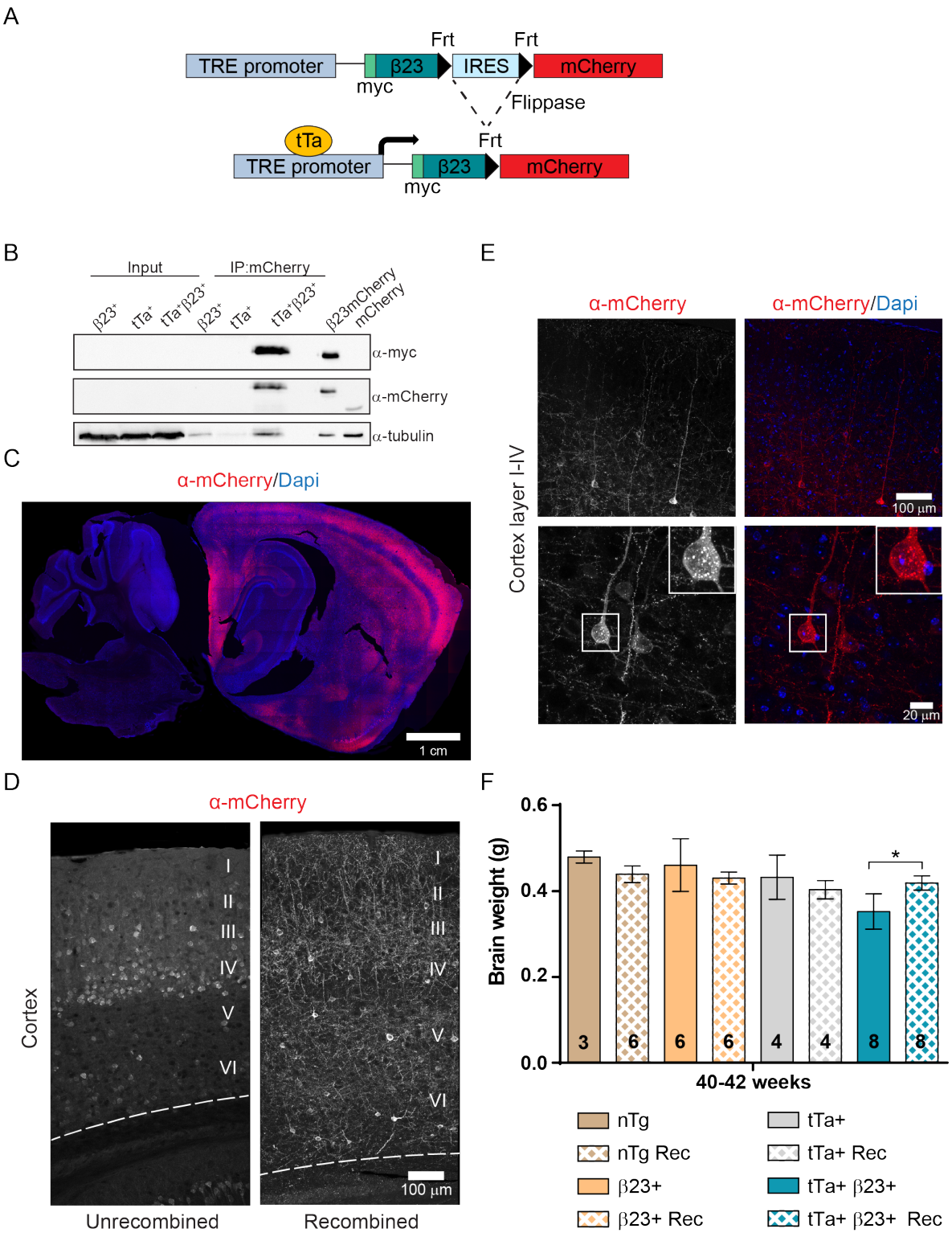
A
TRE promoter
β23
myc
Frt
IRES
Frt
mCherry
Flippase
Frt
tTa
TRE promoter
β23
myc
mCherry
B
Input
IP:mCherry
β23+
tTa+
tTa+β23+
β23+
tTa+
tTa+β23+
β23mCherry mCherry
α-myc
α-mCherry
α-tubulin
C
α-mCherry/Dapi
1 cm
D
α-mCherry
Cortex
I
II
III
IV
V
VI
100 μm
Unrecombined
Recombined
E
α-mCherry
α-mCherry/Dapi
Cortex layer I-IV
100 μm
20 μm
F
Brain weight (g)
0.6
0.4
0.2
0.0
*
3
6
6
6
4
4
8
8
40-42 weeks
nTg
nTg Rec
β23+
β23+ Rec
tTa+
tTa+ Rec
tTa+ β23+
tTa+ β23+ Rec

Figure 4.16 *(previous page)*: **Recombined β23mCherry expression does not lead to brain atrophy.** (A) Schematic of the transgene expressed by CamK;β23 recombined mice. The IRES sequence was excised out by flippase recombination and mice express the fused β23mCherry protein. (B) Western blot after immunoprecipitation against mCherry in forebrain lysates. Only double transgenic mice express β23mCherry. Last two columns are control lysates from Hek293T cells transfected with either β23mCherry or mCherry. Note that β23mCherry runs slightly higher in the brain lysate than in the cell lysate, probably because of the remaining of one frt sequence in the construct after recombination. (C) Expression pattern of β23mCherry in the forebrain, shown by mCherry staining at 20 weeks of age. (D) Comparison of mCherry staining in the cortex of CamK;β23 unrecombined and recombined mice, both females of 20 weeks of age. (E) Higher magnification images revealing β23mCherry aggregates in cortical neurons of a CamK;β23 recombined mouse. (F) Brain weight quantification demonstrating no brain weight reduction in recombined mice, in comparison to unrecombined. The data for the unrecombined mice is the same as shown in Fig. 4.15 B. Only female mice used for unrecombined measurements and both female and male used for the recombined. Statistics: One-way ANOVA + Tukey's multiple comparison test.

4.8 β23 may impair nucleocytoplasmic transport *in vivo*

It has been previously reported that artificial β-sheet proteins impair nucleocytoplasmic transport of proteins and mRNA in Hek293T cells [204]. Interestingly, in our CamK;β23 mouse model, we detected that β23 localized to the nuclear membrane of cortical neurons (Fig.4.17 A, B). Moreover, β23 aggregates accumulated also along neurites (Fig.4.17 C). Interestingly, the nuclear membrane localization of β23 in neurons had not been reported before and the presence of small β23 accumulations in the nuclear membrane suggested a possible interference with the nucleocytoplasmic transport *in vivo*.

Several nuclear pore proteins (Nups) and transport factors have been reported to mislocalize and coaggregate with aggregating proteins such as Huntingtin, TDP-43, and DPRs [135, 134, 137, 130]. Moreover, abnormal localization of Ran GTPase-activating protein 1 (RanGAP1) is recurrent among different diseases. Accordingly, we detected partial colocalization of RanGAP1 with β23 in double transgenic CamK;β23 unrecombined mice (Fig.4.18). In addition, immunostaining against one of the Nups located in the nuclear pore basket, Nup153, showed partial colocalization with β23, as well as sporadic mislocalization of Nup153 to the cytoplasm (Fig.4.19). These qualitative data suggest that β23 might be neurotoxic *in vivo* by hindering nucleocytoplasmic transport. However, experiments to assess transport functionality would be necessary to confirm this hypothesis, and the performance of such experiments would not be trivial *in vivo*.

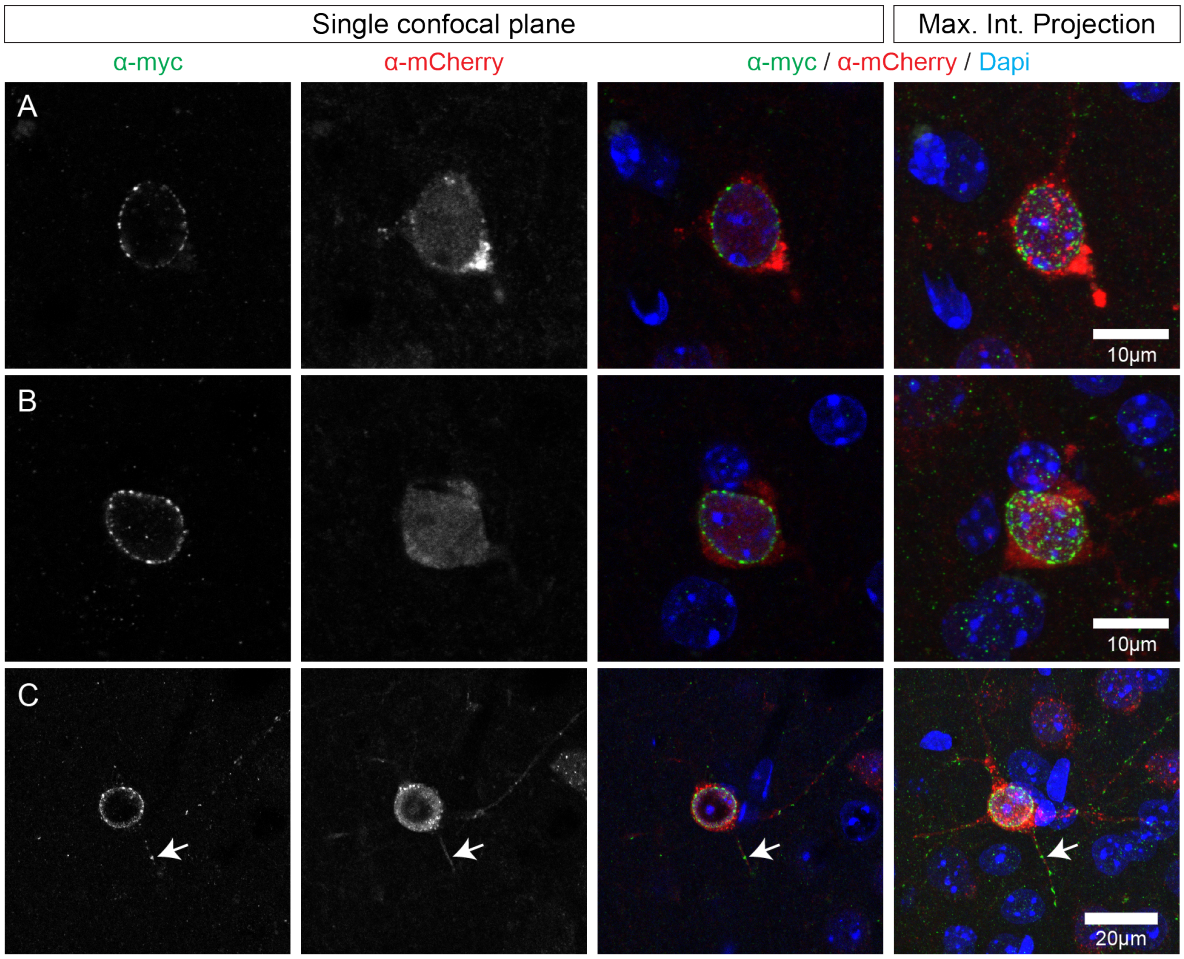

Figure 4.17: **β23 forms inclusions at the nuclear membrane and in neurites.** (A and B) High magnification confocal images, exemplifying neurons in the cortex with β23 inclusions around the nuclear membrane. (C) Low magnification example of a cortical neuron with inclusions around the nuclear membrane and along the neurites (arrow). All images from layers III to VI of the cortex of a 20-week-old, CamK;β23 unrecombined mouse.

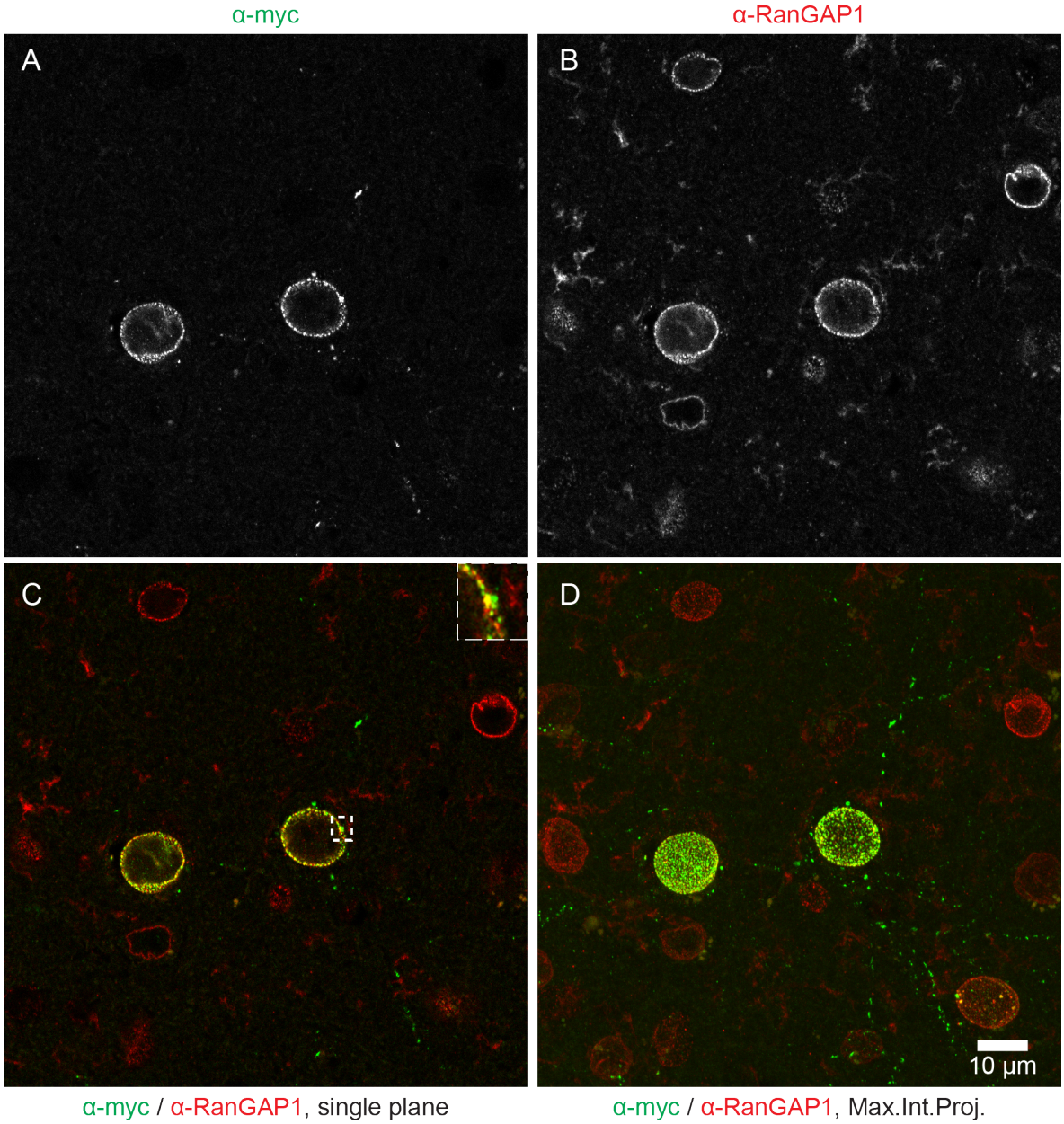

Figure 4.18: **Partial colocalization of β23 inclusions with RanGap1.** Confocal image of a brain section stained against myc and RanGap1, illustrating partial colocalization of β23 with RanGap1. Cortex layers II-III of a 20-week-old, CamK;β23 unrecombined mouse.

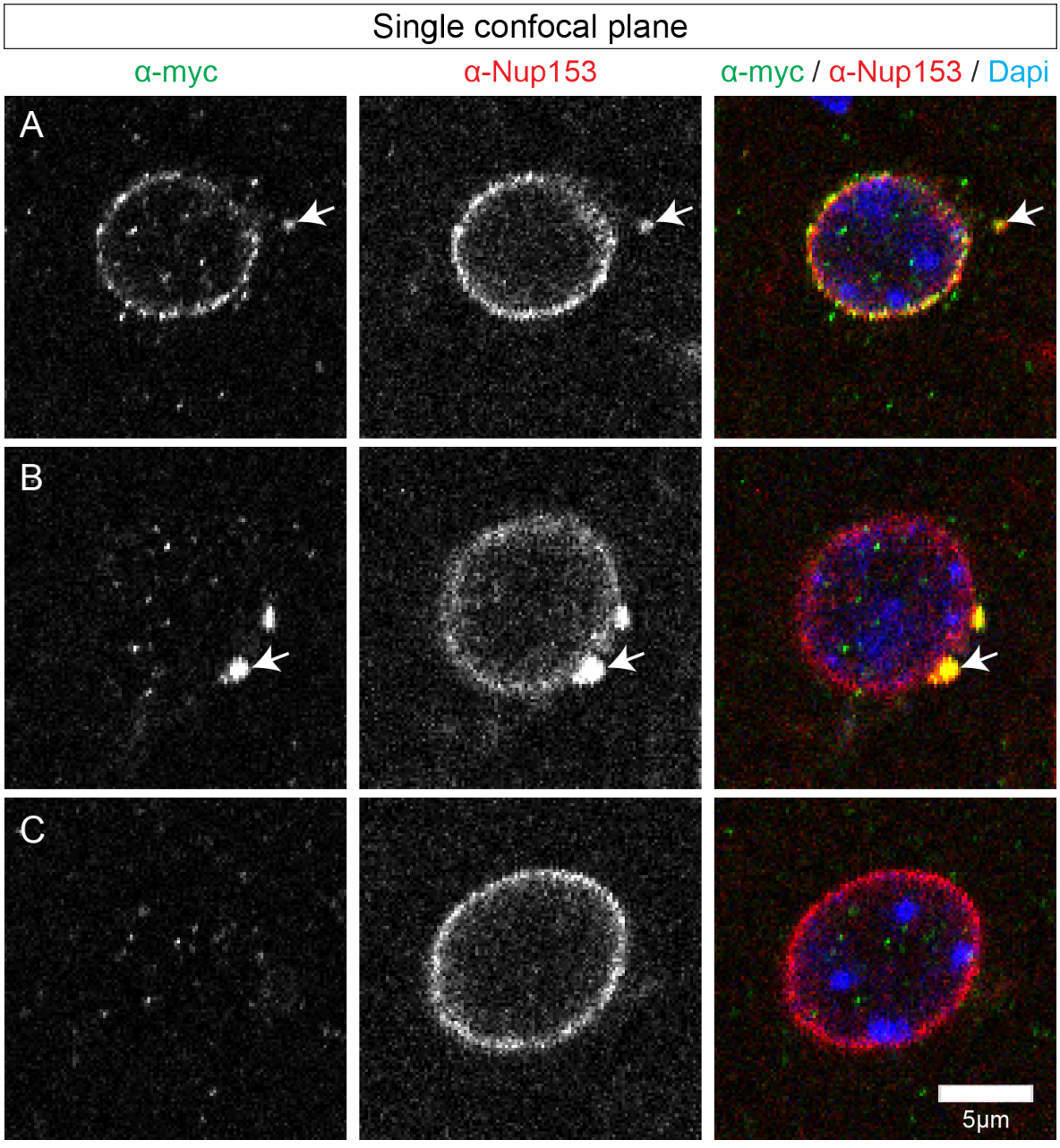

Figure 4.19: **Partial colocalization of β23 inclusions with Nup153.** (A and B) Confocal images of two example neurons with Nup153 mislocalization to β23 aggregates. (C) Example image of a β23 negative neuron showing Nup153 staining only around the nucleus. All images taken from the layer VI of the cortex of a 20-week-old, CamK;β23 unrecombined mouse.

Thus, in order to study nucleocytoplasmic transport functionality in presence of β23 in a simpler system, we have generated a lentiviral construct which is analogous to the mouse construct (Fig.4.20 A). Expression of this construct resulted in aggregate formation and neuronal death in primary cortical neurons (Fig. 4.20 B, C), and could be a valuable tool for further mechanistic experiments.

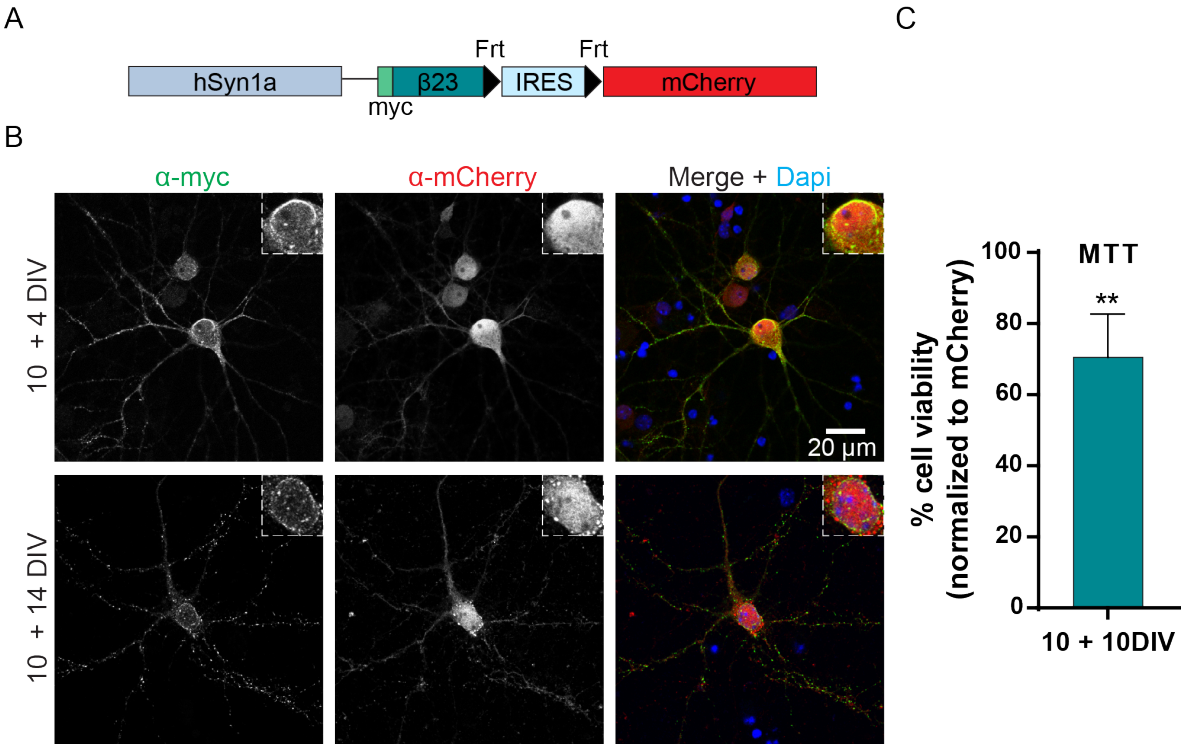

Figure 4.20: **Lentivirus to study β23 effects on nucleocytoplasmic transport *in vitro*.** (A) LV-construct to study NCT in cultured neurons. The mouse pTRE3G promoter was exchanged for a neuronal-specific hSynapsin1 promoter. (B) Single confocal plane image depicting expression of the LV-construct in primary cortical neurons. Early β23 aggregation was detected at 10+4 DIV and abundant aggregation at 10+14 DIV. (C) Quantification of toxicity induced by expression of the construct in E15.5 primary cortical neurons. Viability measured by MTT assay. N=5, Unpaired t-test + Welch's correction.

Of note, we observed that mCherry formed inclusions both *in vitro* and *in vivo* (Fig.4.17 A, Fig.4.20 B). Nevertheless, when expressing the mouse construct *in vitro*, we detected β23 aggregation prior to mCherry aggregation (Fig.4.20 B, upper row). These results suggest that mCherry aggregation was not the driving force for β23 aggregation, but β23 accumulation probably enhanced mCherry aggregation.

4.9 CamK;β23 unrecombined mice present no deficits in behavioral tests

To investigate if artificial aggregating protein β23 expression in the forebrain of CamK;β23 unrecombined mice could lead to behavioral effects, we performed a panel of motor and cognitive tests. These tests were performed in collaboration with the German mouse clinic at the Helmholtz Center in Munich. Analyses were done at a range of 20 to 43 weeks of age in single-transgenic control animals with either β23+ or tTa+ genotype, and double transgenic tTa+ β23+ mice. Both males and females were tested in all tests.

The group of motor tests included open field, grip strength, rotarod, beam walk, and beam ladder analysis. We detected no significant differences among genotypes in the total traveled distance, the total number of rears, and the time spent in the center measured in the open field test (Fig.4.21 A-C). Moreover, although there was a trend towards reduced fore- and hindlimb strength in female double transgenic mice, there were no significant differences among genotypes in limb strength measured in the grip strength test (Fig.4.21 D, E). Furthermore, no impairment in motor coordination and balance was detected in the accelerating rotarod test (Fig.4.21 F). Finally, we assessed fine motor movement with the beam and ladder walk tests. These analyses showed that tTa+ and tTa+ β23+ animals needed more time to traverse the beam and ladder, and stopped more times in comparison to β23+ mice. However, double transgenic performance was not different from that of tTa+ control mice (Fig.4.22 A-D). In summary, we detected no impairment in motor behavior in CamK;β23 mice at analyzed ages.

Moreover, we performed Y-maze, social discrimination, novel object recognition, and Intellicage experiments to study memory capacity of our mice. In Y-maze experiments there was no difference among genotypes neither in spontaneous alternation among arms, nor in the percentage of alternate arm returns. tTa+ β23+ showed a significant reduction in the number of arm entries in comparison to β23+ animals, although the difference to tTa+ mice was not significant (Fig.4.23 A-C). In addition, we detected no difference among genotypes in the social discrimination test (Fig.4.23

D). In the novel object recognition test, double transgenic animals showed a trend towards a reduction in recognition of the novel object after a retention interval of 3h (Fig.4.23 E), whereas the trend was reverted after a retention interval of 24h (Fig.4.23 F). Finally, tTa+ β23+ mice took slightly longer to learn in the place learning test of the Intellicage. However, in the reversal learning, double transgenic mice performed at the same level as β23+ mice, and these two genotypes performed significantly better than tTa+ mice (Fig.4.23 G). In summary, we did not detect any consistent effects in memory in CamK;β23 unrecombined mice. In fact, results overall suggested that there might be slight effects on behavior driven by tTa expression, since double transgenic tTa+ β23+ and single transgenic tTa+ results consistently pointed towards the same direction, while these results were partially different than the results in β23+ single transgenic mice.

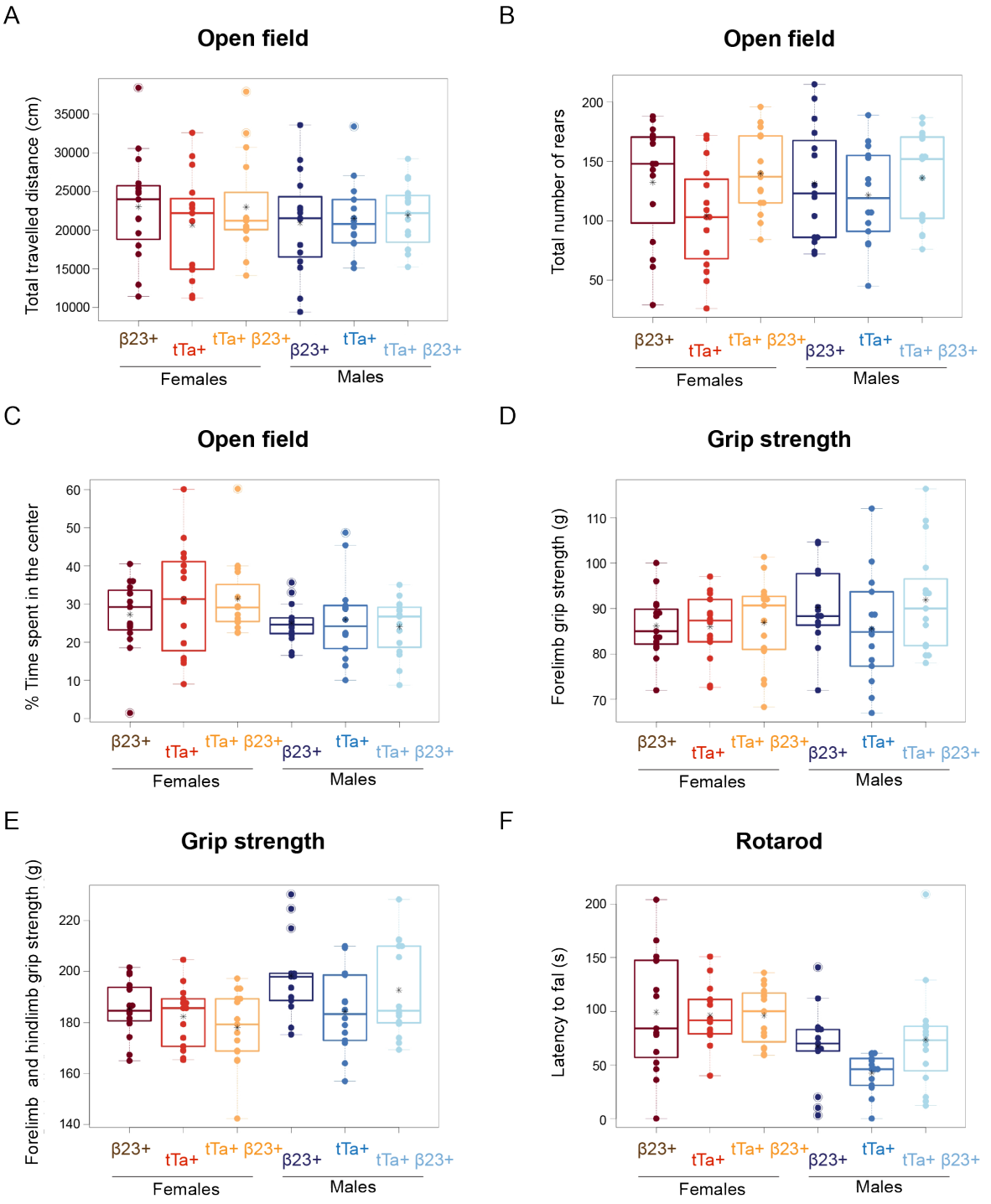

Figure 4.21: **β23 aggregation does not result in impaired motor behavior in CamK;β23 unrecombined mice.** (A-C) Open field results. Test performed at 22 weeks of age. (D and E) Grip strength results. Test performed at 31 weeks of age. (F) Rotarod results. Test performed at 31 weeks of age.

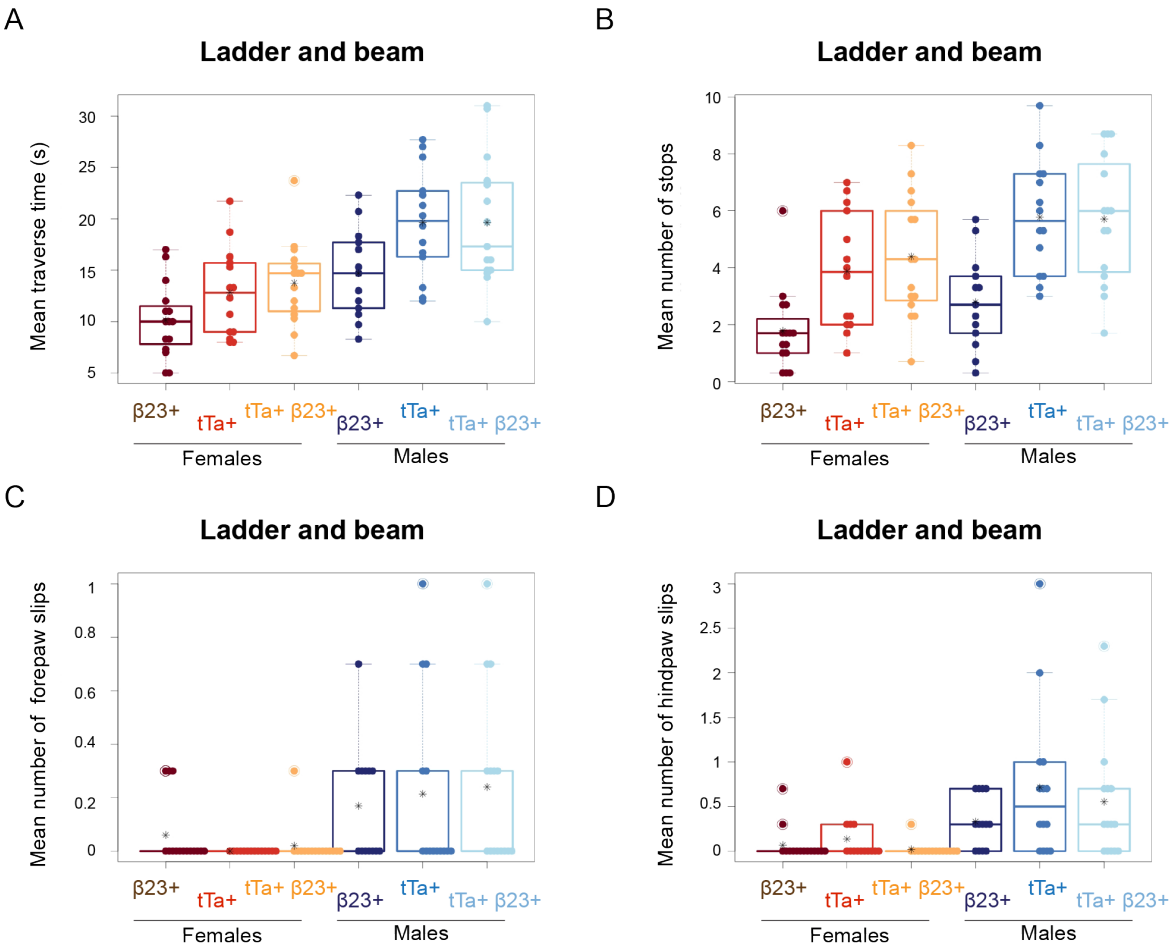

Figure 4.22: **β23 aggregation does not impair fine motor behavior in mice.** (A-D) Pooled results of the beam ladder and balance beam. Tests performed at 33 weeks of age. In (A) β23+ *vs* β23+tTa+ are significantly different by Fisher's Exact test, P = 0.004. In (B) β23+ *vs* β23+tTa+ are significantly different P $<$ 0.001.

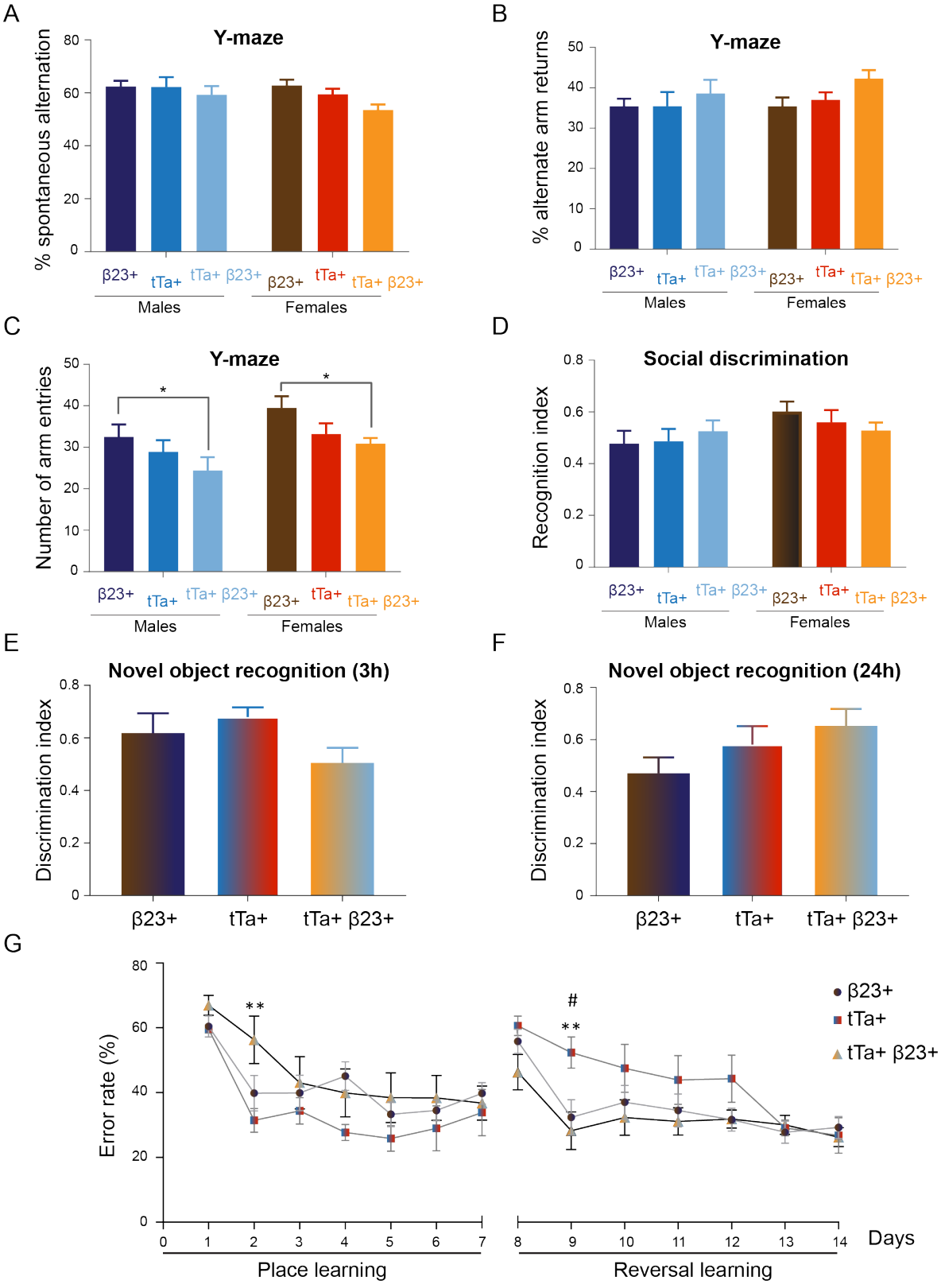
A
Y-maze
% spontaneous alternation
β23+ tTa+ tTa+ β23+ β23+ tTa+ tTa+ β23+
Males
Females
B
Y-maze
% alternate arm returns
C
Y-maze
Number of arm entries
D
Social discrimination
Recognition index
E
Novel object recognition (3h)
Discrimination index
β23+ tTa+ tTa+ β23+
F
Novel object recognition (24h)
G
Error rate (%)
Place learning
Reversal learning
Days
β23+
tTa+
tTa+ β23+

Figure 4.23 *(previous page)*: **β23 aggregation does not result in impaired memory test performance in CamK;β23 unrecombined mice.** (A, B and C) Y-maze results. Test performed at 23 weeks of age. (D) Social discrimination results. Test performed at 34 weeks of age. (E and F) Novel object recognition results. Test performed at 36 weeks of age. (G) Intellicage results. Tests performed at 43 weeks of age.

4.10 β23 expression in the whole CNS is lethal in NEFH;β23 unrecombined mice

In some NDs, such as ALS and SCA, forebrain structures are not the main affected regions in disease, but the spinal cord and the cerebellum. In order to study gain of function toxicity caused by protein aggregation at whole CNS level, we crossed our β23 mice to a different line in which tTa expression is driven by the neurofilament heavy chain (NEFH) promoter [252]. This mice will be further referred to as NEFH;β23. Importantly, all work on NEFH;β23 mice was performed with Miguel da Silva Padilha.

Strikingly, genotyping results of four different litters of 3-week-old unrecombined mice revealed the absence of double transgenic NEFH;β23 animals. We therefore hypothesized that NEFH;β23 mice might die before reaching this age. Interestingly, genotyping of two E15 litters revealed the presence of two normally looking and alive, double transgenic mice. Moreover, we analyzed two more litters at P0 and found that all NEFH;β23 double transgenic mice were dead, while all other littermates were alive (Table 4.4).

To test if β23 expression might be related to the lethality phenotype, we confirmed β23 expression during development by immunostaining against myc in brain sections of E18 mice (Fig.4.24 A). Moreover, we administered Dox to NEFH;β23 mice from conception until P21 to prevent β-sheet protein expression. As expected, Dox-treated double transgenic NEFH;β23 unrecombined mice were viable (data not shown).

Overall, these results suggested that β23 expression in whole CNS exerted strong cytotoxicity effects that impaired viability, leading to the animal's death before or shortly after birth. This lethality phenotype could be prevented by β23 expression inhibition via Dox administration (schematically depicted in Fig.4.24 B). Further experiments on Dox-treated NEFH;β23 mice will be necessary to assess the effects of β-sheet protein expression throughout the CNS in adult mice at mechanistic and behavioral levels.

Analyzed NEFH;β23 unrecombined mice		
Embryonic day 15 (E15)		
Genotype	**♯ of mice**	**Mendelian ratio**
Non-transgenic	1	6%
NEFH:tTa- β23+	3	18%
NEFH:tTa+ β23-	11	65%
NEFH:tTa+ β23+	2	11%
Postnatal day 0 (P0)		
Genotype	**♯ of mice**	**Mendelian ratio**
Non-transgenic	3	25%
NEFH:tTa- β23+	3	25%
NEFH:tTa+ β23-	3	25%
NEFH:tTa+ β23+	3 (non-viable)	25%
3 weeks old		
Genotype	**♯ of mice**	**Mendelian ratio**
Non-transgenic	16	62%
NEFH:tTa- β23+	7	27%
NEFH:tTa+ β23-	3	11%
NEFH:tTa+ β23+	0	0%

Table 4.4: Numbers and ages of analyzed NEFH;β23 unrecombined mice

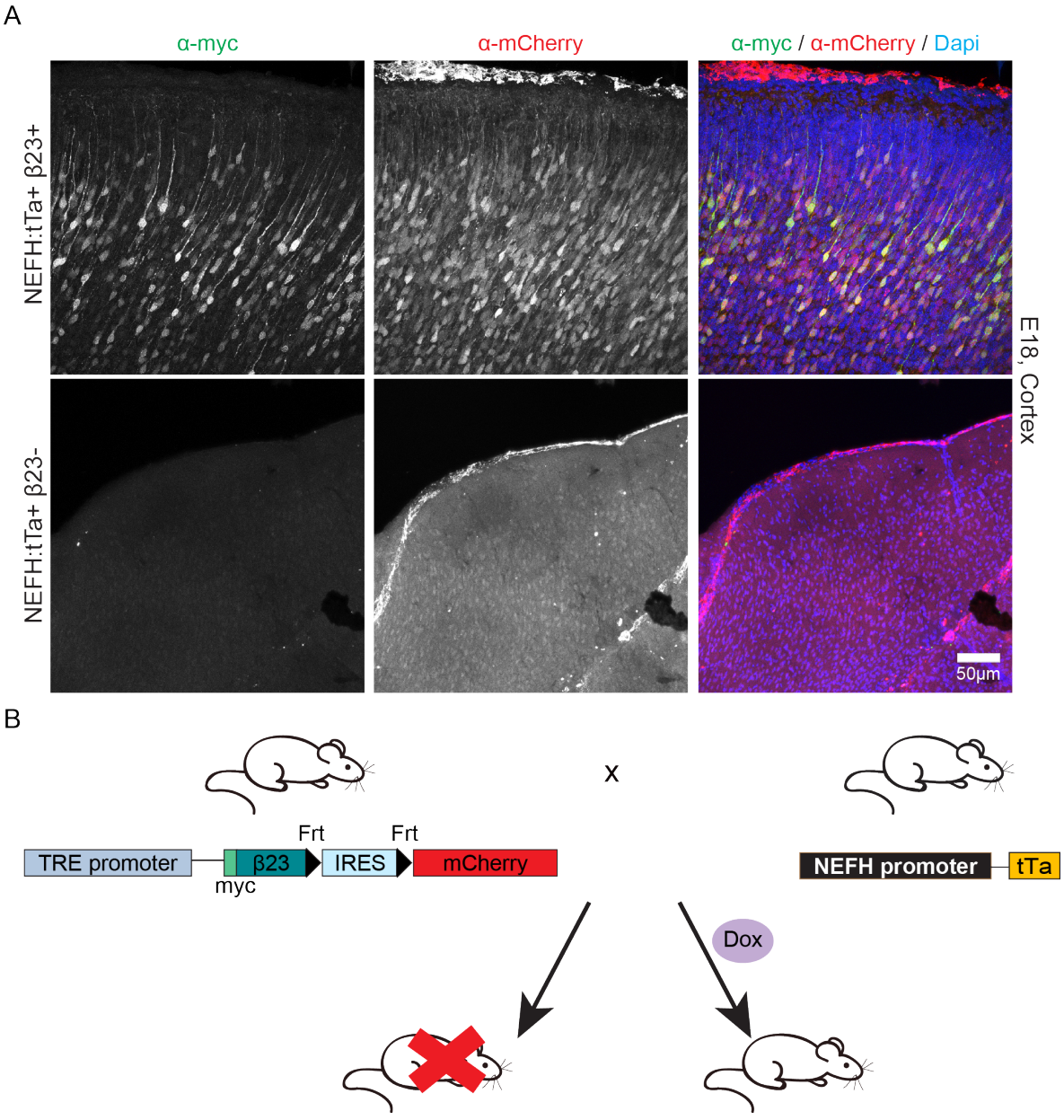

Figure 4.24: **NEFH-driven β23 expression is strong during development and impairs mice viability.** (A) Immunostaining confirming β23 expression in E18 NEFH;β23 unrecombined and non-Dox treated mice. (B) Schematics depicting the lack in viability in NEFH;β23 mice, which can be prevented by Dox-administration during development.

5 Discussion

5.1 Effects of synthetic β-sheet proteins *in vitro*

In this thesis, we characterized the gain of function effects of amyloid-like protein aggregation on neuronal viability by overexpressing artificial β-sheet proteins. These proteins had been previously introduced as a model for protein misfolding and aggregation in a purely *in vitro* system [203]. Moreover, Olzscha *et al.* first characterized their effects on cellular well-being in the Hek293T cell line [81]. However, characterization of artificial β-sheet protein effects in neurons, the cells which are most vulnerable to death in NDs, was missing. Therefore, we aimed to address this issue.

5.1.1 Studying the effects of mCherry-tagged synthetic β-sheet proteins: aggregation

We used myc and mCherry-tagged β-sheet proteins for most experiments, and focused on β4 and β23, while previous studies used myc tagged proteins without mCherry. By adding the mCherry tag, we facilitated detection of protein expression by fluorescence. However, we introduced a possible modifier of protein aggregation, since mCherry is almost three times bigger than the β-sheet proteins (28 vs 10 kDa). Thus, aggregation of mCherry-tagged β-sheet proteins needed to be assessed. In fact, preliminary experiments performed by Dr. Irina Dudanova prior to my thesis, compared β23 and β23mCherry aggregate load and toxicity in Hek293T cells, showing no large differences between the two constructs (data not shown). These results encouraged us to continue working with mCherry-tagged constructs in primary neurons.

In agreement with the above mentioned data in Hek293T cells, β4mCherry and β23mCherry formed aggregates in primary cortical neurons when overexpressed both by transfection (Fig. 4.1 A, B) or lentiviral transduction (Fig. 4.5 A). In transfected neurons, aggregates were abundant already after one day, while in transduced neurons only a few neurons contained aggregates after four days. This time shift could be

explained by two reasons: the first was the delayed expression in transduced neurons, in which β-sheet expression started to be detectable by fluorescence two days after LV-transduction; the second was the differential expression levels, which at the level of individual neurons were probably higher in transfected neurons than in transduced. Comparison of expression levels obtained by the two different overexpression methods is however challenging, since transfection in neurons usually leads to only 1-30% of transfected neurons [208], which greatly complicates the assessment of protein expression by, for example, Western blot. In addition, quantification via immunofluorescence would not be accurate, since aggregates are formed by protein accumulation and are brighter than the diffused protein.

The number of aggregate-bearing neurons was significantly higher in cells overexpressing β4mCherry or β23mCherry, in comparison to control mCherry-overexpressing neurons (Fig. 4.1 B). Nonetheless, it is important to remark that we also detected mCherry forming inclusions in control cells. On the other hand, expression in primary neurons of β23-IRES-mCherry, which leads to β23 and mCherry translation as two separate proteins, suggested that β23 aggregates could be detected earlier than mCherry inclusions, indicating that β23 aggregation was not driven by mCherry (Fig. 4.20 A). mCherry is widely used as a fluorescent tag, it is reported to be monomeric and it is a good compromise between brightness, photostability, and cytotoxicity [253]; nevertheless, alternative fluorescent protein tags such as mScarlet [254] or the widely used eGFP, may be better options for future experiments with aggregating proteins.

5.1.2 Studying the effects of mCherry-tagged synthetic β-sheet proteins: neuronal morphology and apoptosis

We have quantified cellular viability in transfected and LV-transduced primary cortical neurons, providing compelling evidence of β4mCherry and β23mCherry-induced cytotoxicity in neurons. First, quantification of neuronal apoptosis in transfected neurons demonstrated a significant increase in neuronal apoptosis induced by β4mCherry and β23mCherry expression (Fig. 4.1 D). Moreover, considering that naturally aggregating proteins can interfere with neuronal cytoskeleton and morphology maintenance [255], we investigated the effects of the β-sheet proteins on neuronal morphology in transfected hippocampal neurons by Sholl analysis. Similarly, as observed for poly-GA dipeptide repeat aggregates [118], β4mCherry and β23mCherry expression

reduced dendritic arborization (Fig. 4.2). Importantly, impaired neuronal morphology can have dramatic effects on cellular trafficking, affecting cellular processes, such as the maintenance of mitochondrial homeostasis, synaptic morphology, and autophagy-lysosome pathways, which are shared pathological mechanisms in NDs [111].

In addition, we further confirmed the cytotoxic effects of β4mCherry and β23mCherry aggregation, at a population level and in a time-dependent manner, in LV-transduced primary cortical neurons. These experiments revealed the progressive character of β-sheet-induced toxicity, since we measured no effect on neuronal viability three days after transduction, but the viability of β-sheet-expressing neurons started decreasing at four days after transduction. According to the characteristic progressive pathogenesis observed in NDs, cultured β-sheet-expressing neurons continued dying over time, so that only around 10% of neurons were alive on day fourteen after transduction. While β-sheet expression strongly affected neuronal viability, control mCherry-expressing neurons survived as well as untransduced neurons (Fig. 4.5 B), reinforcing that the observed effects are not driven by mCherry expression.

Unexpectedly, all our viability experiments indicated that β4mCherry-induced toxicity occurs faster than β23mCherry-induced toxicity, and these results, at least for LV-transduced neurons, were not a result of differential protein expression levels (Fig. 4.5 D). These toxicity results were in disagreement with a previous publication, which reported that β23 was more toxic than β4 [81]. However, in contrast to our experimental settings, these experiments were performed in Hek293T cells transiently transfected via electroporation.

Therefore, to find out more about this disagreement in the toxicity results, we performed viability analysis in transfected Hek293T cells, comparing the effects on viability exerted by untagged and mCherry-tagged β-sheet proteins. To our surprise, we were not only unable to reproduce the strong reported toxicity measured in Hek293T cells expressing untagged β-sheet proteins, but we did not detect any impairment in viability in Hek293T cells expressing mCherry-tagged proteins (Fig. 4.4 A). Furthermore, as an alternative approach, we also measured cellular viability in a newly generated, inducible Hek293T cell line, which stably expressed β23mCherry upon Dox addition to the media. In the viability experiments performed with the inducible cell line, we detected a mild decrease of around 20-25% in cellular viability

at time-point four days after expression induction (Fig.4.3 B). Nonetheless, this result was also distincly lower than the 60% cell death at three days after transfection reported in Hek293T cells expressing β23 [81, 204]. These discrepancies may however be due to technical reasons.

Finally, we analyzed the cytotoxicity of untagged β-sheet proteins in transfected primary cortical neurons. In accordance to the results with the mCherry-tagged proteins in neurons, untagged β4 was more toxic than β23, although the number of apoptotic neurons was much lower than in β4mCherry transfected neurons (Fig. 4.4 B). Altogether, the robust cell death observed in neurons versus Hek293T cells indicate the existence of neuronal specific toxic mechanisms induced by amyloid-like protein aggregation. Indeed, it is thought that the postmitotic nature of neurons renders them particularly vulnerable to accumulation of disease-related proteins in NDs [110]. Our results therefore, point out the importance of validating results in disease-relevant cell lines. Moreover, our cytotoxicity results suggest that expression levels might play an important role in the degree of cellular apoptosis induced by artificial aggregating proteins. This importance of expression levels is reminiscent of the effects elicited by increased amounts of Aβ and α-synuclein, given that duplications in the Aβ coding gene *APP* lead to familial AD [20], and *SNCA* duplications or triplications lead to familial PD [29].

At this point, further experiments would be needed to discern the cause of the differential cytotoxicity detected between untagged and mCherry-tagged β-sheet proteins in neurons. To test if differences in expression levels were the reason, transduction of all proteins and comparison of protein levels for example via Western Blot, along with analysis of population viability could be performed. Alternatively, differences in toxicity may have been caused by different protein localization of untagged and mCherry-tagged proteins, since untagged β-sheets form abundant aggregates in the nucleus, while mCherry-tagged β-sheets primarily localize to the cytoplasm. In support of this, a study concluded that cytoplasmic localization of the artificial β-sheet proteins leads to higher cytotoxicity than nuclear localization [204].

In addition, further experiments would be needed to find out more about the temporal difference in toxicity elicited by β4mCherry and β23mCherry. Possibly, in-depth biophysical characterization of the structure and dynamics of the aggregates would be

necessary. Given that *in vitro* data indicate that β4 is less prone to aggregation than β23 [81], it is reasonable to speculate that β4 may form more oligomeric species, which could also influence the dynamics of secondary nucleation processes [9]. On the other hand, the sequences of the two artificial proteins are slightly different, and this could also have an influence on their aggregation dynamics and the types of interactions they have with other cellular molecules.

Overall, we have shown that artificial aggregating proteins β4mCherry and β23mCherry form aggregates, lead to neuronal death in a time-dependent manner, and can thus be employed to study toxic mechanisms induced by amyloid-like protein aggregation.

5.2 Identification of molecular candidates with a potential role in common mechanisms of cell toxicity

5.2.1 Neuronal interactome of β-sheet proteins: comparison to other proteomic studies

Aiming to find out more about the molecular underpinnings involved in β-sheet-induced toxicity, we performed interactome mass spectrometry analysis. This approach has successfully been used to identify different molecules and pathways affected by aberrant interactions of cellular components with naturally aggregating proteins (see section 2.2.1) and artificial aggregating proteins [81, 204]. Moreover, *omics* studies are of growing interest for the neurodegeneration community, due to their great value in the systematical and comprehensive understanding of phenotypes related to disease [80].

Importantly, our experimental approach aimed at identifying proteins involved in early stages of toxicity, interactors of predominantly soluble oligomeric β-sheet species. In addition, although the interactomes of β4, β17, and β23 had been analyzed in a previous report [81], this previous study was performed in Hek293T cells and results on β-sheet-induced toxicity in these cells are conflicting (see section 5.1.2). Conversely, our experiments were performed in primary neurons and enabled us to identify neuronal-specific protein interactors, a factor that is of disadvantage in cell lines. In addition, a second published study measured the interactome of

β17GFP in primary cortical neurons, using GFP as a control [204]. While this study identified several interesting candidates in neurons, the experiments were performed in transfected neurons and the number of β17GFP-positive cells was probably low. Moreover, the article did not report neither the time point after transfection in which experiments were performed, nor the neuronal toxicity at that time point. In contrast, our LV-transduction approach allowed a broad neuronal-specific population expression, at an early time point of toxicity (Fig.4.5 B).

We identified close to hundred specific β-sheet interactors with a wide variety of cellular functions (Fig. 4.7 A, Table 4.1). Importantly, expression of these interactors was not altered in β-sheet-expressing neurons (Table 4.2), excluding the possibility that interaction was due to higher protein concentration in the cell. Moreover, in line with proteins that were sequestered by HTT aggregates in the R6/2 mouse model [125], the content of intrinsically disordered regions was higher in β-sheet interacting proteins than in the rest of identified proteins (Fig.4.7 B). This commonality in protein features brings to mind the concept of a metastable fraction of the cellular proteome being particularly vulnerable to protein misfolding [256].

In addition, annotation enrichment of the β-sheet interactors highlighted terms such as transport, microtubule, and cell membrane; suggesting that proteins involved in aberrant interactions with the aggregating proteins, might have a role in the observed impairment of neuronal morphology caused by β4mCherry and β23mCherry (Fig.4.2).

In contrast to the reported interactome in transfected neurons [204], we did not identify any member of the THOC complex enriched as significant β-sheet interactor. This difference might be explained by the different experimental conditions used in the two studies: transfected vs transduced neurons, GFP vs mCherry tag. Furthermore, transfection leads to very high protein expression levels and it is reasonable to think that this might influence outcoming results.

5.2.2 Investigation of individual protein candidates

In order to mimic the loss of function effect that aberrant protein interaction with β-sheet aggregating proteins might have on neuronal viability, we performed a

Crispr/Cas9 knock-out screen of a subset of interactors. To do so, we selected nineteen proteins among all the interactors. This selection was based on literature and according to the criteria determined by the members of the project (Table 4.3). LV-transduction of the Crispr/Cas9 construct in WT primary cortical neurons, followed by viability measurements, revealed that KO of individual interactor proteins significantly reduced neuronal survival (Fig.4.8 B, C).

Particularly, KO of the candidates Ccdc88a, Aimp1, and Stmn2 showed the most consistent results, since neuronal survival was significantly reduced by the protein KO with all three different gRNAs. Interestingly, Aimp1 has been linked to AD and motor neuron degeneration [123, 223], and Stmn2 downregulation was detected in AD patients [230], confirming that we were able to identify disease relevant candidates using the artificial β-sheet aggregating proteins.

Nonetheless, further validation experiments would be needed to complement our screening results, since they are probably an underestimation of the possible effects given that factors like transduction efficiency of each LV and different protein half-lives have not been considered in the experiments. As a consequence, it remains an open question, if the lack of effect in the KO of some candidates was due to low transduction efficiency, very long half-life of the protein, non-functional KO, or if the protein is actually not essential for neuronal survival. Especially important, would be to measure the degree of candidate protein reduction, since we cannot rule out the possibility that we induced a knock-down rather than a knock-out, as a result of achieving transduction in only a fraction of cultured neurons.

Finally, we investigated if overexpression of the candidate Ccdc88a (Girdin) in β-sheet-expressing neurons could rescue neuronal viability. However, girdin overexpression did not improve neuronal viability even at the latest analyzed time point, fourteen days after cotransduction (Fig. 4.9). This result may be explained by girdin levels not being sufficient to counteract the β-sheet effects, but technical difficulties hindered us from further investigation. In our experiments, both β-sheets and girdin constructs were expressed in the same backbone vector and therefore under the same promoter. Thereby, cotransduction of the two vectors might have lead to competition for transcription factors and increasing girdin levels resulted in reduced β-sheet protein levels. Therefore, we were not able to discern between effects on neuronal survival

elicited by girdin or by reduction in β-sheet expression.

Alternatively, maybe girdin overexpression alone was not enough to rescue viability and a combination of several proteins, perhaps involved in various cellular pathways, may be necessary. This option seems reasonable considering the multifactorial pathogenesis described in NDs [111].

5.2.3 Investigation of pathway impairments

Enrichment of the annotation *Protein serine/threonine kinase activity* in β-sheet interactors (Fig. 4.7 C) lead the focus of our attention to neurotrophic signaling, given that its dysregulation is a commonality in NDs (see section 2.2.3). Therefore, we became interested in studying the effects of amyloid-like aggregation on trophic signaling using the artificial β-sheet proteins. As a starting point, we focused on BDNF-TrkB signaling, which has been widely investigated in earlier years of our laboratory.

Usually, binding of neurotrophin BDNF to its receptor TrkB, leads to activation of downstream pathways through three principal tyrosine kinase-mediated pathways: the MAPK–ERK pathway, the PI3K–AKT pathway and the PLCγ1–PKC pathway. In our experiments, we studied the first two pathways, which promote cell survival, whereas the PLCγ1–PKC pathway promotes cell differentiation [139]. Interestingly, we detected impaired Akt phosphorylation in β-sheet expressing neurons (Fig. 4.10), suggesting that β-sheet expression hinders the activation of the survival pathway. Moreover, we detected no difference in Erk1/2 phosphorylation (Fig. 4.11), hinting at a specific dysfunction of the Akt arm of the survival pathways. However, the variability among these experiments was very high and further confirmation would be needed.

Notably, reduced Akt phosphorylative activity caused by its own reduced phosphorylation, may explain why girdin overexpression would not be enough to rescue β-sheet protein toxicity. Girdin gets phosphorylated by Akt [244]. Therefore, girdin overexpression, without solving the upstream problem in Akt, may not be sufficient to improve cell viability.

Our Akt results unraveled another common effect elicited by gain of function in protein aggregation: the impairment of neurotrophic signaling cascades. However, many questions remain open: in β-sheet presence, are the levels of receptor TrkB and P-TrkB maintained? Is the downregulation of P-Akt caused by higher expression of the upstream kinase PTEN? What are the downstream effects of this downregulation? What happens to signaling via the other neurotrophin receptors? Does β-sheet expression *in vivo* impair neurotrophic signaling as well? Further experiments will help unravel some of the answers.

In summary, as observed for naturally aggregating proteins [142], artificial β-sheet proteins might impair neurotrophic signaling in neurons. This shared feature may enable the testing of small molecules in artificial β-sheet expressing neurons as a further validation of therapeutic potential in preclinical studies.

5.2.4 Artificial β-sheets proteins *in vitro*: concluding remarks and outlook

We have assessed the effects of mCherry-tagged artificial β-sheet proteins on neuronal viability. First, we have shown that β4mCherry and β23mCherry form aggregates in primary murine neurons. Moreover, our results revealed that β4mCherry and β23mCherry expression leads to impaired neuronal morphology and to progressive neuronal death in primary neurons. Thus validating the use of artificial amyloid-like proteins to study gain of function toxic mechanisms induced by protein aggregation.

In addition, by analyzing the interactome of the artificial β-sheet proteins in neurons, we have provided a list of protein candidates, which may have a role in common mechanisms driving neurodegeneration.

At a mechanistic level, we could pinpoint the impairment of neurotophic survival signaling as one of the possible causes of β-sheet induced toxicity. Overall, the results reinforce the utility of artificial proteins to mimic and study phenotypes caused by naturally aggregating proteins.

However, there are still further characterization experiments and open questions that one might address. To start with, several protein aggregates are ubiquitinated or tagged by p62 [46, 49]. Checking these features, as well as determining the degradation

pathway of artificial β-sheet proteins, would serve as their further validation as a model to study neurodegeneration.

Moreover, further validation experiments regarding the protein candidates from the interactome should aim at identifying their role in the context of naturally aggregating proteins: are they sequestered by protein aggregates? Can their overexpression improve neuronal viability? If so, by which mechanism? Is the candidate relevant for more than one disease? Is the candidate expression modified in postmortem material of patients?

Finally, further mechanistic studies to answer the fundamental question of how protein aggregation leads to cell death are still necessary. Although vast advances have been made in the past decades to identify the multiple dysfunctional mechanisms in NDs, this fundamental question still cannot be answered. In this regard, artificial β-sheet proteins can be used as a tool to help unravel key mechanisms of aggregation-driven cytotoxicity.

5.3 β23 protein aggregation effects *in vivo* in a new inducible mouse model

Studies in cultured neurons are very valuable for mechanistic investigations. However, processes in a living animal involve several cell types, interconnected with each other in particular manners, and are therefore much more complex. To study the effects of amyloid-like protein aggregation in the brain of a complex living organism, we generated a novel β23 transgenic mouse model of protein aggregation.

5.3.1 Generation of a Tet-inducible β23 mouse model

We made use of a Tet-inducible system to enable temporal and spatial control of β23 expression. A responder transgene was generated consisting of a third generation Tet-responsive element (TRE) placed upstream of the β23-encoding cDNA. We were concerned about how mCherry would influence aggregation *in vivo*, but were interested in generating a model that would be used for functional *in vivo* imaging, which

would require the fusion protein β23mCherry for protein identification. Therefore, we kept both possibilities open by placing an frt-flanked IRES sequence in between β23 and mCherry (Fig. 4.12). The widely used CamKIIα:tTa activator mouse line was used to induce expression and restrict it to forebrain structures [205]. Moreover, the broader NEFH:tTa driver line [252] was used to induce expression in the whole CNS. Of note, most of the following discussion will focus on the CamK;β23 analyses, since these mice have been extensively studied during this thesis. In addition, the final part of the discussion will address the recent results in NEFH;β23 mice.

Before discussing the results from the analyses of the novel β23 models, there are several remarks that can be made regarding the strategy and implications of the line. First, the choice of β23 to be expressed in a mouse was based on the published toxicity data in Hek293T cells, which described this protein as the most aggregating and toxic of the three artificial proteins analyzed [81]. In light of my data in primary neurons, generating and studying a β4 mouse model could bring insight into the toxic mechanisms of a less aggregating protein, which may resemble those of oligomeric species.

Second, placing the cDNA expression construct under the control of the pTRE3G promoter is a new strategy for Tet-inducible mouse models of neurodegeneration. Some models have been generated using the bidirectional tet operator (BiTetO), such as the HD94 model of HD [257], the TauRD models [258], and the mutant α-synuclein model with restricted expression to dopaminergic neurons in the midbrain [182]; while other models, an Aβ model [259], the tauP301L model Tg4510 [77] and two TDP-43 models [260, 252] made use of the prion promoter PrP. In comparison to biTetO, pTRE3G is a further optimized promoter version with very low basal expression and high maximal expression after induction [261], whereas there is no available data comparing expression induction between pTRE3G and PrP.

Next, the recombined line (expressing fused β23mCherry) would allow for functional two-photon *in vivo* imaging, enabling also the characterization of aggregation dynamics over months. This imaging technique has not been applied in many neurodegeneration studies yet, and our mouse model may be useful to study aggregation in different cell populations and its effects on the circuitry *in vivo*. Moreover, mCherry fluorescence would facilitate protein detection avoiding injection of amyloid dyes.

Finally, to restrict β23 expression to excitatory neurons of the forebrain, we decided to use the CamKIIα:tTa driver mouse line [205]. We selected this line because it was previously used to generate and characterize several neurodegeneration mouse models [257, 259, 77, 258, 260], which would enable us to compare our mouse to existing models of naturally aggregating proteins.

However, it has been reported that tTa expression in the CamKIIα:tTa mouse line can lead to dentate gyrus degeneration and influence behavior results depending on the genetic background [251], demonstrating that the tTa is not just an inert control element. This study showed that generation F1 with CBA x C57BL/6 and C3H/He x C57BL/6, but not pure C57BL/6 background induced degeneration, whereas pure C57BL/6 resulted in poor Morris water maze performance. Degeneration in the dentate gyrus could be prevented by Dox treatment during development. Nonetheless, reporting of Dox treatment, genetic background, and single transgenic controls usage among different studies has been very variable and partly misleading. For example, double transgenic animals were compared to non-transgenic controls, instead of to single transgenic animals [260], or non-transgenic and single transgenic animals were pooled in a *control* group [77]. Overall, the use of the activator CamKIIα:tTa line in our project involved careful management of the mouse colony and reporting of control genotypes.

5.3.2 Effects on brain macrostructure by β23 expression

As expected, we detected restricted β23 and mCherry expression in the forebrain of CamK;β23 mice and only in positive double transgenic animals (Fig. 4.13). Immunostaining against mCherry showed conspicuous expression in neurons of several brain regions, such as the olfactory bulb, the whole cortex, including the motor, somatosensory, and entorhinal cortex; the striatum, the hippocampus, and the amygdala. These regions of expression coincide with previously published expression data of the CamKIIα:tTa line [262]. However, in the hippocampus of our mice, expression was restricted to CA1, although expression in CA1, CA2, CA3, and dentate gyrus was expected. Given that our mouse line is a transgenic line, this limited expression might be related to the transgene's integration site.

Moreover, we confirmed β23 expression via myc immunostaining. Noteworthy, laborious troubleshooting was required for myc staining to work *in vivo* (see section 3.2.16). Nevertheless, we did not detect myc-positive neurons in the CA1 region of the hippocampus and only a few in the striatum. This differential expression suggests that in the CamK;β23 unrecombined line β23 and mCherry might not be expressed at equimolar ratios and only the mCherry part of the construct is expressed in CA1. This issue is however surprising, since it was reported that in constructs containing IRES, the upstream to the IRES part of the construct is usually expressed higher than the downstream part [263], and not the opposite.

Importantly, neither myc nor mCherry expression were detected in absence of tTa transactivator in single transgenic β23+ mice, indicating the absence of leakiness in expression (Fig. 4.13 B). This lack of leakiness supports our choice of the pTRE3G promoter, given that tau expression has been identified in transactivator absence in the Tet-inducible P301L tau model [264], which is driven by the PrP promoter.

At whole-brain level, we measured a reduction in brain weight in double positive CamK;β23 transgenic mice, along with a reduction in cortical width, while the body weight remained constant (Fig. 4.15). Importantly, reduced brain weight and progressive body weight loss are common phenotypes observed in mouse models of neurodegenerative diseases [77, 182, 252, 202]. In our mice, the difference in brain weight of double transgenic versus control mice became more pronounced with increasing age. However, this difference was given by the augmentation in brain weight in control mice, not because brains of double transgenic mice progressively lost weight, as it is commonly observed for ND mouse models. In addition, already at the early age of 4 weeks, we detected a slight reduction in the brain weight of double transgenic CamK;β23 unrecombined mice. Altogether, these data suggest that the reduced brain weight detected in double transgenic mice might be caused by an effect of β23 expression (maybe also due to combined tTa expression) during brain development, rather than by a progressive neurodegenerative phenotype.

Finally, to prevent the possible neurodevelopmental effect, we administered Dox to CamK;β23 unrecombined mice from conception until weaning and measured their brain weight. Unfortunately, although the effects on development were circumvented, we detected no brain weight loss in Dox-treated mice even in very aged mice (Fig.

4.15 F). Nonetheless, we noticed in preliminary observations of mCherry fluorescence that expression levels in Dox-treated mice were low and expression was detected in fewer cells than in non-treated mice. In addition, expression levels stayed low with age, which might have resulted in the lack of brain atrophy derived from β23 expression. Considering that other studies using the CamKIIα:tTa driver line reported good expression-induction and development of neurodegenerative phenotypes after Dox removal [257, 77], the low expression levels in our mice might be linked to the integration site of the transgene. Hence integration mapping would be necessary to investigate how β23 expression is regulated during and after development.

Differences between the unrecombined and recombined line in CamK;β23 mice

Besides working with unrecombined mice, we also studied mice of our recombined line, in which the fused protein β23mCherry was expressed in double transgenic mice upon breeding with CamKIIα:tTa mice. Notably, when observing the perfused brains directly after withdrawal, we noticed that fluorescence in brains of recombined mice was clearly brighter than fluorescence in unrecombined brains. This observation fitted to accumulation of the fused protein, since β23mCherry aggregates in cultured neurons also appeared brighter than the diffused protein or than mCherry alone.

As we had done for the CamK;β23 unrecombined line, we confirmed expression in the forebrain of recombined mice by staining against mCherry. The expression pattern of the recombined line looked very similar to that of the unrecombined line. However, although in principle the unrecombined and recombined mice should present expression in the same brain regions, recombined mice lacked hippocampal CA1 expression (Fig.4.16 C).

In addition, comparison of cortical expression between unrecombined and recombined mice, showed strong β23mCherry expression in neural processes of recombined mice, while mCherry was stronger in the soma in the unrecombined animals (Fig.4.16 D). Possibly, less neurons were labeled in the cortex of β23mCherry-expressing mice, suggesting that myc staining might be more accurate to detect transgene expression in unrecombined mice, especially given that β23 and mCherry might not be expressed at equimolar levels. These observations should be taken into account for further studies in NEFH;β23 mice.

Furthermore, β23mCherry aggregates were readily detected in the recombined line via mCherry staining, although β23mCherry did not seem to localize to the nuclear membrane, as observed for β23 in unrecombined mice (Fig.4.17 E). Analysis of myc staining in CamK;β23 unrecombined and recombined mice would be necessary for precise comparison of expression between the two lines. Moreover, the number of expressing neurons should also be quantified in further experiments.

Finally, we measured the brain weights of non-Dox treated CamK;β23 unrecombined and recombined mice. As mentioned above, unrecombined β23-expressing double transgenic mice presented reduced brain weight when compared to controls. However, we did not detect a reduction in brain weight in recombined β23mCherry-expressing mice at 40-42 weeks of age (Fig.4.16 F). These data indicated that β23 and β23mCherry expression may lead to different effects, β23mCherry being less toxic *in vivo*. It is possible then that mCherry fusion alters aggregate structure and reduces its toxicity. To investigate this hypothesis, in-depth structural characterization of β23 and β23mCherry aggregates in neurons, for example by Cryo-electron tomography [265], would be necessary. Moreover, amyloid stainings such as Thioflavin could be useful to detect if β23mCherry may be less amyloidogenic than β23.

Overall, we have detected β23 in the forebrain of CamK;β23 unrecombined and recombined mice. Moreover, we have confirmed the presence of protein aggregates in both lines. However, β23 expression showed an effect in brain weight only in CamK;β23 unrecombined mice. Our data does not exclude that CamK;β23 recombined mice may develop a degeneration phenotype at a later age, as indeed many neurodegeneration models develop a phenotype at very advanced ages [181, 266]. Nonetheless, we decided to focus our further experiments on CamK;β23 unrecombined mice.

5.3.3 β23 mice as a model to study nucleocytoplasmic transport

At cellular level, we detected β23 aggregates in the soma and neurites in CamK;β23 mice (Fig.4.17 C and 4.18 D). Remarkably, we noticed an enrichment of small β23 aggregates around the nucleus, probably at the nuclear membrane (Fig.4.17 A,B). This particular aggregation localization opened up the possibility that β23 interferes with NCT *in vivo*. In fact, a previous report showed impairment of NCT due to artificial

β-sheet expression *in vitro* [204].

Nucleocytoplasmic transport impairment arose as a potential unifying toxicity mechanism in NDs in recent years (see section 2.2.2). Therefore, we performed immunostainings to identify possible signs of NCT malfunction in neurons of CamK;β23 unrecombined mice. Indeed, we could identify RanGAP1 partial colocalization with β23 aggregates, possibly interfering with RanGap1 correct function. However, this colocalization was observed by confocal imaging and should be confirmed with a microscopy technique that allows for better resolution, such as STED microscopy [267]. Given that RanGAP1 is important to maintain the gradient of Ran-GTP in the nucleus and Ran-GDP in the cytoplasm, providing directionality to nucleocytoplasmic transport, alterations in RanGAP1 might lead to changes in the rate and direction of active transport [128].

Moreover, we identified Nup153 mislocalization to β23 aggregates (Fig.4.19). This nuclear pore protein is a member of the nuclear pore basket and is critical for nuclear pore biogenesis [268]. Thus, its mislocalization may impair nuclear pore integrity.

To date, our observations regarding nucleocytoplasmic transport integrity in β23 mice have been qualitative and further experiments that quantify the degree of protein mislocalization will be necessary. In addition, studying how the number of neurons with β23 localization at the nuclear envelope varies with age, would also shed light on the age-dependent mechanisms and dynamics of NCT impairment. Moreover, it will be interesting to find out, if β23 expression can interfere with RNA export, or if it interferes with both RNA and protein transport by clogging the nuclear pores, as observed for DPRs in ALS/FTD [129, 133]. All these open questions can be addressed as well using NEFH;β23 mice, in which we also detected β23 aggregates around the nucleus in preliminary observations. In addition, our lentivirus harboring the same construct as the mouse model will be a potent tool for mechanistic studies on NCT function.

5.3.4 Lack of behavioral abnormalities in Camk;β23 unrecombined mice

In humans affected by NDs, the consequences of aggregate pathology and neurodegeneration are clinical symptoms affecting cognition and motor function. Therefore, we

investigated if aggregation of artificial β23 protein could lead to effects in behavioral function in our mouse model.

We performed a wide variety of memory and motor tests in big Camk;β23 unrecombined mice cohorts including male and female mice. Importantly, and in contrast to what was done in previously published studies, we included the two single transgenic control groups in the studies and analyzed them as independent groups, instead of pooling them together.

Overall, we did not detect any remarkable differences among the three genotypes, neither in motor nor in memory tests (Figs.4.21, 4.22 and 4.23). Although we detected some trends or significant effects suggesting impaired function in some memory tests in tTa+β23+ mice, these effects were only significant in comparison to β23+ control mice, but not to tTa+ control mice. Similarly, performance in fine movement tests, such as the balance beam and beam ladder, was worse in tTa+ and tTa+β23+ mice in comparison to β23+ mice, but there was no difference between the two groups. Thus, these data indicate that tTa expression by itself might be affecting behavioral outcome.

As mentioned above, it was reported that tTa expression in CamkIIα:tTa mice has a neurodegenerative effect on dentate gyrus granule cell layer and this effect is dependent on genetic background [251]. Aiming to overcome this effect, we adopted a breeding strategy that resulted in 25% CBA / 75% C57BL/6 genetic background in our F1. Nevertheless, as shown by the brain weight and behavior data, tTa expression in this genetic background still had an effect. Therefore, tTa expression might have masked subtle effects driven by β23 expression. Perhaps strengthening of β23 over tTa driven effects may be achieved by studying β23 homozygous mice.

Finally, as mentioned in section 2.3 of the introduction, most mouse models of NDs do not reproduce the whole spectrum of the disease phenotype. For example, mice in which Aβ deposition is driven in absence of APP overexpression, including knock-in models, show plaques and gliosis, but subtle behavioral abnormalities [172, 173]. Moreover, neurodegenerative diseases are characterized by their progression and overt manifestation at an advanced age. In agreement, some mouse models show behavioral deficits very late in life, such as some PD models, which present behavior phenotypes

not earlier than at 16 months of age [167]. Thus, analysis of further aged mice may shed light on the validity of Camk;β23 mice as a neurodegeneration model.

5.3.5 Embryonic lethality in NEFH;β23 unrecombined mice

To circumvent the effects driven by CamkIIα:tTa expression and to target a broader neuronal population throughout the CNS, we decided to cross our β23 mice to NEFH:tTa mice. The strategy of changing the driver has already been used in a TDP-43 mouse model of ALS: a first report characterized the line under expression control of CamkIIα:tTa [260], and a second report used the same TDP-43 mouse model in combination with tTa expression driven by the NEFH promoter [252]. Indeed, our NEFH;β23 mice might be most valuable to study protein aggregation toxicity mechanisms with a focus on ALS.

In Camk;β23 unrecombined mice, β23 expression during development resulted in brain atrophy, while the animal's survival was not affected. On the other hand, NEFH;β23 unrecombined were not viable, unless animals were raised on Dox to prevent β23 expression during development. Why and how can the same protein lead to such different outcomes? As it has been pointed out throughout the thesis, different expression levels induced by different promoters could likely have an effect. Moreover, based on the NEFH promoter expression pattern, we would expect β23 expression in motor neurons [252]. Perhaps proteostatic dysfunction and malfunctioning NCT caused by β23 aggregation could be particularly detrimental for vulnerable motor neurons in NEFH;β23 mice, as detected in ALS cellular and animal models [269, 130]. Further experimental analysis will help unravel the mechanistics of β23 aggregation toxicity and its behavioral consequences in NEFH;β23 mice.

5.3.6 β23 *in vivo*: concluding remarks and outlook

We have generated a novel Tet-inducible β23 transgenic mouse model. Two variants of β23 mice have been studied in this thesis: unrecombined and recombined mice. Interestingly, while the two lines presented aggregate pathology in the forebrain of Camk;β23 mice, only unrecombined mice presented reduced brain weight and cortical thickness. Moreover, in unrecombined mice, small β23 inclusions accumulated in

the nuclear envelope of neurons, suggesting an interference with nucleocytoplasmic transport. Despite these observations, β23 expression did not lead to the development of any behavioral impairment in Camk;β23 mice, at least at the measured ages.

Overall, taking into consideration both *in vitro* and *in vivo* data, there might be a discrepancy with regard to the cytotoxicity induced by the different constructs in the two systems. That is, we have shown that fused protein β23mCherry expression is more toxic than β23 to cultured neurons, whereas β23 *in vivo* seems to be more toxic than β23mCherry. However, further experiments would be needed to clarify this issue. As mentioned above, we did not compare the expression levels of β23 and β23mCherry in cultured neurons. This comparison, along with the neuronal viability assessment, would be necessary to make any final conclusion on the cytotoxicity of the constructs. Moreover, confirming that the two mouse lines express the same levels of β-sheet protein would as well be needed.

At this point, taking into consideration our results in Camk;β23 and NEFH;β23 mice, our data suggest that the presence of an amyloid-like aggregated protein in the CNS is enough to drive a neurodegeneration phenotype. However, vulnerability of different neuronal subpopulations can strongly influence the phenotype severity. This is reminiscent of the selective vulnerability of particular neuronal subpopulations in the development of different NDs [110].

Importantly, further studies should address the age-dependency of the neurodegeneration in β23 mice. We need to make sure that mice develop a progressive phenotype with age, not only a developmental phenotype. HD mice with HTT expression restricted to development recapitulated characteristic features of HD [270], suggesting that aberrant mechanisms during development are crucial to disease progression. However, relevance of these findings for other NDs or human disease has not been confirmed. Analysis of aged Dox-treated NEFH;β23 unrecombined mice will be crucial to address this issue.

Moreover, our studies have been very much focused on neuronal effects. Recent research has reinforced the role of glial cells as driving forces in neurodegeneration [65] and investigating glial reactivity mechanisms in β23 mice would be necessary for complete pathology characterization in this model. In addition, another option would

be expressing β23 in glial cells and analyzing the effects on neuronal survival and at circuit level to study the non-cell autonomous component of neurodegeneration.

Further research avenues using the β23 mice could focus on molecular mechanisms. Especially, analyzing nucleocytoplasmic transport function might be particularly relevant for the neurodegeneration field, given that it is still an open question whether common NCT pathways are disrupted by different protein aggregates.

Finally, there are three more lines of investigation that we did not exploit yet, which might help shed light on fundamental questions of protein aggregation toxicity. One is the investigation of protein aggregation effects at circuit level. Functional *in vivo* imaging of neurons bearing aggregates versus neurons without aggregates could be done in the recombined line to study effects of aggregation on neuronal activity. Moreover, β23mCherry expression could be stopped at different ages with Dox to monitor the aggregate clearing capacity with aging *in vivo*, along with its effects on neuronal activity. These experiments may be useful for assessment of the ideal timepoint to administer therapeutics to reverse disease progression. Alternatively, the third experimental line would focus on protein seeding and spreading. It has not been tested yet, whether artificial amyloid-like protein aggregation can be seeded, whether it can spread to other brain regions, or whether artificial proteins can seed naturally aggregating proteins, such as tau or synuclein. If amyloid-like protein aggregation could be seeded, it would indicate that amyloid structure is sufficient to induce conformational changes in soluble proteins leading to aggregation. This would imply the possibility of proteins cross-seeding each other, which may lead the field into the development of structure-targeting therapeutics [7].

6 Conclusions

In this thesis, I provide the first characterization of the effects elicited by artificial amyloid-like aggregating proteins on cultured neurons and in a novel mouse model. We show that β4mCherry and β23mCherry form aggregates in primary neurons. Moreover, expression of β4mCherry and β23mCherry results in neuronal morphology and progressive time-dependent neuronal death. Given that we detect reduced phosphorylated Akt after BDNF treatment in β-sheet protein expressing neurons, impaired neurotrophic signaling might be involved in the cause of neuronal death.

In addition, we identify the neuronal interactome of mCherry-tagged artificial β-sheet proteins. Thereby, we show that aggregating proteins engage in aberrant interactions with proteins involved in a variety of cellular functions. Some of these proteins are necessary for neuronal survival, as revealed by a loss of function Crispr/Cas9 screen. The list of interactor proteins we provide constitutes a resource of candidates potentially involved in common mechanisms of aggregation toxicity.

Finally, we generated a novel inducible transgenic mouse line to study amyloid-like aggregation effects *in vivo*. β-sheet protein expression in the forebrain results in aggregate formation, brain atrophy, and engagement of nucleocytoplasmic transport components with the aggregates. However, we detect no behavioral deficits in these animals. β-sheet protein expression in the whole CNS is on the other hand lethal. These novel mouse lines may be useful tools to study effects on nucleocytoplasmic transport which result from protein aggregation.

Overall, we identified neurodegeneration-relevant pathways, such as neurotrophic signaling and nucleocytoplasmic transport, by utilizing artificial amyloid-like aggregating proteins. Our results confirm the validity of these model proteins to investigate gain of function mechanisms of protein aggregation. Further investigations combining the use of artificial and naturally aggregating proteins may enhance the identification of therapeutic targets for neurodegenerative diseases.

7 Supplementary methods

This section contains the description of methods that were key to my thesis, but performed by collaborators. Proteomic analyses were performed by Daniel Hornburg, who kindly provided the protocols. Behavior tests were performed by the German mouse clinic (Helmholtz Zentrum Muenchen) and the protocols were kindly provided by the staff.

7.1 Proteomics: methods description

LC-MS/MS

We separated peptides on a Thermo Scientific EASY-nLC 1000 HPLC system (Thermo Fisher). Columns (75 μm inner diameter, 40-cm length) were in-house packed with 1.9 μm C18 particles (Dr. Maisch GmbH). Peptides were loaded in buffer A (0.5% formic acid) and separated with a gradient from 7% to 60% buffer B (80% acetonitrile, 0.5% formic acid) within 3.5 h at 200 nl/min. The column temperature was set to $60°C$. A quadrupole Orbitrap mass spectrometer (Q Exactive, Thermo Fisher Scientific) was directly coupled to the liquid chromatograph via a nano-electrospray source. The Q Exactive was operated in a data-dependent mode. The survey scan range was set to 300 to 1.650 m/z, with a resolution of 70.000 at m/z 200. Up to the 15 most abundant isotope patterns with a charge of =2 were subjected to Higher-energy collisional dissociation [271] with a normalized collision energy of 25, an isolation window of 2 Th, and a resolution of 17.500 at m/z 200. To limit repeated sequencing, dynamic exclusion of sequenced peptides was set to 30 s. Thresholds for ion injection time and ion target value were set to 20 ms and $3x10^6$ for the survey scans and to 60 ms and 106 for the MS/MS scans. Data were acquired using Xcalibur software (Thermo Scientific).

Solid phase extraction (StageTips)

Stage tips were prepared with 3xC18 material for rapid desalting and step elution of the peptide mixtures. The stage tips were rinsed with Methanol and Buffer A (0,5%

acetic acid). Then, the samples were added to the staging tips and washed with buffer A. Buffer B (80% ACN, 0.5% acetic acid) was used to elute the samples. To remove the solvent from the samples a Speedvac was used. Finally, the samples were resuspended in 10 μl buffer A* (0.5% Acetic acid, 0.1% T rifluoroacetic acid (TFA), 2% Acetonitrile (ACN)).

Complete proteome analysis

In order to identify all the proteins present in the cortical neurons after lysis, complete proteome analysis was performed. Lysis buffer (4% SDS, 10 mM DTT, 10 mM Hepes pH=8) was applied for 10 min. Then, proteins were subjected to 45 min of alkylation with 55 mM iodoacetamide. Acetone precipitation was performed to remove the detergent. Acetone (-20°C) was added to 100 μg of proteins to a final concentration of 80% v/v, and proteins were precipitated overnight at -20°C. The supernatant was removed after 15 min of centrifugation (4°C, 16,000xg) followed by washing with 80% acetone (-20°C). Residual acetone was evaporated at RT. The protein pellet was dissolved in 50 μl of 6 M urea/2 M thiourea, 10 mM Hepes, pH=8.0. Lys C (1 μg) digestion was carried out for 2 h at RT. Then, samples were incubated with 1 μg Trypsin for overnight digestion. Finally, peptides were desalted on C18 StageTips.

Data Analysis and Statistics of MS data

To process MS raw files, we employed MaxQuant software (v. 1.5.7.10)[272]. We used Andromeda [273], which is integrated into MaxQuant, to search MS/MS spectra against the UniProtKB FASTA database. For the standard immunoprecipitation and pre-loaded serum, enzyme specificity was set to trypsin and Lysine C. For the antigen pre-digestion, the specificity was set only to Lysine C. For all the experiments, N-terminal cleavage to proline and up to two miscleavages were allowed. Peptides had to have a minimum length of seven amino acids to be considered for identification. Oxidation, acetylation and deamidation were set as variable modifications (maximum number of modifications per peptide=5). A false discovery rate (FDR) cutoff of 1% was applied at the peptide and protein levels. Initial precursor mass deviation of up to 4.5 ppm and fragment mass deviation up to 20 ppm were allowed. Precursor ion mass accuracy was improved by time-dependent recalibration algorithms in MaxQuant. The cutoff score (delta score) for accepting individual MS/MS spectra was 17. As

a library for matches we used the proteome fasta file from Mus musculus (Taxon identifier: 10090). Nonlinear retention time alignment [274] of all measured samples was performed in MaxQuant. "Match between runs," which allows the transfer of peptide identifications in the absence of sequencing, was enabled with a maximum retention time window of 0.7 min. Furthermore, we filtered our data by requiring a minimum peptide ratio count of 1 in MaxLFQ [275]. Protein identification required at least one razor peptide [272]. Proteins that could not be discriminated on the basis of unique peptides were grouped into protein groups. For statistical and bioinformatic analysis, as well as for visualization, we used the open PERSEUS environment, which is part of MaxQuant. To gain better behavior of the data in statistical tests, we transformed the numerical data to log2(x). Moreover, proteins were filtered for common contaminants and proteins identified only by site modification and reverse proteins were excluded from further analysis. To figure out, if any of the samples is an out layer, we displayed a hierarchical clustering map. To identify the most discriminating proteins in group wise comparisons, first we performed imputation of missing values with a normal distribution (width = 0.3; shift = 1.8) as described elsewhere [274]. For pairwise comparison of proteomes and determination of significant differences in protein abundances, t-test statistics were applied with a permutation-based FDR of 5% and S0 of 1. The resulting significant outliers for each of the sample pairs were analyzed for gene ontology cellular component (GOCC)[216], biological process (GOBP), Molecular function (GOMF), protein complexes (Corum)[276] and protein families and domains (Pfam) [277] annotation enrichment. For visual representation, we displayed the data in a scatter plot.

To calculate the content of disordered regions, we employed R (rjson and seqinr libraries). First, we mapped amino acids that are predicted with low complexity long region (IUPred-L) to sequences of proteins that are significant outliers in either of the β-sheet interactomes as well as for the entire population of proteins identified in the interactomes. Proteins were only considered if they were detected with at least three valid values in at least one condition. Next the ratio of all amino acids and those predicted with low complexity was calculated. To determine the significance of differences between the individual populations, a two-sample Wilcoxon tests was performed on the ratio distributions.

Finally, to depict common and exclusively interaction proteins we employed R

basic and igraph functions. Significantly enriched proteins were plotted with the edge width scaled by enrichment score.

7.2 Mouse behavior analysis

Male and female mice of the three following genotypes were analyzed: β23+, tTa+, tTa+ β23+. Fifteen animals per sex and genotype were analyzed in all tests, except for tTa+ males, which were only fourteen. Therefore, a total of 89 mice were studied. Mice were acclimatized to the lab environment at least 15 minutes, before the start of each habituation or test session. Table 7.1 summarizes all performed tests and the age at which they were performed.

Behavior test	**Age in weeks**
Open field	22
Y-maze test	23
Grip strength	31
Rotarod	31
Balance beam	33
Horizontal ladder	33
Social discrimination	34
Object recognition	36
Place and reversal learning in Intellicage	43

Table 7.1: List of behavior tests.

7.2.1 Open field

The Open Field test was carried out according to the standardized phenotyping screens utilized by the International Mouse Phenotyping Consortium (IMPC) and available at https://www.mousephenotype.org/impress/protocol/81/7. The light apparatus and software ActiMot2 were purchased from TSE-system. The light apparatus consisted of a square-shaped frame with two pairs of light-beam strips, each pair consisting of one transmitter strip and one receiver strip. These basic light barrier strips were arranged at right angles to each other in the same plane to determine the

X and Y coordinates of the animal, and thus its location (XY frame). Each strip was equipped with 16 infrared sensors with a distance of 28mm between adjacent sensors. With two further pairs of uni-dimensional light-barrier strips (Z1 and Z2), rearing could be detected in addition to location.

The test apparatus where the mouse was placed consisted of a transparent and infrared light permeable acrylic test arena (internal measurements: 45.5 x 45.5 x 39.5 cm) with a smooth floor. The illumination levels were set at approximately 150 lux in the corners and 200 lux in the middle of the test arena. At the beginning of the experiment, all animals were transported to the test room and left undisturbed for at least 30 minutes before the testing started. Then each animal was placed individually into the middle of one side of the arena facing the wall and allowed to freely explore the arena for 20 min.

7.2.2 Y-maze

Spontaneous alternations were assessed using the Y-Maze, which was made of opaque light grey PVC and had 3 identical arms (30 x 5 x 15 cm) placed at 120° from each other; illumination in the center of the maze was 100 lux. Each mouse was placed at the end of one arm and allowed to move freely through the maze during a 5-minute session. Spontaneous alternations (defined as consecutive entries into all three arms without repetitions in overlapping triplet sets) were scored. Total numbers of arm entries were collected cumulatively over the 5 minutes. Spontaneous alternation performance percentage is defined as the ratio of actual (total alternations) to possible alternations (total number of triplets) x 100. Measured parameters included spontaneous alternations, alternate arm returns and same arm returns.

7.2.3 Grip strength

The grip strength meter system was purchased from Bioseb. Mice were allowed to catch the grid with either 2 or 4 paws. Three trials, all measured within one minute, were undertaken for each mouse.

7.2.4 Rotarod

Mice were placed on the Rotarod (Bioseb) at an accelerating speed from 4 to 40 rpm for 300 sec with 15 min between each trial. They were given three trials at the accelerating speed on one day. The mean latency to fall off the Rotarod during the trials was recorded.

7.2.5 Beam walk

In the beam walk test, mice had to traverse a distance of 90 cm on series of elevated, narrow beams (diameters beams 1-4: square 20 mm, round 22 mm, square 12 mm, round 15 mm) to reach their respective home cage. Mice were trained before with the largest beam by habituating them to the apparatus and letting them cross the beam from each near, mid and far distance once. The quantified parameters in the test were: traversing time, number of stops, and fore- and hind-paw slips; which were recorded manually. The means of 3 trials per mouse were used for data analysis.

7.2.6 Beam ladder

The beam ladder test was performed shortly after the beam walk, without previous habituation. In this test, mice were required to traverse a narrow horizontal ladder equipped with metal beams of 1 mm in diameter to reach their respective home cage. The beams were placed in various and irregular distances to each other. Traversing time as well as fore- and hind-paw slips were recorded manually, and the means of 3 trials per mouse were used for data analysis.

7.2.7 Social discrimination

The Social Discrimination procedure consisted of two 4 min exposures of stimulus animals (ovariectomized 129Sv females) to the test animal in a fresh cage to which the test animal had been moved 2 h prior to testing. All stimulus animals are identified using coloured non-toxic non-permanent paint markers on the tail. After a retention interval of 2 h, the stimulus animal was presented to the test animal together with an additional, previously not presented stimulus animal. A separate “familiar” and “unfamiliar” stimulus animal was assigned to each test animal. The

duration of investigatory behavior of the test animal towards the stimulus animals (familiar and unfamiliar) during this test phase was again recorded by a trained observer with a hand-held computer. A social recognition index was calculated as time spent investigating the unfamiliar stimulus mouse / time spent investigating both the familiar and unfamiliar stimulus mouse.

7.2.8 Novel object recognition

Test mice were transferred to the behavior room 15 min prior to habituation or testing. Habituation was done on two consecutive days before testing and mice were placed in the empty arena and allowed to freely explore it for 10 minutes. On the testing day, two identical objects were placed into the arena and the test mouse was allowed to explore them for 5 minutes. This sample phase was performed a total of three times. After retention intervals of 3 hours and 24 hours one of the previous encountered familiar objects was substituted by a new, unfamiliar one. The mouse was put back into the arena for another 5 minutes and exploration time was recorded. Mice were recorded with the Ethovision video-tracking system and the analysis performed with the Observer software (Noldus).

7.2.9 Place and reversal learning in Intellicage

Place and reversal learning were tested using the IntelliCage (NewBehavior, TSE Systems). Mice were first injected with a transponder "White Label" (Planet ID) under isoflurane anesthesia and given a recovery period of one week. Up to 10 mice were then introduced into each Intellicage. Mice were housed according to genotype.

During the habituation phase (days 1-4), all doors protecting the water bottles were open and mice had access to all corners to obtain water. On days 4-7, a nosepoke adaptation period trained the mice to nosepoke for water. All doors closed during this time and the mice had to nosepoke to open the door to get water. The door opened only with the first nosepoke and closed 4 seconds later. They could access water in all four corners. On days 7-14, controlled by the Intellicage software, each mouse could only obtain water in one of the Intellicage corners (designated the "correct corner"). This was, for each mouse, the least preferred corner during the nosepoke

adaptation phase. Any attempts to access water in the other three corners were recorded as an error ("incorrect nosepoke"). The percentage error rate (Number incorrect nosepokes/total number nosepokes x 100) was calculated.

For the reversal learning paradigm, on days 14-21, the assigned corner in which each mouse could access water switched to the opposite corner. The percentage error rate (as calculated for place learning) was determined for each animal.

List of Figures

List of Tables

List of Abbreviations

dH_2**O** destilled water.

3G Third generation.

A Ampere.

AChE Acetylcholinesterase.

AD Alzheimer's disease.

ALS Amyotrophic lateral sclerosis.

Amp Ampicillin.

APS Ammonium persulfate.

BAC Bacterial artificial chromosome.

BDNF Brain-derived neurotrophic factor.

BSA Bovine serum albumin.

C Celsius.

C9 C9orf72.

CamKIIα calcium-calmodulin-dependent kinase II.

Chat Choline acetyltransferase.

CMV Cytomegalovirus.

CNS Central nervous system.

Crispr Clustered regularly interspaced short palindromic repeats.

DA Dopamine.

DIV Days in vitro.

DMEM Dulbecco's Modified Eagle Medium.

DNA Deoxyribonucleic acid.

Dox Doxycycline.

DPR Dipeptide repeat.

DSB Double-stranded breaks.

DTT Dithiothreitol.

E Embryonic day.

FBS Fetal Bovine Serum.

frt Flippase recognition target.

FTD Frontotemporal dementia.

GABA gamma-Aminobutyric acid.

GDP Guanosine diphosphate.

GEF guanine nucleotide exchange factor.

GPCR G protein-coupled receptor.

GTP Guanosine triphosphate.

h hour.

hBDNF human Brain-derived neurotrophic factor.

HBSS Hank's balanced salt solution.

HD Huntington's disease.

hTau human Tau.

HTT Huntingtin.

IDR Intrinsically disordered region.

IP Immunoprecipitation.

IP Immunoprecipitation.

IRES Internal ribosome entry site.

Kan Kanamycin.

Kb Kilobase.

LB Luria-Bertani.

LTP Long-term potentiation.

Luc Luciferase.

LV Lentivirus.

MCI Mild cognitive impairment.

mg milligram.

min minutes.

ml milliliter.

mm millimeter.

MS Mass Spectrometry.

MSN Medium spiny neuron.

MTT Thiazolyl Blue Tetrazolium Bromide.

NCT Nucleocytoplasmic transport.

NDs Neurodegenerative diseases.

NEAA Non-essential aminoacids.

NEFH Neurofilament heavy chain.

NGF nerve growth factor.

NHEJ Non-homologous end joining.

NPC Nuclear pore complex.

NTF Neurotrophin.

PAM Protospacer adjacent motif.

PCR Polymerase chain reaction.

PD Parkinson's disease.

Pen/Strep Penicillin/Streptomycin.

PFA Paraformaldehyde.

Pfu *Pyrococcus furiosus*.

PrD Prion diseases.

PVDF Polyvinylidene difluoride.

RLU Relative light units.

RNA Ribonucleic acid.

rpm revolutions per minute.

RT Room temperature.

rtTa Reverse tetracycline transactivator.

SA Sodium azide.

SCA Spinocerebellar ataxia.

SD Standard deviation.

sgRNA single guide RNA.

SPF Specific-pathogen-free.

TAE Tris-Acetate-EDTA.

TBS-T Tris-buffered saline with Tween20.

TE Tris-EDTA.

TEMED Tetramethylethylenediamine.

Tet Tetracycline.

TRE Tetracycline responsive element.

tTa Tetracycline transactivator.

UPS Ubiquitin-proteasome system.

V Volts.

wt wild-type.

References

[1] M. Prince, R. Bryce, E. Albanese, A. Wimo, W. Ribeiro, and C. P. Ferri, "The global prevalence of dementia: a systematic review and metaanalysis," *Alzheimer's & dementia*, vol. 9, no. 1, pp. 63–75, 2013.

[2] G. Livingston, A. Sommerlad, V. Orgeta, S. G. Costafreda, J. Huntley, D. Ames, C. Ballard, S. Banerjee, A. Burns, J. Cohen-Mansfield, *et al.*, "Dementia prevention, intervention, and care," *The Lancet*, vol. 390, no. 10113, pp. 2673–2734, 2017.

[3] R. G. Canter, J. Penney, and L.-H. Tsai, "The road to restoring neural circuits for the treatment of Alzheimer's disease," *Nature*, vol. 539, no. 7628, p. 187, 2016.

[4] A. Abeliovich and A. D. Gitler, "Defects in trafficking bridge Parkinson's disease pathology and genetics," *Nature*, vol. 539, no. 7628, p. 207, 2016.

[5] J. Labbadia and R. I. Morimoto, "Huntington's disease: underlying molecular mechanisms and emerging concepts," *Trends in biochemical sciences*, vol. 38, no. 8, pp. 378–385, 2013.

[6] J. P. Taylor, R. H. Brown Jr, and D. W. Cleveland, "Decoding ALS: from genes to mechanism," *Nature*, vol. 539, no. 7628, p. 197, 2016.

[7] C. Soto and S. Pritzkow, "Protein misfolding, aggregation, and conformational strains in neurodegenerative diseases," *Nature Neuroscience*, vol. 21, pp. 1332–1340, sep 2018.

[8] A. W. Fitzpatrick, G. T. Debelouchina, M. J. Bayro, D. K. Clare, M. A. Caporini, V. S. Bajaj, C. P. Jaroniec, L. Wang, V. Ladizhansky, S. A. Müller, *et al.*, "Atomic structure and hierarchical assembly of a cross-β amyloid fibril," *Proceedings of the National Academy of Sciences*, p. 201219476, 2013.

[9] F. Chiti and C. M. Dobson, "Protein misfolding, amyloid formation, and human disease: a summary of progress over the last decade," *Annual review of biochemistry*, vol. 86, pp. 27–68, 2017.

[10] J. T. Jarrett and P. T. Lansbury Jr, "Seeding "one-dimensional crystallization" of amyloid: a pathogenic mechanism in Alzheimer's disease and scrapie?," *Cell*, vol. 73, no. 6, pp. 1055–1058, 1993.

[11] G. Meisl, L. Rajah, S. A. Cohen, M. Pfammatter, A. Šarić, E. Hellstrand, A. K. Buell, A. Aguzzi, S. Linse, M. Vendruscolo, *et al.*, "Scaling behaviour and rate-determining steps in filamentous self-assembly," *Chemical science*, vol. 8, no. 10, pp. 7087–7097, 2017.

[12] B. M. Broome and M. H. Hecht, "Nature disfavors sequences of alternating polar and non-polar amino acids: implications for amyloidogenesis," *Journal of molecular biology*, vol. 296, no. 4, pp. 961–968, 2000.

[13] D. Balchin, M. Hayer-Hartl, and F. U. Hartl, "In vivo aspects of protein folding and quality control," *Science*, vol. 353, no. 6294, p. aac4354, 2016.

[14] A. Goate, M.-C. Chartier-Harlin, M. Mullan, J. Brown, F. Crawford, L. Fidani, L. Giuffra, A. Haynes, N. Irving, L. James, *et al.*, "Segregation of a missense mutation in the amyloid precursor protein gene with familial Alzheimer's disease," *Nature*, vol. 349, no. 6311, p. 704, 1991.

[15] G. D. Schellenberg, T. D. Bird, E. M. Wijsman, H. T. Orr, L. Anderson, E. Nemens, J. A. White, L. Bonnycastle, J. L. Weber, M. E. Alonso, *et al.*, "Genetic linkage evidence for a familial Alzheimer's disease locus on chromosome 14," *Science*, vol. 258, no. 5082, pp. 668–671, 1992.

[16] E. Levy-Lahad, W. Wasco, P. Poorkaj, D. M. Romano, J. Oshima, W. H. Pettingell, C. E. Yu, P. D. Jondro, S. D. Schmidt, K. Wang, *et al.*, "Candidate gene for the chromosome 1 familial Alzheimer's disease locus," *Science*, vol. 269, no. 5226, pp. 973–977, 1995.

[17] B. De Strooper, P. Saftig, K. Craessaerts, H. Vanderstichele, G. Guhde, W. Annaert, K. Von Figura, and F. Van Leuven, "Deficiency of presenilin-1 inhibits the normal cleavage of amyloid precursor protein," *Nature*, vol. 391, no. 6665, p. 387, 1998.

[18] Y.-M. Li, M. Xu, M.-T. Lai, Q. Huang, J. L. Castro, J. DiMuzio-Mower, T. Harrison, C. Lellis, A. Nadin, J. G. Neduvelil, *et al.*, "Photoactivated γ-secretase inhibitors directed to the active site covalently label presenilin 1," *Nature*, vol. 405, no. 6787, p. 689, 2000.

[19] W. P. Esler, W. T. Kimberly, B. L. Ostaszewski, T. S. Diehl, C. L. Moore, J.-Y. Tsai, T. Rahmati, W. Xia, D. J. Selkoe, and M. S. Wolfe, "Transition-state analogue inhibitors of γ-secretase bind directly to presenilin-1," *Nature cell biology*, vol. 2, no. 7, p. 428, 2000.

[20] A. Rovelet-Lecrux, D. Hannequin, G. Raux, N. Le Meur, A. Laquerrière, A. Vital, C. Dumanchin, S. Feuillette, A. Brice, M. Vercelletto, *et al.*, "APP locus duplication causes autosomal dominant early-onset Alzheimer disease with cerebral amyloid angiopathy," *Nature genetics*, vol. 38, no. 1, p. 24, 2006.

[21] J. A. Hardy and G. A. Higgins, "Alzheimer's disease: the amyloid cascade hypothesis," *Science*, vol. 256, no. 5054, p. 184, 1992.

[22] E. H. Corder, A. M. Saunders, W. J. Strittmatter, D. E. Schmechel, P. C. Gaskell, G. Small, A. D. Roses, J. Haines, and M. A. Pericak-Vance, "Gene dose of apolipoprotein E type 4 allele and the risk of Alzheimer's disease in late onset families," *Science*, vol. 261, no. 5123, pp. 921–923, 1993.

[23] J. C. Morris, C. M. Roe, C. Xiong, A. M. Fagan, A. M. Goate, D. M. Holtzman, and M. A. Mintun, "APOE predicts amyloid-beta but not tau Alzheimer pathology in cognitively normal aging," *Annals of neurology*, vol. 67, no. 1, pp. 122–131, 2010.

[24] Y. Wang, M. Cella, K. Mallinson, J. D. Ulrich, K. L. Young, M. L. Robinette, S. Gilfillan, G. M. Krishnan, S. Sudhakar, B. H. Zinselmeyer, *et al.*, "TREM2 lipid sensing sustains the microglial response in an Alzheimer's disease model," *Cell*, vol. 160, no. 6, pp. 1061–1071, 2015.

[25] M. Hutton, C. L. Lendon, P. Rizzu, M. Baker, S. Froelich, H. Houlden, S. Pickering-Brown, S. Chakraverty, A. Isaacs, A. Grover, *et al.*, "Association of

missense and 5-splice-site mutations in tau with the inherited dementia FTDP-17," *Nature*, vol. 393, no. 6686, p. 702, 1998.

[26] M. G. Spillantini, M. L. Schmidt, V. M.-Y. Lee, J. Q. Trojanowski, R. Jakes, and M. Goedert, "α-Synuclein in Lewy bodies," *Nature*, vol. 388, no. 6645, p. 839, 1997.

[27] M. H. Polymeropoulos, J. J. Higgins, L. I. Golbe, W. G. Johnson, S. E. Ide, G. Di Iorio, G. Sanges, E. S. Stenroos, L. T. Pho, A. A. Schaffer, *et al.*, "Mapping of a gene for Parkinson's disease to chromosome 4q21-q23," *Science*, vol. 274, no. 5290, pp. 1197–1199, 1996.

[28] A. Singleton, M. Farrer, J. Johnson, A. Singleton, S. Hague, J. Kachergus, M. Hulihan, T. Peuralinna, A. Dutra, R. Nussbaum, *et al.*, "α-Synuclein locus triplication causes Parkinson's disease," *Science*, vol. 302, no. 5646, pp. 841–841, 2003.

[29] M.-C. Chartier-Harlin, J. Kachergus, C. Roumier, V. Mouroux, X. Douay, S. Lincoln, C. Levecque, L. Larvor, J. Andrieux, M. Hulihan, *et al.*, "α-synuclein locus duplication as a cause of familial Parkinson's disease," *The Lancet*, vol. 364, no. 9440, pp. 1167–1169, 2004.

[30] A. Zimprich, S. Biskup, P. Leitner, P. Lichtner, M. Farrer, S. Lincoln, J. Kachergus, M. Hulihan, R. J. Uitti, D. B. Calne, *et al.*, "Mutations in LRRK2 cause autosomal-dominant parkinsonism with pleomorphic pathology," *Neuron*, vol. 44, no. 4, pp. 601–607, 2004.

[31] C. Paisán-Ruız, S. Jain, E. W. Evans, W. P. Gilks, J. Simón, M. Van Der Brug, A. L. De Munain, S. Aparicio, A. M. Gil, N. Khan, *et al.*, "Cloning of the gene containing mutations that cause PARK8-linked Parkinson's disease," *Neuron*, vol. 44, no. 4, pp. 595–600, 2004.

[32] J. R. Mazzulli, Y.-H. Xu, Y. Sun, A. L. Knight, P. J. McLean, G. A. Caldwell, E. Sidransky, G. A. Grabowski, and D. Krainc, "Gaucher disease glucocerebrosidase and α-synuclein form a bidirectional pathogenic loop in synucleinopathies," *Cell*, vol. 146, no. 1, pp. 37–52, 2011.

[33] T. Kitada, S. Asakawa, N. Hattori, H. Matsumine, Y. Yamamura, S. Minoshima, M. Yokochi, Y. Mizuno, and N. Shimizu, "Mutations in the parkin gene cause

autosomal recessive juvenile parkinsonism," *nature*, vol. 392, no. 6676, p. 605, 1998.

[34] M. Periquet, M. Latouche, E. Lohmann, N. Rawal, G. De Michele, S. Ricard, H. Teive, V. Fraix, M. Vidailhet, D. Nicholl, *et al.*, "Parkin mutations are frequent in patients with isolated early-onset parkinsonism," *Brain*, vol. 126, no. 6, pp. 1271–1278, 2003.

[35] E. M. Valente, P. M. Abou-Sleiman, V. Caputo, M. M. Muqit, K. Harvey, S. Gispert, Z. Ali, D. Del Turco, A. R. Bentivoglio, D. G. Healy, *et al.*, "Hereditary early-onset Parkinson's disease caused by mutations in PINK1," *Science*, vol. 304, no. 5674, pp. 1158–1160, 2004.

[36] V. Bonifati, P. Rizzu, M. J. Van Baren, O. Schaap, G. J. Breedveld, E. Krieger, M. C. Dekker, F. Squitieri, P. Ibanez, M. Joosse, *et al.*, "Mutations in the DJ-1 gene associated with autosomal recessive early-onset parkinsonism," *science*, vol. 299, no. 5604, pp. 256–259, 2003.

[37] C. A. Ross and S. J. Tabrizi, "Huntington's disease: from molecular pathogenesis to clinical treatment," *The Lancet Neurology*, vol. 10, no. 1, pp. 83–98, 2011.

[38] R. Morigaki and S. Goto, "Striatal vulnerability in Huntington's disease: Neuroprotection versus neurotoxicity," *Brain sciences*, vol. 7, no. 6, p. 63, 2017.

[39] P. McColgan and S. J. Tabrizi, "Huntington's disease: a clinical review," *European journal of neurology*, vol. 25, no. 1, pp. 24–34, 2018.

[40] M. E. MacDonald, C. M. Ambrose, M. P. Duyao, R. H. Myers, C. Lin, L. Srinidhi, G. Barnes, S. A. Taylor, M. James, N. Groot, *et al.*, "A novel gene containing a trinucleotide repeat that is expanded and unstable on Huntington's disease chromosomes," *Cell*, vol. 72, no. 6, pp. 971–983, 1993.

[41] D. R. Rosen, T. Siddique, D. Patterson, D. A. Figlewicz, P. Sapp, A. Hentati, D. Donaldson, J. Goto, J. P. O'Regan, H.-X. Deng, *et al.*, "Mutations in Cu/Zn superoxide dismutase gene are associated with familial amyotrophic lateral sclerosis," *Nature*, vol. 362, no. 6415, p. 59, 1993.

[42] L. Bruijn, M. Becher, M. Lee, K. Anderson, N. Jenkins, N. Copeland, S. Sisodia, J. Rothstein, D. Borchelt, D. Price, *et al.*, "ALS-linked SOD1 mutant G85R

mediates damage to astrocytes and promotes rapidly progressive disease with SOD1-containing inclusions," *neuron*, vol. 18, no. 2, pp. 327–338, 1997.

[43] J. Sreedharan, I. P. Blair, V. B. Tripathi, X. Hu, C. Vance, B. Rogelj, S. Ackerley, J. C. Durnall, K. L. Williams, E. Buratti, *et al.*, "TDP-43 mutations in familial and sporadic amyotrophic lateral sclerosis," *Science*, vol. 319, no. 5870, pp. 1668–1672, 2008.

[44] C. Vance, B. Rogelj, T. Hortobágyi, K. J. De Vos, A. L. Nishimura, J. Sreedharan, X. Hu, B. Smith, D. Ruddy, P. Wright, *et al.*, "Mutations in FUS, an RNA processing protein, cause familial amyotrophic lateral sclerosis type 6," *Science*, vol. 323, no. 5918, pp. 1208–1211, 2009.

[45] H. Maruyama, H. Morino, H. Ito, Y. Izumi, H. Kato, Y. Watanabe, Y. Kinoshita, M. Kamada, H. Nodera, H. Suzuki, *et al.*, "Mutations of optineurin in amyotrophic lateral sclerosis," *Nature*, vol. 465, no. 7295, p. 223, 2010.

[46] M. Neumann, D. M. Sampathu, L. K. Kwong, A. C. Truax, M. C. Micsenyi, T. T. Chou, J. Bruce, T. Schuck, M. Grossman, C. M. Clark, *et al.*, "Ubiquitinated TDP-43 in frontotemporal lobar degeneration and amyotrophic lateral sclerosis," *Science*, vol. 314, no. 5796, pp. 130–133, 2006.

[47] M. DeJesus-Hernandez, I. R. Mackenzie, B. F. Boeve, A. L. Boxer, M. Baker, N. J. Rutherford, A. M. Nicholson, N. A. Finch, H. Flynn, J. Adamson, *et al.*, "Expanded GGGGCC hexanucleotide repeat in noncoding region of C9ORF72 causes chromosome 9p-linked FTD and ALS," *Neuron*, vol. 72, no. 2, pp. 245–256, 2011.

[48] A. E. Renton, E. Majounie, A. Waite, J. Simón-Sánchez, S. Rollinson, J. R. Gibbs, J. C. Schymick, H. Laaksovirta, J. C. Van Swieten, L. Myllykangas, *et al.*, "A hexanucleotide repeat expansion in C9ORF72 is the cause of chromosome 9p21-linked ALS-FTD," *Neuron*, vol. 72, no. 2, pp. 257–268, 2011.

[49] S. Al-Sarraj, A. King, C. Troakes, B. Smith, S. Maekawa, I. Bodi, B. Rogelj, A. Al-Chalabi, T. Hortobágyi, and C. E. Shaw, "p62 positive, TDP-43 negative, neuronal cytoplasmic and intranuclear inclusions in the cerebellum and hippocampus define the pathology of C9orf72-linked FTLD and MND/ALS," *Acta neuropathologica*, vol. 122, no. 6, pp. 691–702, 2011.

[50] P. E. Ash, K. F. Bieniek, T. F. Gendron, T. Caulfield, W.-L. Lin, M. DeJesus-Hernandez, M. M. Van Blitterswijk, K. Jansen-West, J. W. Paul III, R. Rademakers, *et al.*, "Unconventional translation of C9ORF72 GGGGCC expansion generates insoluble polypeptides specific to c9FTD/ALS," *Neuron*, vol. 77, no. 4, pp. 639–646, 2013.

[51] K. Mori, S.-M. Weng, T. Arzberger, S. May, K. Rentzsch, E. Kremmer, B. Schmid, H. A. Kretzschmar, M. Cruts, C. Van Broeckhoven, *et al.*, "The C9orf72 GGGGCC repeat is translated into aggregating dipeptide-repeat proteins in FTLD/ALS," *Science*, vol. 339, no. 6125, pp. 1335–1338, 2013.

[52] T. Zu, B. Gibbens, N. S. Doty, M. Gomes-Pereira, A. Huguet, M. D. Stone, J. Margolis, M. Peterson, T. W. Markowski, M. A. Ingram, *et al.*, "Non-ATG-initiated translation directed by microsatellite expansions," *Proceedings of the National Academy of Sciences*, vol. 108, no. 1, pp. 260–265, 2011.

[53] M. Bañez-Coronel, F. Ayhan, A. D. Tarabochia, T. Zu, B. A. Perez, S. K. Tusi, O. Pletnikova, D. R. Borchelt, C. A. Ross, R. L. Margolis, *et al.*, "RAN translation in Huntington disease," *Neuron*, vol. 88, no. 4, pp. 667–677, 2015.

[54] C. Soto, "Unfolding the role of protein misfolding in neurodegenerative diseases," *Nature Reviews Neuroscience*, vol. 4, no. 1, p. 49, 2003.

[55] J. Nasir, S. B. Floresco, J. R. O'Kusky, V. M. Diewert, J. M. Richman, J. Zeisler, A. Borowski, J. D. Marth, A. G. Phillips, and M. R. Hayden, "Targeted disruption of the Huntington's disease gene results in embryonic lethality and behavioral and morphological changes in heterozygotes," *Cell*, vol. 81, no. 5, pp. 811–823, 1995.

[56] S. Zeitlin, J.-P. Liu, D. L. Chapman, V. E. Papaioannou, and A. Efstratiadis, "Increased apoptosis and early embryonic lethality in mice nullizygous for the Huntington's disease gene homologue," *Nature genetics*, vol. 11, no. 2, p. 155, 1995.

[57] A. G. Reaume, J. L. Elliott, E. K. Hoffman, N. W. Kowall, R. J. Ferrante, D. R. Siwek, H. M. Wilcox, D. G. Flood, M. F. Beal, R. H. Brown Jr, *et al.*, "Motor neurons in Cu/Zn superoxide dismutase-deficient mice develop normally but exhibit enhanced cell death after axonal injury," *Nature genetics*, vol. 13, no. 1, p. 43, 1996.

[58] H. Zheng, M. Jiang, M. Trumbauer, R. Hopkins, D. Sirinathsinghji, K. Stevens, M. Conner, H. Slunt, S. Sisodia, H. Chen, *et al.*, "Mice deficient for the amyloid precursor protein gene," *Annals of the New York Academy of Sciences*, vol. 777, no. 1, pp. 421–426, 1996.

[59] A. Abeliovich, Y. Schmitz, I. Fariñas, D. Choi-Lundberg, W.-H. Ho, P. E. Castillo, N. Shinsky, J. M. G. Verdugo, M. Armanini, A. Ryan, *et al.*, "Mice lacking α-synuclein display functional deficits in the nigrostriatal dopamine system," *Neuron*, vol. 25, no. 1, pp. 239–252, 2000.

[60] M. Koppers, A. M. Blokhuis, H.-J. Westeneng, M. L. Terpstra, C. A. Zundel, R. Vieira de Sá, R. D. Schellevis, A. J. Waite, D. J. Blake, J. H. Veldink, *et al.*, "C9orf72 ablation in mice does not cause motor neuron degeneration or motor deficits," *Annals of neurology*, vol. 78, no. 3, pp. 426–438, 2015.

[61] J. O'rourke, L. Bogdanik, A. Yanez, D. Lall, A. Wolf, A. Muhammad, R. Ho, S. Carmona, J. Vit, J. Zarrow, *et al.*, "C9orf72 is required for proper macrophage and microglial function in mice," *Science*, vol. 351, no. 6279, pp. 1324–1329, 2016.

[62] C. K. Glass, K. Saijo, B. Winner, M. C. Marchetto, and F. H. Gage, "Mechanisms underlying inflammation in neurodegeneration," *Cell*, vol. 140, no. 6, pp. 918–934, 2010.

[63] T. Wyss-Coray, J. D. Loike, T. C. Brionne, E. Lu, R. Anankov, F. Yan, S. C. Silverstein, and J. Husemann, "Adult mouse astrocytes degrade amyloid-β in vitro and in situ," *Nature medicine*, vol. 9, no. 4, p. 453, 2003.

[64] T. Wyss-Coray, C. Lin, F. Yan, G.-Q. Yu, M. Rohde, L. McConlogue, E. Masliah, and L. Mucke, "TGF-β1 promotes microglial amyloid-β clearance and reduces plaque burden in transgenic mice," *Nature medicine*, vol. 7, no. 5, p. 612, 2001.

[65] B. De Strooper and E. Karran, "The cellular phase of Alzheimer's disease," *Cell*, vol. 164, no. 4, pp. 603–615, 2016.

[66] S. F. Carter, M. Schöll, O. Almkvist, A. Wall, H. Engler, B. Långström, and A. Nordberg, "Evidence for astrocytosis in prodromal Alzheimer disease provided by 11C-deuterium-L-deprenyl: a multitracer PET paradigm combining 11C-pittsburgh compound B and 18F-FDG," *Journal of Nuclear Medicine*, vol. 53, no. 1, pp. 37–46, 2012.

[67] D. B. Re, V. Le Verche, C. Yu, M. W. Amoroso, K. A. Politi, S. Phani, B. Ikiz, L. Hoffmann, M. Koolen, T. Nagata, *et al.*, "Necroptosis drives motor neuron death in models of both sporadic and familial ALS," *Neuron*, vol. 81, no. 5, pp. 1001–1008, 2014.

[68] R. Guerreiro, A. Wojtas, J. Bras, M. Carrasquillo, E. Rogaeva, E. Majounie, C. Cruchaga, C. Sassi, J. S. Kauwe, S. Younkin, *et al.*, "TREM2 variants in Alzheimer's disease," *New England Journal of Medicine*, vol. 368, no. 2, pp. 117–127, 2013.

[69] T. Jonsson, H. Stefansson, S. Steinberg, I. Jonsdottir, P. V. Jonsson, J. Snaedal, S. Bjornsson, J. Huttenlocher, A. I. Levey, J. J. Lah, *et al.*, "Variant of TREM2 associated with the risk of Alzheimer's disease," *New England Journal of Medicine*, vol. 368, no. 2, pp. 107–116, 2013.

[70] B. Zhang, C. Gaiteri, L.-G. Bodea, Z. Wang, J. McElwee, A. A. Podtelezhnikov, C. Zhang, T. Xie, L. Tran, R. Dobrin, *et al.*, "Integrated systems approach identifies genetic nodes and networks in late-onset Alzheimer's disease," *Cell*, vol. 153, no. 3, pp. 707–720, 2013.

[71] M. Baker, I. R. Mackenzie, S. M. Pickering-Brown, J. Gass, R. Rademakers, C. Lindholm, J. Snowden, J. Adamson, A. D. Sadovnick, S. Rollinson, *et al.*, "Mutations in progranulin cause tau-negative frontotemporal dementia linked to chromosome 17," *Nature*, vol. 442, no. 7105, p. 916, 2006.

[72] S. Hong, V. F. Beja-Glasser, B. M. Nfonoyim, A. Frouin, S. Li, S. Ramakrishnan, K. M. Merry, Q. Shi, A. Rosenthal, B. A. Barres, *et al.*, "Complement and microglia mediate early synapse loss in Alzheimer mouse models," *Science*, vol. 352, no. 6286, pp. 712–716, 2016.

[73] D. T. Loo, A. Copani, C. J. Pike, E. R. Whittemore, A. J. Walencewicz, and C. W. Cotman, "Apoptosis is induced by beta-amyloid in cultured central nervous system neurons," *Proceedings of the National Academy of Sciences*, vol. 90, no. 17, pp. 7951–7955, 1993.

[74] A. Lunkes and J.-L. Mandel, "A cellular model that recapitulates major pathogenic steps of Huntington's disease," *Human molecular genetics*, vol. 7, no. 9, pp. 1355–1361, 1998.

[75] O. M. El-Agnaf, R. Jakes, M. D. Curran, D. Middleton, R. Ingenito, E. Bianchi, A. Pessi, D. Neill, and A. Wallace, "Aggregates from mutant and wild-type α-synuclein proteins and NAC peptide induce apoptotic cell death in human neuroblastoma cells by formation of β-sheet and amyloid-like filaments," *FEBS letters*, vol. 440, no. 1-2, pp. 71–75, 1998.

[76] L. Mangiarini, K. Sathasivam, M. Seller, B. Cozens, A. Harper, C. Hetherington, M. Lawton, Y. Trottier, H. Lehrach, S. W. Davies, *et al.*, "Exon 1 of the HD gene with an expanded CAG repeat is sufficient to cause a progressive neurological phenotype in transgenic mice," *Cell*, vol. 87, no. 3, pp. 493–506, 1996.

[77] K. Santacruz, J. Lewis, T. Spires, J. Paulson, L. Kotilinek, M. Ingelsson, A. Guimaraes, M. DeTure, M. Ramsden, E. McGowan, *et al.*, "Tau suppression in a neurodegenerative mouse model improves memory function," *Science*, vol. 309, no. 5733, pp. 476–481, 2005.

[78] J. L. Jankowsky, D. J. Fadale, J. Anderson, G. M. Xu, V. Gonzales, N. A. Jenkins, N. G. Copeland, M. K. Lee, L. H. Younkin, S. L. Wagner, *et al.*, "Mutant presenilins specifically elevate the levels of the 42 residue β-amyloid peptide in vivo: evidence for augmentation of a 42-specific γ secretase," *Human molecular genetics*, vol. 13, no. 2, pp. 159–170, 2003.

[79] H. Oakley, S. L. Cole, S. Logan, E. Maus, P. Shao, J. Craft, A. Guillozet-Bongaarts, M. Ohno, J. Disterhoft, L. Van Eldik, *et al.*, "Intraneuronal β-amyloid aggregates, neurodegeneration, and neuron loss in transgenic mice with five familial Alzheimer's disease mutations: potential factors in amyloid plaque formation," *Journal of Neuroscience*, vol. 26, no. 40, pp. 10129–10140, 2006.

[80] T. M. Dawson, T. E. Golde, and C. Lagier-Tourenne, "Animal models of neurodegenerative diseases," *Nat. Neurosci*, vol. 21, pp. 1370–1379, 2018.

[81] H. Olzscha, S. M. Schermann, A. C. Woerner, S. Pinkert, M. H. Hecht, G. G. Tartaglia, M. Vendruscolo, M. Hayer-Hartl, F. U. Hartl, and R. M. Vabulas, "Amyloid-like aggregates sequester numerous metastable proteins with essential cellular functions," *Cell*, vol. 144, no. 1, pp. 67–78, 2011.

[82] M. Bucciantini, E. Giannoni, F. Chiti, F. Baroni, L. Formigli, J. Zurdo, N. Taddei, G. Ramponi, C. M. Dobson, and M. Stefani, "Inherent toxicity of aggregates

implies a common mechanism for protein misfolding diseases," *nature*, vol. 416, no. 6880, p. 507, 2002.

[83] C. Haass and D. J. Selkoe, "Soluble protein oligomers in neurodegeneration: lessons from the Alzheimer's amyloid β-peptide," *Nature reviews Molecular cell biology*, vol. 8, no. 2, p. 101, 2007.

[84] G. M. Shankar, S. Li, T. H. Mehta, A. Garcia-Munoz, N. E. Shepardson, I. Smith, F. M. Brett, M. A. Farrell, M. J. Rowan, C. A. Lemere, *et al.*, "Amyloid-β protein dimers isolated directly from Alzheimer's brains impair synaptic plasticity and memory," *Nature medicine*, vol. 14, no. 8, p. 837, 2008.

[85] Y. Zhang, L. Lu, J. Jia, L. Jia, C. Geula, J. Pei, Z. Xu, W. Qin, R. Liu, D. Li, *et al.*, "A lifespan observation of a novel mouse model: in vivo evidence supports aβ oligomer hypothesis," *PloS one*, vol. 9, no. 1, p. e85885, 2014.

[86] B. Winner, R. Jappelli, S. K. Maji, P. A. Desplats, L. Boyer, S. Aigner, C. Hetzer, T. Loher, M. Vilar, S. Campioni, *et al.*, "In vivo demonstration that α-synuclein oligomers are toxic," *Proceedings of the National Academy of Sciences*, vol. 108, no. 10, pp. 4194–4199, 2011.

[87] L.-F. Lue, Y.-M. Kuo, A. E. Roher, L. Brachova, Y. Shen, L. Sue, T. Beach, J. H. Kurth, R. E. Rydel, and J. Rogers, "Soluble amyloid β peptide concentration as a predictor of synaptic change in Alzheimer's disease," *The American journal of pathology*, vol. 155, no. 3, pp. 853–862, 1999.

[88] M. P. Lambert, A. Barlow, B. A. Chromy, C. Edwards, R. Freed, M. Liosatos, T. Morgan, I. Rozovsky, B. Trommer, K. L. Viola, *et al.*, "Diffusible, nonfibrillar ligands derived from Aβ1-42 are potent central nervous system neurotoxins," *Proceedings of the National Academy of Sciences*, vol. 95, no. 11, pp. 6448–6453, 1998.

[89] A. R. A. Ladiwala, J. Litt, R. S. Kane, D. S. Aucoin, S. O. Smith, S. Ranjan, J. Davis, W. E. Van Nostrand, and P. M. Tessier, "Conformational differences between two amyloid β oligomers of similar size and dissimilar toxicity," *Journal of Biological Chemistry*, vol. 287, no. 29, pp. 24765–24773, 2012.

[90] B. O'Nuallain, D. B. Freir, A. J. Nicoll, E. Risse, N. Ferguson, C. E. Herron, J. Collinge, and D. M. Walsh, "Amyloid β-protein dimers rapidly form stable

synaptotoxic protofibrils," *Journal of Neuroscience*, vol. 30, no. 43, pp. 14411–14419, 2010.

[91] N. Lorenzen, S. B. Nielsen, A. K. Buell, J. D. Kaspersen, P. Arosio, B. S. Vad, W. Paslawski, G. Christiansen, Z. Valnickova-Hansen, M. Andreasen, *et al.*, "The role of stable α-synuclein oligomers in the molecular events underlying amyloid formation," *Journal of the American Chemical Society*, vol. 136, no. 10, pp. 3859–3868, 2014.

[92] M. Arrasate, S. Mitra, E. S. Schweitzer, M. R. Segal, and S. Finkbeiner, "Inclusion body formation reduces levels of mutant huntingtin and the risk of neuronal death," *nature*, vol. 431, no. 7010, p. 805, 2004.

[93] R. M. Koffie, M. Meyer-Luehmann, T. Hashimoto, K. W. Adams, M. L. Mielke, M. Garcia-Alloza, K. D. Micheva, S. J. Smith, M. L. Kim, V. M. Lee, *et al.*, "Oligomeric amyloid β associates with postsynaptic densities and correlates with excitatory synapse loss near senile plaques," *Proceedings of the National Academy of Sciences*, vol. 106, no. 10, pp. 4012–4017, 2009.

[94] M. Meyer-Luehmann, J. Coomaraswamy, T. Bolmont, S. Kaeser, C. Schaefer, E. Kilger, A. Neuenschwander, D. Abramowski, P. Frey, A. L. Jaton, *et al.*, "Exogenous induction of cerebral ß-amyloidogenesis is governed by agent and host," *Science*, vol. 313, no. 5794, pp. 1781–1784, 2006.

[95] F. Clavaguera, T. Bolmont, R. A. Crowther, D. Abramowski, S. Frank, A. Probst, G. Fraser, A. K. Stalder, M. Beibel, M. Staufenbiel, *et al.*, "Transmission and spreading of tauopathy in transgenic mouse brain," *Nature cell biology*, vol. 11, no. 7, p. 909, 2009.

[96] F. Clavaguera, H. Akatsu, G. Fraser, R. A. Crowther, S. Frank, J. Hench, A. Probst, D. T. Winkler, J. Reichwald, M. Staufenbiel, *et al.*, "Brain homogenates from human tauopathies induce tau inclusions in mouse brain," *Proceedings of the National Academy of Sciences*, vol. 110, no. 23, pp. 9535–9540, 2013.

[97] K. C. Luk, V. M. Kehm, B. Zhang, P. O'Brien, J. Q. Trojanowski, and V. M. Lee, "Intracerebral inoculation of pathological α-synuclein initiates a rapidly progressive neurodegenerative α-synucleinopathy in mice," *Journal of Experimental Medicine*, vol. 209, no. 5, pp. 975–986, 2012.

[98] C. Münch, J. O'Brien, and A. Bertolotti, "Prion-like propagation of mutant superoxide dismutase-1 misfolding in neuronal cells," *Proceedings of the National Academy of Sciences*, vol. 108, no. 9, pp. 3548–3553, 2011.

[99] E. Pecho-Vrieseling, C. Rieker, S. Fuchs, D. Bleckmann, M. S. Esposito, P. Botta, C. Goldstein, M. Bernhard, I. Galimberti, M. Müller, *et al.*, "Transneuronal propagation of mutant huntingtin contributes to non–cell autonomous pathology in neurons," *Nature neuroscience*, vol. 17, no. 8, p. 1064, 2014.

[100] I. Jeon, F. Cicchetti, G. Cisbani, S. Lee, E. Li, J. Bae, N. Lee, L. Li, W. Im, M. Kim, *et al.*, "Human-to-mouse prion-like propagation of mutant huntingtin protein," *Acta neuropathologica*, vol. 132, no. 4, pp. 577–592, 2016.

[101] K. C. Luk, V. Kehm, J. Carroll, B. Zhang, P. O'Brien, J. Q. Trojanowski, and V. M.-Y. Lee, "Pathological α-synuclein transmission initiates Parkinson-like neurodegeneration in nontransgenic mice," *Science*, vol. 338, no. 6109, pp. 949–953, 2012.

[102] J. L. Guo, S. Narasimhan, L. Changolkar, Z. He, A. Stieber, B. Zhang, R. J. Gathagan, M. Iba, J. D. McBride, J. Q. Trojanowski, *et al.*, "Unique pathological tau conformers from Alzheimer's brains transmit tau pathology in nontransgenic mice," *Journal of Experimental Medicine*, vol. 213, no. 12, pp. 2635–2654, 2016.

[103] W. Qiang, W.-M. Yau, J.-X. Lu, J. Collinge, and R. Tycko, "Structural variation in amyloid-β fibrils from Alzheimer's disease clinical subtypes," *Nature*, vol. 541, no. 7636, p. 217, 2017.

[104] S. K. Kaufman, D. W. Sanders, T. L. Thomas, A. J. Ruchinskas, J. Vaquer-Alicea, A. M. Sharma, T. M. Miller, and M. I. Diamond, "Tau prion strains dictate patterns of cell pathology, progression rate, and regional vulnerability in vivo," *Neuron*, vol. 92, no. 4, pp. 796–812, 2016.

[105] S. Narasimhan, J. L. Guo, L. Changolkar, A. Stieber, J. D. McBride, L. V. Silva, Z. He, B. Zhang, R. J. Gathagan, J. Q. Trojanowski, *et al.*, "Pathological tau strains from human brains recapitulate the diversity of tauopathies in nontransgenic mouse brain," *Journal of Neuroscience*, vol. 37, no. 47, pp. 11406–11423, 2017.

[106] L. Bousset, L. Pieri, G. Ruiz-Arlandis, J. Gath, P. H. Jensen, B. Habenstein, K. Madiona, V. Olieric, A. Böckmann, B. H. Meier, *et al.*, "Structural and func-

tional characterization of two alpha-synuclein strains," *Nature communications*, vol. 4, p. 2575, 2013.

[107] W. Peelaerts, L. Bousset, A. Van der Perren, A. Moskalyuk, R. Pulizzi, M. Giugliano, C. Van den Haute, R. Melki, and V. Baekelandt, "α-synuclein strains cause distinct synucleinopathies after local and systemic administration," *Nature*, vol. 522, no. 7556, p. 340, 2015.

[108] H. Braak and K. Del Tredici, "Neuropathological staging of brain pathology in sporadic Parkinson's disease: separating the wheat from the chaff," *Journal of Parkinson's disease*, vol. 7, no. s1, pp. S71–S85, 2017.

[109] H. Braak, J. Brettschneider, A. C. Ludolph, V. M. Lee, J. Q. Trojanowski, and K. Del Tredici, "Amyotrophic lateral sclerosis—a model of corticofugal axonal spread," *Nature Reviews Neurology*, vol. 9, no. 12, p. 708, 2013.

[110] H. Fu, J. Hardy, and K. E. Duff, "Selective vulnerability in neurodegenerative diseases," *Nature neuroscience*, p. 1, 2018.

[111] L. Gan, M. R. Cookson, L. Petrucelli, and A. R. La Spada, "Converging pathways in neurodegeneration, from genetics to mechanisms," *Nature neuroscience*, vol. 21, no. 10, p. 1300, 2018.

[112] L. S. Kaltenbach, E. Romero, R. R. Becklin, R. Chettier, R. Bell, A. Phansalkar, A. Strand, C. Torcassi, J. Savage, A. Hurlburt, *et al.*, "Huntingtin interacting proteins are genetic modifiers of neurodegeneration," *PLoS genetics*, vol. 3, no. 5, p. e82, 2007.

[113] M. Gray, D. I. Shirasaki, C. Cepeda, V. M. Andre, B. Wilburn, X.-H. Lu, J. Tao, I. Yamazaki, S.-H. Li, Y. E. Sun, *et al.*, "Full-length human mutant huntingtin with a stable polyglutamine repeat can elicit progressive and selective neuropathogenesis in BACHD mice," *Journal of Neuroscience*, vol. 28, no. 24, pp. 6182–6195, 2008.

[114] D. I. Shirasaki, E. R. Greiner, I. Al-Ramahi, M. Gray, P. Boontheung, D. H. Geschwind, J. Botas, G. Coppola, S. Horvath, J. A. Loo, *et al.*, "Network organization of the huntingtin proteomic interactome in mammalian brain," *Neuron*, vol. 75, no. 1, pp. 41–57, 2012.

[115] Y. E. Kim, F. Hosp, F. Frottin, H. Ge, M. Mann, M. Hayer-Hartl, and F. U. Hartl, "Soluble oligomers of polyQ-expanded huntingtin target a multiplicity of key cellular factors," *Molecular cell*, vol. 63, no. 6, pp. 951–964, 2016.

[116] C. G. Gunawardana, M. Mehrabian, X. Wang, I. Mueller, I. B. Lubambo, J. E. Jonkman, H. Wang, and G. Schmitt-Ulms, "The human tau interactome: binding to the ribonucleoproteome, and impaired binding of the P301L mutant to chaperones and the proteasome," *Molecular & Cellular Proteomics*, pp. mcp–M115, 2015.

[117] P. Wang, G. Joberty, A. Buist, A. Vanoosthuyse, I.-C. Stancu, B. Vasconcelos, N. Pierrot, M. Faelth-Savitski, P. Kienlen-Campard, J.-N. Octave, *et al.*, "Tau interactome mapping based identification of Otub1 as tau deubiquitinase involved in accumulation of pathological tau forms in vitro and in vivo," *Acta neuropathologica*, vol. 133, no. 5, pp. 731–749, 2017.

[118] S. May, D. Hornburg, M. H. Schludi, T. Arzberger, K. Rentzsch, B. M. Schwenk, F. A. Grässer, K. Mori, E. Kremmer, J. Banzhaf-Strathmann, *et al.*, "C9orf72 FTLD/ALS-associated Gly-Ala dipeptide repeat proteins cause neuronal toxicity and Unc119 sequestration," *Acta neuropathologica*, vol. 128, no. 4, pp. 485–503, 2014.

[119] H. Hartmann, D. Hornburg, M. Czuppa, J. Bader, M. Michaelsen, D. Farny, T. Arzberger, M. Mann, F. Meissner, and D. Edbauer, "Proteomics and C9orf72 neuropathology identify ribosomes as poly-GR/PR interactors driving toxicity," *Life science alliance*, vol. 1, no. 2, p. e201800070, 2018.

[120] A. M. Blokhuis, M. Koppers, E. J. Groen, D. M. van den Heuvel, S. D. Modigliani, J. J. Anink, K. Fumoto, F. van Diggelen, A. Snelting, P. Sodaar, *et al.*, "Comparative interactomics analysis of different ALS-associated proteins identifies converging molecular pathways," *Acta neuropathologica*, vol. 132, no. 2, pp. 175–196, 2016.

[121] F. Hosp, H. Vossfeldt, M. Heinig, D. Vasiljevic, A. Arumughan, E. Wyler, M. Landthaler, N. Hubner, E. E. Wanker, L. Lannfelt, *et al.*, "Quantitative interaction proteomics of neurodegenerative disease proteins," *Cell reports*, vol. 11, no. 7, pp. 1134–1146, 2015.

[122] B. Bai, C. M. Hales, P.-C. Chen, Y. Gozal, E. B. Dammer, J. J. Fritz, X. Wang, Q. Xia, D. M. Duong, C. Street, *et al.*, "U1 small nuclear ribonucleoprotein complex and RNA splicing alterations in Alzheimer's disease," *Proceedings of the National Academy of Sciences*, vol. 110, no. 41, pp. 16562–16567, 2013.

[123] C. M. Hales, E. B. Dammer, Q. Deng, D. M. Duong, M. Gearing, J. C. Troncoso, M. Thambisetty, J. J. Lah, J. M. Shulman, A. I. Levey, *et al.*, "Changes in the detergent-insoluble brain proteome linked to amyloid and tau in Alzheimer's disease progression," *Proteomics*, vol. 16, no. 23, pp. 3042–3053, 2016.

[124] P. Langfelder, J. P. Cantle, D. Chatzopoulou, N. Wang, F. Gao, I. Al-Ramahi, X.-H. Lu, E. M. Ramos, K. El-Zein, Y. Zhao, *et al.*, "Integrated genomics and proteomics define huntingtin CAG length-dependent networks in mice," *Nature neuroscience*, vol. 19, no. 4, p. 623, 2016.

[125] F. Hosp, S. Gutiérrez-Ángel, M. H. Schaefer, J. Cox, F. Meissner, M. S. Hipp, F.-U. Hartl, R. Klein, I. Dudanova, and M. Mann, "Spatiotemporal proteomic profiling of Huntington's disease inclusions reveals widespread loss of protein function," *Cell reports*, vol. 21, no. 8, pp. 2291–2303, 2017.

[126] M. C. Pace, G. Xu, S. Fromholt, J. Howard, K. Crosby, B. I. Giasson, J. Lewis, and D. R. Borchelt, "Changes in proteome solubility indicate widespread proteostatic disruption in mouse models of neurodegenerative disease," *Acta neuropathologica*, vol. 136, no. 6, pp. 919–938, 2018.

[127] K. E. Knockenhauer and T. U. Schwartz, "The nuclear pore complex as a flexible and dynamic gate," *Cell*, vol. 164, no. 6, pp. 1162–1171, 2016.

[128] H. J. Kim and J. P. Taylor, "Lost in transportation: nucleocytoplasmic transport defects in ALS and other neurodegenerative diseases," *Neuron*, vol. 96, no. 2, pp. 285–297, 2017.

[129] B. D. Freibaum, Y. Lu, R. Lopez-Gonzalez, N. C. Kim, S. Almeida, K.-H. Lee, N. Badders, M. Valentine, B. L. Miller, P. C. Wong, *et al.*, "GGGGCC repeat expansion in C9orf72 compromises nucleocytoplasmic transport," *Nature*, vol. 525, no. 7567, p. 129, 2015.

[130] K. Zhang, C. J. Donnelly, A. R. Haeusler, J. C. Grima, J. B. Machamer, P. Steinwald, E. L. Daley, S. J. Miller, K. M. Cunningham, S. Vidensky, *et al.*,

"The C9orf72 repeat expansion disrupts nucleocytoplasmic transport," *Nature*, vol. 525, no. 7567, p. 56, 2015.

[131] S. Boeynaems, E. Bogaert, E. Michiels, I. Gijselinck, A. Sieben, A. Jovičić, G. De Baets, W. Scheveneels, J. Steyaert, I. Cuijt, *et al.*, "Drosophila screen connects nuclear transport genes to DPR pathology in c9ALS/FTD," *Scientific reports*, vol. 6, p. 20877, 2016.

[132] A. Jovičić, J. Mertens, S. Boeynaems, E. Bogaert, N. Chai, S. B. Yamada, J. W. Paul III, S. Sun, J. R. Herdy, G. Bieri, *et al.*, "Modifiers of C9orf72 DPR toxicity implicate nucleocytoplasmic transport impairments in c9FTD/ALS," *Nature neuroscience*, vol. 18, no. 9, p. 1226, 2015.

[133] K. Y. Shi, E. Mori, Z. F. Nizami, Y. Lin, M. Kato, S. Xiang, L. C. Wu, M. Ding, Y. Yu, J. G. Gall, *et al.*, "Toxic PRn poly-dipeptides encoded by the C9orf72 repeat expansion block nuclear import and export," *Proceedings of the National Academy of Sciences*, vol. 114, no. 7, pp. E1111–E1117, 2017.

[134] J. C. Grima, J. G. Daigle, N. Arbez, K. C. Cunningham, K. Zhang, J. Ochaba, C. Geater, E. Morozko, J. Stocksdale, J. C. Glatzer, *et al.*, "Mutant huntingtin disrupts the nuclear pore complex," *Neuron*, vol. 94, no. 1, pp. 93–107, 2017.

[135] F. Gasset-Rosa, C. Chillon-Marinas, A. Goginashvili, R. S. Atwal, J. W. Artates, R. Tabet, V. C. Wheeler, A. G. Bang, D. W. Cleveland, and C. Lagier-Tourenne, "Polyglutamine-expanded huntingtin exacerbates age-related disruption of nuclear integrity and nucleocytoplasmic transport," *Neuron*, vol. 94, no. 1, pp. 48–57, 2017.

[136] N. Li and C. Lagier-Tourenne, "Nuclear pores: the gate to neurodegeneration," *Nature neuroscience*, vol. 21, no. 2, p. 156, 2018.

[137] C.-C. Chou, Y. Zhang, M. E. Umoh, S. W. Vaughan, I. Lorenzini, F. Liu, M. Sayegh, P. G. Donlin-Asp, Y. H. Chen, D. M. Duong, *et al.*, "TDP-43 pathology disrupts nuclear pore complexes and nucleocytoplasmic transport in ALS/FTD," *Nature neuroscience*, vol. 21, no. 2, p. 228, 2018.

[138] B. Eftekharzadeh, J. G. Daigle, L. E. Kapinos, A. Coyne, J. Schiantarelli, Y. Carlomagno, C. Cook, S. J. Miller, S. Dujardin, A. S. Amaral, *et al.*, "Tau protein disrupts nucleocytoplasmic transport in Alzheimer's disease," *Neuron*, vol. 99, no. 5, pp. 925–940, 2018.

[139] M. V. Chao, "Neurotrophins and their receptors: a convergence point for many signalling pathways," *Nature Reviews Neuroscience*, vol. 4, no. 4, p. 299, 2003.

[140] A. Nykjaer, R. Lee, K. K. Teng, P. Jansen, P. Madsen, M. S. Nielsen, C. Jacobsen, M. Kliemannel, E. Schwarz, T. E. Willnow, *et al.*, "Sortilin is essential for proNGF-induced neuronal cell death," *Nature*, vol. 427, no. 6977, p. 843, 2004.

[141] F. M. Longo and S. M. Massa, "Small-molecule modulation of neurotrophin receptors: a strategy for the treatment of neurological disease," *Nature reviews Drug discovery*, vol. 12, no. 7, p. 507, 2013.

[142] S. Josephy-Hernandez, S. Jmaeff, I. Pirvulescu, T. Aboulkassim, and H. U. Saragovi, "Neurotrophin receptor agonists and antagonists as therapeutic agents: An evolving paradigm," *Neurobiology of disease*, vol. 97, pp. 139–155, 2017.

[143] S. A. Scott, E. J. Mufson, J. A. Weingartner, K. A. Skau, and K. A. Crutcher, "Nerve growth factor in Alzheimer's disease: increased levels throughout the brain coupled with declines in nucleus basalis," *Journal of Neuroscience*, vol. 15, no. 9, pp. 6213–6221, 1995.

[144] M. Fahnestock, B. Michalski, B. Xu, and M. D. Coughlin, "The precursor pro-nerve growth factor is the predominant form of nerve growth factor in brain and is increased in Alzheimer's disease," *Molecular and Cellular Neuroscience*, vol. 18, no. 2, pp. 210–220, 2001.

[145] S. Peng, J. Wuu, E. J. Mufson, and M. Fahnestock, "Increased proNGF levels in subjects with mild cognitive impairment and mild Alzheimer disease," *Journal of Neuropathology & Experimental Neurology*, vol. 63, no. 6, pp. 641–649, 2004.

[146] S. E. Counts, M. Nadeem, J. Wuu, S. D. Ginsberg, H. U. Saragovi, and E. J. Mufson, "Reduction of cortical TrkA but not p75NTR protein in early-stage Alzheimer's disease," *Annals of Neurology: Official Journal of the American Neurological Association and the Child Neurology Society*, vol. 56, no. 4, pp. 520–531, 2004.

[147] C. N. Svendsen, J. D. Cooper, and M. V. Sofroniew, "Trophic factor effects on septal cholinergic neuronsa," *Annals of the New York Academy of Sciences*, vol. 640, no. 1, pp. 91–94, 1991.

[148] M. Yaar, S. Zhai, P. F. Pilch, S. M. Doyle, P. B. Eisenhauer, R. E. Fine, and B. A. Gilchrest, "Binding of beta-amyloid to the p75 neurotrophin receptor induces apoptosis. a possible mechanism for Alzheimer's disease.," *The Journal of clinical investigation*, vol. 100, no. 9, pp. 2333–2340, 1997.

[149] C. Costantini, F. Rossi, E. Formaggio, R. Bernardoni, D. Cecconi, and V. Della-Bianca, "Characterization of the signaling pathway downstream p75 neurotrophin receptor involved in β-amyloid peptide-dependent cell death," *Journal of molecular neuroscience*, vol. 25, no. 2, pp. 141–156, 2005.

[150] H. S. Phillips, J. M. Hains, M. Armanini, G. R. Laramee, S. A. Johnson, and J. W. Winslow, "BDNF mRNA is decreased in the hippocampus of individuals with Alzheimer's disease," *Neuron*, vol. 7, no. 5, pp. 695–702, 1991.

[151] I. Ferrer, C. Marín, M. J. Rey, T. Ribalta, E. Goutan, R. Blanco, E. Tolosa, and E. Martí, "BDNF and full-length and truncated TrkB expression in Alzheimer disease. implications in therapeutic strategies," *Journal of neuropathology and experimental neurology*, vol. 58, no. 7, pp. 729–739, 1999.

[152] S. Peng, J. Wuu, E. J. Mufson, and M. Fahnestock, "Precursor form of brain-derived neurotrophic factor and mature brain-derived neurotrophic factor are decreased in the pre-clinical stages of Alzheimer's disease," *Journal of neurochemistry*, vol. 93, no. 6, pp. 1412–1421, 2005.

[153] A. H. Nagahara, D. A. Merrill, G. Coppola, S. Tsukada, B. E. Schroeder, G. M. Shaked, L. Wang, A. Blesch, A. Kim, J. M. Conner, *et al.*, "Neuroprotective effects of brain-derived neurotrophic factor in rodent and primate models of Alzheimer's disease," *Nature medicine*, vol. 15, no. 3, p. 331, 2009.

[154] M. Mogi, A. Togari, T. Kondo, Y. Mizuno, O. Komure, S. Kuno, H. Ichinose, and T. Nagatsu, "Brain-derived growth factor and nerve growth factor concentrations are decreased in the substantia nigra in Parkinson's disease," *Neuroscience letters*, vol. 270, no. 1, pp. 45–48, 1999.

[155] L. L. Pedre, N. P. Fuentes, L. A. González, A. McRae, T. S. Sánchez, L. B. Lescano, and R. M. González, "Nerve growth factor levels in Parkinson disease and experimental parkinsonian rats," *Brain research*, vol. 952, no. 1, pp. 122–127, 2002.

[156] N. B. Chauhan, G. J. Siegel, and J. M. Lee, "Depletion of glial cell line-derived neurotrophic factor in substantia nigra neurons of Parkinson's disease brain," *Journal of chemical neuroanatomy*, vol. 21, no. 4, pp. 277–288, 2001.

[157] S. S. Gill, N. K. Patel, G. R. Hotton, K. O'Sullivan, R. McCarter, M. Bunnage, D. J. Brooks, C. N. Svendsen, and P. Heywood, "Direct brain infusion of glial cell line-derived neurotrophic factor in Parkinson disease," *Nature medicine*, vol. 9, no. 5, p. 589, 2003.

[158] A. E. Lang, S. Gill, N. K. Patel, A. Lozano, J. G. Nutt, R. Penn, D. J. Brooks, G. Hotton, E. Moro, P. Heywood, *et al.*, "Randomized controlled trial of intraputamenal glial cell line-derived neurotrophic factor infusion in Parkinson disease," *Annals of neurology*, vol. 59, no. 3, pp. 459–466, 2006.

[159] C. Zuccato, A. Ciammola, D. Rigamonti, B. R. Leavitt, D. Goffredo, L. Conti, M. E. MacDonald, R. M. Friedlander, V. Silani, M. R. Hayden, *et al.*, "Loss of huntingtin-mediated BDNF gene transcription in Huntington's disease," *Science*, vol. 293, no. 5529, pp. 493–498, 2001.

[160] C. Zuccato, M. Marullo, P. Conforti, M. E. MacDonald, M. Tartari, and E. Cattaneo, "Systematic assessment of BDNF and its receptor levels in human cortices affected by Huntington's disease," *Brain pathology*, vol. 18, no. 2, pp. 225–238, 2008.

[161] S. Ginés, M. Bosch, S. Marco, N. Gavalda, M. Díaz-Hernández, J. J. Lucas, J. M. Canals, and J. Alberch, "Reduced expression of the trkb receptor in huntington's disease mouse models and in human brain," *European Journal of Neuroscience*, vol. 23, no. 3, pp. 649–658, 2006.

[162] L. R. Gauthier, B. C. Charrin, M. Borrell-Pagès, J. P. Dompierre, H. Rangone, F. P. Cordelières, J. De Mey, M. E. MacDonald, V. Leßmann, S. Humbert, *et al.*, "Huntingtin controls neurotrophic support and survival of neurons by enhancing BDNF vesicular transport along microtubules," *Cell*, vol. 118, no. 1, pp. 127–138, 2004.

[163] E. Colin, D. Zala, G. Liot, H. Rangone, M. Borrell-Pagès, X.-J. Li, F. Saudou, and S. Humbert, "Huntingtin phosphorylation acts as a molecular switch for anterograde/retrograde transport in neurons," *The EMBO journal*, vol. 27, no. 15, pp. 2124–2134, 2008.

[164] G. Liot, D. Zala, P. Pla, G. Mottet, M. Piel, and F. Saudou, "Mutant Huntingtin alters retrograde transport of TrkB receptors in striatal dendrites," *Journal of Neuroscience*, vol. 33, no. 15, pp. 6298–6309, 2013.

[165] J. L. Plotkin, M. Day, J. D. Peterson, Z. Xie, G. J. Kress, I. Rafalovich, J. Kondapalli, T. S. Gertler, M. Flajolet, P. Greengard, *et al.*, "Impaired TrkB receptor signaling underlies corticostriatal dysfunction in Huntington's disease," *Neuron*, vol. 83, no. 1, pp. 178–188, 2014.

[166] A. M. Weissmiller and C. Wu, "Current advances in using neurotrophic factors to treat neurodegenerative disorders," *Translational neurodegeneration*, vol. 1, no. 1, p. 14, 2012.

[167] J. B. Koprich, L. V. Kalia, and J. M. Brotchie, "Animal models of α-synucleinopathy for Parkinson disease drug development," *Nature Reviews Neuroscience*, vol. 18, no. 9, p. 515, 2017.

[168] L. M. Ittner, G. M. Halliday, J. J. Kril, J. Götz, J. R. Hodges, and M. C. Kiernan, "FTD and ALS—translating mouse studies into clinical trials," *Nature Reviews Neurology*, vol. 11, no. 6, p. 360, 2015.

[169] D. M. Holtzman, J. C. Morris, and A. M. Goate, "Alzheimer's disease: the challenge of the second century," *Science translational medicine*, vol. 3, no. 77, pp. 77sr1–77sr1, 2011.

[170] F. M. LaFerla and K. N. Green, "Animal models of Alzheimer disease," *Cold Spring Harbor perspectives in medicine*, vol. 2, no. 11, p. a006320, 2012.

[171] K. H. Ashe and K. R. Zahs, "Probing the biology of Alzheimer's disease in mice," *Neuron*, vol. 66, no. 5, pp. 631–645, 2010.

[172] T. Saito, Y. Matsuba, N. Mihira, J. Takano, P. Nilsson, S. Itohara, N. Iwata, and T. C. Saido, "Single App knock-in mouse models of Alzheimer's disease," *Nature neuroscience*, vol. 17, no. 5, p. 661, 2014.

[173] A. Masuda, Y. Kobayashi, N. Kogo, T. Saito, T. C. Saido, and S. Itohara, "Cognitive deficits in single App knock-in mouse models," *Neurobiology of learning and memory*, vol. 135, pp. 73–82, 2016.

[174] C. Andorfer, Y. Kress, M. Espinoza, R. De Silva, K. L. Tucker, Y.-A. Barde, K. Duff, and P. Davies, "Hyperphosphorylation and aggregation of tau in mice

expressing normal human tau isoforms," *Journal of neurochemistry*, vol. 86, no. 3, pp. 582–590, 2003.

[175] I. Espuny-Camacho, A. M. Arranz, M. Fiers, A. Snellinx, K. Ando, S. Munck, J. Bonnefont, L. Lambot, N. Corthout, L. Omodho, *et al.*, "Hallmarks of Alzheimer's disease in stem-cell-derived human neurons transplanted into mouse brain," *Neuron*, vol. 93, no. 5, pp. 1066–1081, 2017.

[176] C. Andorfer, C. M. Acker, Y. Kress, P. R. Hof, K. Duff, and P. Davies, "Cell-cycle reentry and cell death in transgenic mice expressing nonmutant human tau isoforms," *Journal of Neuroscience*, vol. 25, no. 22, pp. 5446–5454, 2005.

[177] J. Lewis, D. W. Dickson, W.-L. Lin, L. Chisholm, A. Corral, G. Jones, S.-H. Yen, N. Sahara, L. Skipper, D. Yager, *et al.*, "Enhanced neurofibrillary degeneration in transgenic mice expressing mutant tau and APP," *Science*, vol. 293, no. 5534, pp. 1487–1491, 2001.

[178] S. Oddo, A. Caccamo, J. D. Shepherd, M. P. Murphy, T. E. Golde, R. Kayed, R. Metherate, M. P. Mattson, Y. Akbari, and F. M. LaFerla, "Triple-transgenic model of Alzheimer's disease with plaques and tangles: intracellular Aβ and synaptic dysfunction," *Neuron*, vol. 39, no. 3, pp. 409–421, 2003.

[179] J. Götz, F. v. Chen, J. Van Dorpe, and R. Nitsch, "Formation of neurofibrillary tangles in p301l tau transgenic mice induced by Aβ42 fibrils," *Science*, vol. 293, no. 5534, pp. 1491–1495, 2001.

[180] C. Olanow, K. Kieburtz, and R. Katz, "Clinical approaches to the development of a neuroprotective therapy for PD," *Experimental neurology*, vol. 298, pp. 246–251, 2017.

[181] S. Janezic, S. Threlfell, P. D. Dodson, M. J. Dowie, T. N. Taylor, D. Potgieter, L. Parkkinen, S. L. Senior, S. Anwar, B. Ryan, *et al.*, "Deficits in dopaminergic transmission precede neuron loss and dysfunction in a new Parkinson model," *Proceedings of the National Academy of Sciences*, vol. 110, no. 42, pp. E4016–E4025, 2013.

[182] X. Lin, L. Parisiadou, C. Sgobio, G. Liu, J. Yu, L. Sun, H. Shim, X.-L. Gu, J. Luo, C.-X. Long, *et al.*, "Conditional expression of parkinson's disease-related mutant

α-synuclein in the midbrain dopaminergic neurons causes progressive neurodegeneration and degradation of transcription factor nuclear receptor related 1," *Journal of Neuroscience*, vol. 32, no. 27, pp. 9248–9264, 2012.

[183] Y. Lee, V. L. Dawson, and T. M. Dawson, "Animal models of Parkinson's disease: vertebrate genetics," *Cold Spring Harbor perspectives in medicine*, vol. 2, no. 10, p. a009324, 2012.

[184] V. Picher-Martel, P. N. Valdmanis, P. V. Gould, J.-P. Julien, and N. Dupré, "From animal models to human disease: a genetic approach for personalized medicine in ALS," *Acta neuropathologica communications*, vol. 4, no. 1, p. 70, 2016.

[185] J. D. Rothstein, L. J. Martin, and R. W. Kuncl, "Decreased glutamate transport by the brain and spinal cord in amyotrophic lateral sclerosis," *New England Journal of Medicine*, vol. 326, no. 22, pp. 1464–1468, 1992.

[186] A. Clement, M. Nguyen, E. Roberts, M. Garcia, S. Boillee, M. Rule, A. McMahon, W. Doucette, D. Siwek, R. Ferrante, *et al.*, "Wild-type nonneuronal cells extend survival of SOD1 mutant motor neurons in ALS mice," *science*, vol. 302, no. 5642, pp. 113–117, 2003.

[187] H. Ilieva, M. Polymenidou, and D. W. Cleveland, "Non–cell autonomous toxicity in neurodegenerative disorders: ALS and beyond," *The Journal of cell biology*, vol. 187, no. 6, pp. 761–772, 2009.

[188] T. Philips and J. D. Rothstein, "Rodent models of amyotrophic lateral sclerosis," *Current protocols in pharmacology*, vol. 69, no. 1, pp. 5–67, 2015.

[189] V. Swarup, D. Phaneuf, N. Dupré, S. Petri, M. Strong, J. Kriz, and J.-P. Julien, "Deregulation of TDP-43 in amyotrophic lateral sclerosis triggers nuclear factor b–mediated pathogenic pathways," *Journal of Experimental Medicine*, vol. 208, no. 12, pp. 2429–2447, 2011.

[190] J. G. O'Rourke, L. Bogdanik, A. Muhammad, T. F. Gendron, K. J. Kim, A. Austin, J. Cady, E. Y. Liu, J. Zarrow, S. Grant, *et al.*, "C9orf72 BAC transgenic mice display typical pathologic features of ALS/FTD," *Neuron*, vol. 88, no. 5, pp. 892–901, 2015.

[191] O. M. Peters, G. T. Cabrera, H. Tran, T. F. Gendron, J. E. McKeon, J. Metterville, A. Weiss, N. Wightman, J. Salameh, J. Kim, *et al.*, "Human C9ORF72 hexanucleotide expansion reproduces RNA foci and dipeptide repeat proteins but not neurodegeneration in BAC transgenic mice," *Neuron*, vol. 88, no. 5, pp. 902–909, 2015.

[192] Y. Liu, A. Pattamatta, T. Zu, T. Reid, O. Bardhi, D. R. Borchelt, A. T. Yachnis, and L. P. Ranum, "C9orf72 BAC mouse model with motor deficits and neurodegenerative features of ALS/FTD," *Neuron*, vol. 90, no. 3, pp. 521–534, 2016.

[193] C. Rinaldi and M. J. Wood, "Antisense oligonucleotides: the next frontier for treatment of neurological disorders," *Nature Reviews Neurology*, vol. 14, no. 1, p. 9, 2018.

[194] R. S. Finkel, E. Mercuri, B. T. Darras, A. M. Connolly, N. L. Kuntz, J. Kirschner, C. A. Chiriboga, K. Saito, L. Servais, E. Tizzano, *et al.*, "Nusinersen versus sham control in infantile-onset spinal muscular atrophy," *New England Journal of Medicine*, vol. 377, no. 18, pp. 1723–1732, 2017.

[195] J. Jiang, Q. Zhu, T. F. Gendron, S. Saberi, M. McAlonis-Downes, A. Seelman, J. E. Stauffer, P. Jafar-Nejad, K. Drenner, D. Schulte, *et al.*, "Gain of toxicity from ALS/FTD-linked repeat expansions in C9ORF72 is alleviated by antisense oligonucleotides targeting GGGGCC-containing RNAs," *Neuron*, vol. 90, no. 3, pp. 535–550, 2016.

[196] G. Schilling, M. W. Becher, A. H. Sharp, H. A. Jinnah, K. Duan, J. A. Kotzuk, H. H. Slunt, T. Ratovitski, J. K. Cooper, N. A. Jenkins, *et al.*, "Intranuclear inclusions and neuritic aggregates in transgenic mice expressing a mutant N-terminal fragment of huntingtin," *Human molecular genetics*, vol. 8, no. 3, pp. 397–407, 1999.

[197] H. S. Group *et al.*, "A randomized, placebo-controlled trial of coenzyme Q10 and remacemide in Huntington's disease," *Neurology*, vol. 57, no. 3, pp. 397–404, 2001.

[198] G. B. Landwehrmeyer, B. Dubois, J. G. de Yébenes, B. Kremer, W. Gaus, P. H. Kraus, H. Przuntek, M. Dib, A. Doble, W. Fischer, *et al.*, "Riluzole in Huntington's disease: a 3-year, randomized controlled study," *Annals of Neurology:*

Official Journal of the American Neurological Association and the Child Neurology Society, vol. 62, no. 3, pp. 262–272, 2007.

[199] D. E. Ehrnhoefer, S. L. Butland, M. A. Pouladi, and M. R. Hayden, "Mouse models of Huntington disease: variations on a theme," *Disease models & mechanisms*, vol. 2, no. 3-4, pp. 123–129, 2009.

[200] E. J. Slow, J. Van Raamsdonk, D. Rogers, S. H. Coleman, R. K. Graham, Y. Deng, R. Oh, N. Bissada, S. M. Hossain, Y.-Z. Yang, *et al.*, "Selective striatal neuronal loss in a YAC128 mouse model of Huntington disease," *Human molecular genetics*, vol. 12, no. 13, pp. 1555–1567, 2003.

[201] L. B. Menalled, A. E. Kudwa, S. Miller, J. Fitzpatrick, J. Watson-Johnson, N. Keating, M. Ruiz, R. Mushlin, W. Alosio, K. McConnell, *et al.*, "Comprehensive behavioral and molecular characterization of a new knock-in mouse model of Huntington's disease: zQ175," *PloS one*, vol. 7, no. 12, p. e49838, 2012.

[202] A. L. Southwell, A. Smith-Dijak, C. Kay, M. Sepers, E. B. Villanueva, M. P. Parsons, Y. Xie, L. Anderson, B. Felczak, S. Waltl, *et al.*, "An enhanced Q175 knock-in mouse model of huntington disease with higher mutant huntingtin levels and accelerated disease phenotypes," *Human molecular genetics*, vol. 25, no. 17, pp. 3654–3675, 2016.

[203] M. W. West, W. Wang, J. Patterson, J. D. Mancias, J. R. Beasley, and M. H. Hecht, "De novo amyloid proteins from designed combinatorial libraries," *Proceedings of the National Academy of Sciences*, vol. 96, no. 20, pp. 11211–11216, 1999.

[204] A. C. Woerner, F. Frottin, D. Hornburg, L. R. Feng, F. Meissner, M. Patra, J. Tatzelt, M. Mann, K. F. Winklhofer, F. U. Hartl, *et al.*, "Cytoplasmic protein aggregates interfere with nucleocytoplasmic transport of protein and RNA," *Science*, vol. 351, no. 6269, pp. 173–176, 2016.

[205] M. Mayford, M. E. Bach, Y.-Y. Huang, L. Wang, R. D. Hawkins, and E. R. Kandel, "Control of memory formation through regulated expression of a CaMKII transgene," *Science*, vol. 274, no. 5293, pp. 1678–1683, 1996.

[206] C. I. Rodríguez, F. Buchholz, J. Galloway, R. Sequerra, J. Kasper, R. Ayala, A. F. Stewart, and S. M. Dymecki, "High-efficiency deleter mice show that FLPe is an alternative to Cre-loxP," *Nature genetics*, vol. 25, no. 2, p. 139, 2000.

[207] R. H. Kutner, X.-Y. Zhang, and J. Reiser, "Production, concentration and titration of pseudotyped hiv-1-based lentiviral vectors," *Nature protocols*, vol. 4, no. 4, p. 495, 2009.

[208] M. Jiang and G. Chen, "High Ca 2+-phosphate transfection efficiency in low-density neuronal cultures," *Nature protocols*, vol. 1, no. 2, p. 695, 2006.

[209] K. Meyer, M. Kirchner, B. Uyar, J.-Y. Cheng, G. Russo, L. R. Hernandez-Miranda, A. Szymborska, H. Zauber, I.-M. Rudolph, T. E. Willnow, *et al.*, "Mutations in disordered regions can cause disease by creating dileucine motifs," *Cell*, vol. 175, no. 1, pp. 239–253, 2018.

[210] A. Cumberworth, G. Lamour, M. M. Babu, and J. Gsponer, "Promiscuity as a functional trait: intrinsically disordered regions as central players of interactomes," *Biochemical Journal*, vol. 454, no. 3, pp. 361–369, 2013.

[211] M. Ashburner, C. A. Ball, J. A. Blake, D. Botstein, H. Butler, J. M. Cherry, A. P. Davis, K. Dolinski, S. S. Dwight, J. T. Eppig, *et al.*, "Gene Ontology: tool for the unification of biology," *Nature genetics*, vol. 25, no. 1, p. 25, 2000.

[212] J. Cox and M. Mann, "1D and 2D annotation enrichment: a statistical method integrating quantitative proteomics with complementary high-throughput data," *BMC bioinformatics*, vol. 13, no. 16, p. S12, 2012.

[213] E. Rogaeva, Y. Meng, J. H. Lee, Y. Gu, T. Kawarai, F. Zou, T. Katayama, C. T. Baldwin, R. Cheng, H. Hasegawa, *et al.*, "The neuronal sortilin-related receptor SORL1 is genetically associated with Alzheimer disease," *Nature genetics*, vol. 39, no. 2, p. 168, 2007.

[214] C. Reitz, R. Cheng, E. Rogaeva, J. H. Lee, S. Tokuhiro, F. Zou, K. Bettens, K. Sleegers, E. K. Tan, R. Kimura, *et al.*, "Meta-analysis of the association between variants in SORL1 and Alzheimer disease," *Archives of neurology*, vol. 68, no. 1, pp. 99–106, 2011.

[215] J. Durieux, S. Wolff, and A. Dillin, "The cell-non-autonomous nature of electron transport chain-mediated longevity," *Cell*, vol. 144, no. 1, pp. 79–91, 2011.

[216] G. O. Consortium, "The Gene Ontology (GO) database and informatics resource," *Nucleic acids research*, vol. 32, no. suppl_1, pp. D258–D261, 2004.

[217] M. Kanehisa and S. Goto, "Kegg: kyoto encyclopedia of genes and genomes," *Nucleic acids research*, vol. 28, no. 1, pp. 27–30, 2000.

[218] N. E. Sanjana, O. Shalem, and F. Zhang, "Improved vectors and genome-wide libraries for CRISPR screening," *Nature methods*, vol. 11, no. 8, p. 783, 2014.

[219] S. Incontro, C. S. Asensio, R. H. Edwards, and R. A. Nicoll, "Efficient, complete deletion of synaptic proteins using CRISPR," *Neuron*, vol. 83, no. 5, pp. 1051–1057, 2014.

[220] F. M. Menzies, A. Fleming, A. Caricasole, C. F. Bento, S. P. Andrews, A. Ashkenazi, J. Füllgrabe, A. Jackson, M. J. Sanchez, C. Karabiyik, *et al.*, "Autophagy and neurodegeneration: pathogenic mechanisms and therapeutic opportunities," *Neuron*, vol. 93, no. 5, pp. 1015–1034, 2017.

[221] L. Brichta, W. Shin, V. Jackson-Lewis, J. Blesa, E.-L. Yap, Z. Walker, J. Zhang, J.-P. Roussarie, M. J. Alvarez, A. Califano, *et al.*, "Identification of neurodegenerative factors using translatome-regulatory network analysis," *Nature neuroscience*, vol. 18, no. 9, p. 1325, 2015.

[222] M. S. Nahorski, M. Asai, E. Wakeling, A. Parker, N. Asai, N. Canham, S. E. Holder, Y.-C. Chen, J. Dyer, A. F. Brady, *et al.*, "CCDC88A mutations cause PEHO-like syndrome in humans and mouse," *Brain*, vol. 139, no. 4, pp. 1036–1044, 2016.

[223] X. Zhu, Y. Liu, Y. Yin, A. Shao, B. Zhang, S. Kim, and J. Zhou, "MSC p43 required for axonal development in motor neurons," *Proceedings of the National Academy of Sciences*, vol. 106, no. 37, pp. 15944–15949, 2009.

[224] L. Armstrong, R. Biancheri, C. Shyr, A. Rossi, G. Sinclair, C. Ross, M. Tarailo-Graovac, W. Wasserman, and C. van Karnebeek, "AIMP1 deficiency presents as a cortical neurodegenerative disease with infantile onset," *neurogenetics*, vol. 15, no. 3, pp. 157–159, 2014.

[225] P. Andrés-Benito, J. Moreno, E. Aso, M. Povedano, and I. Ferrer, "Amyotrophic lateral sclerosis, gene deregulation in the anterior horn of the spinal cord and frontal cortex area 8: implications in frontotemporal lobar degeneration," *Aging (Albany NY)*, vol. 9, no. 3, p. 823, 2017.

[226] S. E. Baranzini, R. Srinivasan, P. Khankhanian, D. T. Okuda, S. J. Nelson, P. M. Matthews, S. L. Hauser, J. R. Oksenberg, and D. Pelletier, "Genetic variation influences glutamate concentrations in brains of patients with multiple sclerosis," *Brain*, vol. 133, no. 9, pp. 2603–2611, 2010.

[227] F. Desmots, H. R. Russell, Y. Lee, K. Boyd, and P. J. McKinnon, "The reaper-binding protein scythe modulates apoptosis and proliferation during mammalian development," *Molecular and cellular biology*, vol. 25, no. 23, pp. 10329–10337, 2005.

[228] Z.-Q. Song, L.-F. Yang, Y.-S. Wang, T. Zhu, X.-M. Zhou, X.-M. Yin, H.-Q. Yao, and D.-M. Zhao, "Overexpression of BAT3 alleviates prion protein fragment PrP106-126-induced neuronal apoptosis," *CNS neuroscience & therapeutics*, vol. 20, no. 8, pp. 737–747, 2014.

[229] M. Zhao, N. Maani, and J. J. Dowling, "Dynamin 2 (DNM2) as cause of, and modifier for, human neuromuscular disease," *Neurotherapeutics*, pp. 1–10, 2018.

[230] L.-W. Jin, E. Masliah, D. Iimoto, R. Deteresa, M. Mallory, M. Sundsmo, N. Mori, A. Sobel, and T. Saitoh, "Neurofibrillary tangle-associated alteration of stathmin in Alzheimer's disease," *Neurobiology of aging*, vol. 17, no. 3, pp. 331–341, 1996.

[231] S. Bahn, M. Mimmack, M. Ryan, M. A. Caldwell, E. Jauniaux, M. Starkey, C. N. Svendsen, and P. Emson, "Neuronal target genes of the neuron-restrictive silencer factor in neurospheres derived from fetuses with Down's syndrome: a gene expression study," *The Lancet*, vol. 359, no. 9303, pp. 310–315, 2002.

[232] S. E. Lloyd, S. Mead, and J. Collinge, "Genetics of prion diseases," *Current opinion in genetics & development*, vol. 23, no. 3, pp. 345–351, 2013.

[233] M. D. Li, T. C. Burns, A. A. Morgan, and P. Khatri, "Integrated multi-cohort transcriptional meta-analysis of neurodegenerative diseases," *Acta neuropathologica communications*, vol. 2, no. 1, p. 1, 2014.

[234] S. Crimmins, Y. Jin, C. Wheeler, A. K. Huffman, C. Chapman, L. E. Dobrunz, A. Levey, K. A. Roth, J. A. Wilson, and S. M. Wilson, "Transgenic rescue of ataxia mice with neuronal-specific expression of ubiquitin-specific protease 14," *Journal of Neuroscience*, vol. 26, no. 44, pp. 11423–11431, 2006.

[235] H. Kanuka, E. Kuranaga, T. Hiratou, T. Igaki, B. Nelson, H. Okano, and M. Miura, "Cytosol-endoplasmic reticulum interplay by Sec61α translocon in polyglutamine-mediated neurotoxicity in Drosophila," *Proceedings of the National Academy of Sciences*, vol. 100, no. 20, pp. 11723–11728, 2003.

[236] A. G. Fitzmaurice, S. L. Rhodes, A. Lulla, N. P. Murphy, H. A. Lam, K. C. O'Donnell, L. Barnhill, J. E. Casida, M. Cockburn, A. Sagasti, *et al.*, "Aldehyde dehydrogenase inhibition as a pathogenic mechanism in Parkinson disease," *Proceedings of the National Academy of Sciences*, vol. 110, no. 2, pp. 636–641, 2013.

[237] M. C.-Y. Wey, E. Fernandez, P. A. Martinez, P. Sullivan, D. S. Goldstein, and R. Strong, "Neurodegeneration and motor dysfunction in mice lacking cytosolic and mitochondrial aldehyde dehydrogenases: implications for Parkinson's disease," *PloS one*, vol. 7, no. 2, p. e31522, 2012.

[238] M. Yoshikawa, S. Uchida, J. Ezaki, T. Rai, A. Hayama, K. Kobayashi, Y. Kida, M. Noda, M. Koike, Y. Uchiyama, *et al.*, "CLC-3 deficiency leads to phenotypes similar to human neuronal ceroid lipofuscinosis," *Genes to Cells*, vol. 7, no. 6, pp. 597–605, 2002.

[239] V. Buggia-Prévot, C. G. Fernandez, V. Udayar, K. S. Vetrivel, A. Elie, J. Roseman, V. A. Sasse, M. Lefkow, X. Meckler, S. Bhattacharyya, *et al.*, "A function for EHD family proteins in unidirectional retrograde dendritic transport of BACE1 and Alzheimer's disease Aβ production," *Cell reports*, vol. 5, no. 6, pp. 1552–1563, 2013.

[240] J. V. Louis, E. Martens, P. Borghgraef, C. Lambrecht, W. Sents, S. Longin, K. Zwaenepoel, R. Pijnenborg, I. Landrieu, G. Lippens, *et al.*, "Mice lacking phosphatase PP2A subunit PR61/B'δ (Ppp2r5d) develop spatially restricted tauopathy by deregulation of CDK5 and GSK3β," *Proceedings of the National Academy of Sciences*, vol. 108, no. 17, pp. 6957–6962, 2011.

[241] J. Wegiel, C.-X. Gong, and Y.-W. Hwang, "The role of DYRK1A in neurodegenerative diseases," *The FEBS journal*, vol. 278, no. 2, pp. 236–245, 2011.

[242] J. Cornett, F. Cao, C.-E. Wang, C. A. Ross, G. P. Bates, S.-H. Li, and X.-J. Li, "Polyglutamine expansion of huntingtin impairs its nuclear export," *Nature genetics*, vol. 37, no. 2, p. 198, 2005.

[243] J. E. Galvin, K. Uryu, V. M.-Y. Lee, and J. Q. Trojanowski, "Axon pathology in Parkinson's disease and Lewy body dementia hippocampus contains α-, β-, and γ-synuclein," *Proceedings of the National Academy of Sciences*, vol. 96, no. 23, pp. 13450–13455, 1999.

[244] A. Enomoto, H. Murakami, N. Asai, N. Morone, T. Watanabe, K. Kawai, Y. Murakumo, J. Usukura, K. Kaibuchi, and M. Takahashi, "Akt/PKB regulates actin organization and cell motility via Girdin/APE," *Developmental cell*, vol. 9, no. 3, pp. 389–402, 2005.

[245] C. Lin, J. Ear, K. Midde, I. Lopez-Sanchez, N. Aznar, M. Garcia-Marcos, I. Kufareva, R. Abagyan, and P. Ghosh, "Structural basis for activation of trimeric Gi proteins by multiple growth factor receptors via GIV/Girdin," *Molecular biology of the cell*, vol. 25, no. 22, pp. 3654–3671, 2014.

[246] T. Kitamura, N. Asai, A. Enomoto, K. Maeda, T. Kato, M. Ishida, P. Jiang, T. Watanabe, J. Usukura, T. Kondo, *et al.*, "Regulation of VEGF-mediated angiogenesis by the Akt/PKB substrate Girdin," *Nature cell biology*, vol. 10, no. 3, p. 329, 2008.

[247] N. Aznar, A. Patel, C. C. Rohena, Y. Dunkel, L. P. Joosen, V. Taupin, I. Kufareva, M. G. Farquhar, and P. Ghosh, "AMP-activated protein kinase fortifies epithelial tight junctions during energetic stress via its effector GIV/Girdin," *Elife*, vol. 5, p. e20795, 2016.

[248] C. Krueger, K. Pfleiderer, W. Hillen, and C. Berens, "Tetracycline derivatives: alternative effectors for Tet transregulators," *Biotechniques*, vol. 37, no. 4, pp. 546–550, 2004.

[249] M. Gossen and H. Bujard, "Tight control of gene expression in mammalian cells by tetracycline-responsive promoters.," *Proceedings of the National Academy of Sciences*, vol. 89, no. 12, pp. 5547–5551, 1992.

[250] M. Gossen, S. Freundlieb, G. Bender, G. Muller, W. Hillen, and H. Bujard, "Transcriptional activation by tetracyclines in mammalian cells," *Science*, vol. 268, no. 5218, pp. 1766–1769, 1995.

[251] H. J. Han, C. C. Allen, C. M. Buchovecky, M. J. Yetman, H. A. Born, M. A. Marin, S. P. Rodgers, B. J. Song, H.-C. Lu, M. J. Justice, *et al.*, "Strain back-

ground influences neurotoxicity and behavioral abnormalities in mice expressing the tetracycline transactivator," *Journal of Neuroscience*, vol. 32, no. 31, pp. 10574–10586, 2012.

[252] A. K. Walker, K. J. Spiller, G. Ge, A. Zheng, Y. Xu, M. Zhou, K. Tripathy, L. K. Kwong, J. Q. Trojanowski, and V. M.-Y. Lee, "Functional recovery in new mouse models of ALS/FTLD after clearance of pathological cytoplasmic TDP-43," *Acta neuropathologica*, vol. 130, no. 5, pp. 643–660, 2015.

[253] N. C. Shaner, R. E. Campbell, P. A. Steinbach, B. N. Giepmans, A. E. Palmer, and R. Y. Tsien, "Improved monomeric red, orange and yellow fluorescent proteins derived from Discosoma sp. red fluorescent protein," *Nature biotechnology*, vol. 22, no. 12, p. 1567, 2004.

[254] D. S. Bindels, L. Haarbosch, L. Van Weeren, M. Postma, K. E. Wiese, M. Mastop, S. Aumonier, G. Gotthard, A. Royant, M. A. Hink, *et al.*, "mScarlet: a bright monomeric red fluorescent protein for cellular imaging," *Nature methods*, vol. 14, no. 1, p. 53, 2017.

[255] K. R. Brunden, V. M. Lee, A. B. Smith III, J. Q. Trojanowski, and C. Ballatore, "Altered microtubule dynamics in neurodegenerative disease: Therapeutic potential of microtubule-stabilizing drugs," *Neurobiology of disease*, vol. 105, pp. 328–335, 2017.

[256] M. S. Hipp, S.-H. Park, and F. U. Hartl, "Proteostasis impairment in protein-misfolding and-aggregation diseases," *Trends in cell biology*, vol. 24, no. 9, pp. 506–514, 2014.

[257] A. Yamamoto, J. J. Lucas, and R. Hen, "Reversal of neuropathology and motor dysfunction in a conditional model of Huntington's disease," *Cell*, vol. 101, no. 1, pp. 57–66, 2000.

[258] A. Sydow, A. Van der Jeugd, F. Zheng, T. Ahmed, D. Balschun, O. Petrova, D. Drexler, L. Zhou, G. Rune, E. Mandelkow, *et al.*, "Tau-induced defects in synaptic plasticity, learning, and memory are reversible in transgenic mice after switching off the toxic tau mutant," *Journal of Neuroscience*, vol. 31, no. 7, pp. 2511–2525, 2011.

[259] J. L. Jankowsky, H. H. Slunt, V. Gonzales, A. V. Savonenko, J. C. Wen, N. A. Jenkins, N. G. Copeland, L. H. Younkin, H. A. Lester, S. G. Younkin, *et al.*,

"Persistent amyloidosis following suppression of Aβ production in a transgenic model of Alzheimer disease," *PLoS medicine*, vol. 2, no. 12, p. e355, 2005.

[260] L. M. Igaz, L. K. Kwong, E. B. Lee, A. Chen-Plotkin, E. Swanson, T. Unger, J. Malunda, Y. Xu, M. J. Winton, J. Q. Trojanowski, *et al.*, "Dysregulation of the ALS-associated gene TDP-43 leads to neuronal death and degeneration in mice," *The Journal of clinical investigation*, vol. 121, no. 2, pp. 726–738, 2011.

[261] R. Loew, N. Heinz, M. Hampf, H. Bujard, and M. Gossen, "Improved Tet-responsive promoters with minimized background expression," *BMC biotechnology*, vol. 10, no. 1, p. 81, 2010.

[262] F. Odeh, T. B. Leergaard, J. Boy, T. Schmidt, O. Riess, and J. G. Bjaalie, "Atlas of transgenic Tet-Off Ca2+/calmodulin-dependent protein kinase ii and prion protein promoter activity in the mouse brain," *Neuroimage*, vol. 54, no. 4, pp. 2603–2611, 2011.

[263] J. Goedhart, L. Van Weeren, M. J. Adjobo-Hermans, I. Elzenaar, M. A. Hink, and T. W. Gadella Jr, "Quantitative co-expression of proteins at the single cell level–application to a multimeric FRET sensor," *PloS one*, vol. 6, no. 11, p. e27321, 2011.

[264] D. M. Barten, G. W. Cadelina, N. Hoque, L. B. DeCarr, V. L. Guss, L. Yang, S. Sankaranarayanan, P. D. Wes, M. E. Flynn, J. E. Meredith, *et al.*, "Tau transgenic mice as models for cerebrospinal fluid tau biomarkers," *Journal of Alzheimer's Disease*, vol. 24, no. supplement2, pp. 127–141, 2011.

[265] J. Wagner, M. Schaffer, and R. Fernández-Busnadiego, "Cryo-electron tomography—the cell biology that came in from the cold," *FEBS letters*, vol. 591, no. 17, pp. 2520–2533, 2017.

[266] E. K. Richfield, M. J. Thiruchelvam, D. A. Cory-Slechta, C. Wuertzer, R. R. Gainetdinov, M. G. Caron, D. A. Di Monte, and H. J. Federoff, "Behavioral and neurochemical effects of wild-type and mutated human α-synuclein in transgenic mice," *Experimental neurology*, vol. 175, no. 1, pp. 35–48, 2002.

[267] S. W. Hell, "Microscopy and its focal switch," *Nature methods*, vol. 6, no. 1, p. 24, 2009.

[268] B. Vollmer, M. Lorenz, D. Moreno-Andrés, M. Bodenhöfer, P. De Magistris, S. A. Astrinidis, A. Schooley, M. Flötenmeyer, S. Leptihn, and W. Antonin, "Nup153 recruits the Nup107-160 complex to the inner nuclear membrane for interphasic nuclear pore complex assembly," *Developmental cell*, vol. 33, no. 6, pp. 717–728, 2015.

[269] U. Woehlbier, A. Colombo, M. J. Saaranen, V. Pérez, J. Ojeda, F. J. Bustos, C. I. Andreu, M. Torres, V. Valenzuela, D. B. Medinas, *et al.*, "Als-linked protein disulfide isomerase variants cause motor dysfunction," *The EMBO journal*, vol. 35, no. 8, pp. 845–865, 2016.

[270] A. E. Molero, E. E. Arteaga-Bracho, C. H. Chen, M. Gulinello, M. L. Winchester, N. Pichamoorthy, S. Gokhan, K. Khodakhah, and M. F. Mehler, "Selective expression of mutant huntingtin during development recapitulates characteristic features of Huntington's disease," *Proceedings of the National Academy of Sciences*, vol. 113, no. 20, pp. 5736–5741, 2016.

[271] J. V. Olsen, B. Macek, O. Lange, A. Makarov, S. Horning, and M. Mann, "Higher-energy C-trap dissociation for peptide modification analysis," *Nature methods*, vol. 4, no. 9, p. 709, 2007.

[272] J. Cox and M. Mann, "MaxQuant enables high peptide identification rates, individualized ppb-range mass accuracies and proteome-wide protein quantification," *Nature biotechnology*, vol. 26, no. 12, p. 1367, 2008.

[273] J. Cox, N. Neuhauser, A. Michalski, R. A. Scheltema, J. V. Olsen, and M. Mann, "Andromeda: a peptide search engine integrated into the MaxQuant environment," *Journal of proteome research*, vol. 10, no. 4, pp. 1794–1805, 2011.

[274] K. Podwojski, A. Fritsch, D. C. Chamrad, W. Paul, B. Sitek, K. Stühler, P. Mutzel, C. Stephan, H. E. Meyer, W. Urfer, *et al.*, "Retention time alignment algorithms for LC/MS data must consider non-linear shifts," *Bioinformatics*, vol. 25, no. 6, pp. 758–764, 2009.

[275] D. Hornburg, *Development and application of quantitative proteomics strategies to analyze molecular mechanisms of neurodegeneration*. PhD thesis, lmu, 2015.

[276] A. Ruepp, B. Waegele, M. Lechner, B. Brauner, I. Dunger-Kaltenbach, G. Fobo, G. Frishman, C. Montrone, and H.-W. Mewes, "CORUM: the comprehensive

resource of mammalian protein complexes—2009," *Nucleic acids research*, vol. 38, no. suppl_1, pp. D497–D501, 2009.

[277] R. D. Finn, A. Bateman, J. Clements, P. Coggill, R. Y. Eberhardt, S. R. Eddy, A. Heger, K. Hetherington, L. Holm, J. Mistry, *et al.*, "Pfam: the protein families database," *Nucleic acids research*, vol. 42, no. D1, pp. D222–D230, 2013.

Acknowledgements

I would like to thank Rüdiger for giving me the opportunity to work in his lab and for all the support during all these years.

I am especially grateful to Irina for all her guidance, supervision, and patience. When I look back to the beginning of my PhD, I realize how much I have learned and evolved as a scientist, and this is mostly thanks to her.

Big thanks to all my colleagues and collaborators for all the discussions and help throughout the project. I am particularly grateful to Sara and Kerstin for the healthy working atmosphere. Working in the lab has been a lot of fun and Dani, Augusto, and Marion made it even better.

I was very lucky to supervise two fantastic master students. Heartfelt thanks to Alan and Miguel for all their enthusiasm and efforts. I am sure that I have learned from them at least as much as I have taught them. Thank you also to all our Hiwis for all the technical help.

I am profoundly grateful to Sara and to Philipp for being my friends from the beginning until the end. All these years would have been dull without you. I am also deeply grateful to my Munich familia for keeping me smiling after so many years.

Finally, I would like to thank my family and Georg. My family has supported me in every decision and they actually made possible that I could pursue a PhD. Georg has patiently listened to me, has been an extraordinary scientific and personal role model, and has helped me by pushing my limits every day a little further. Thank you.